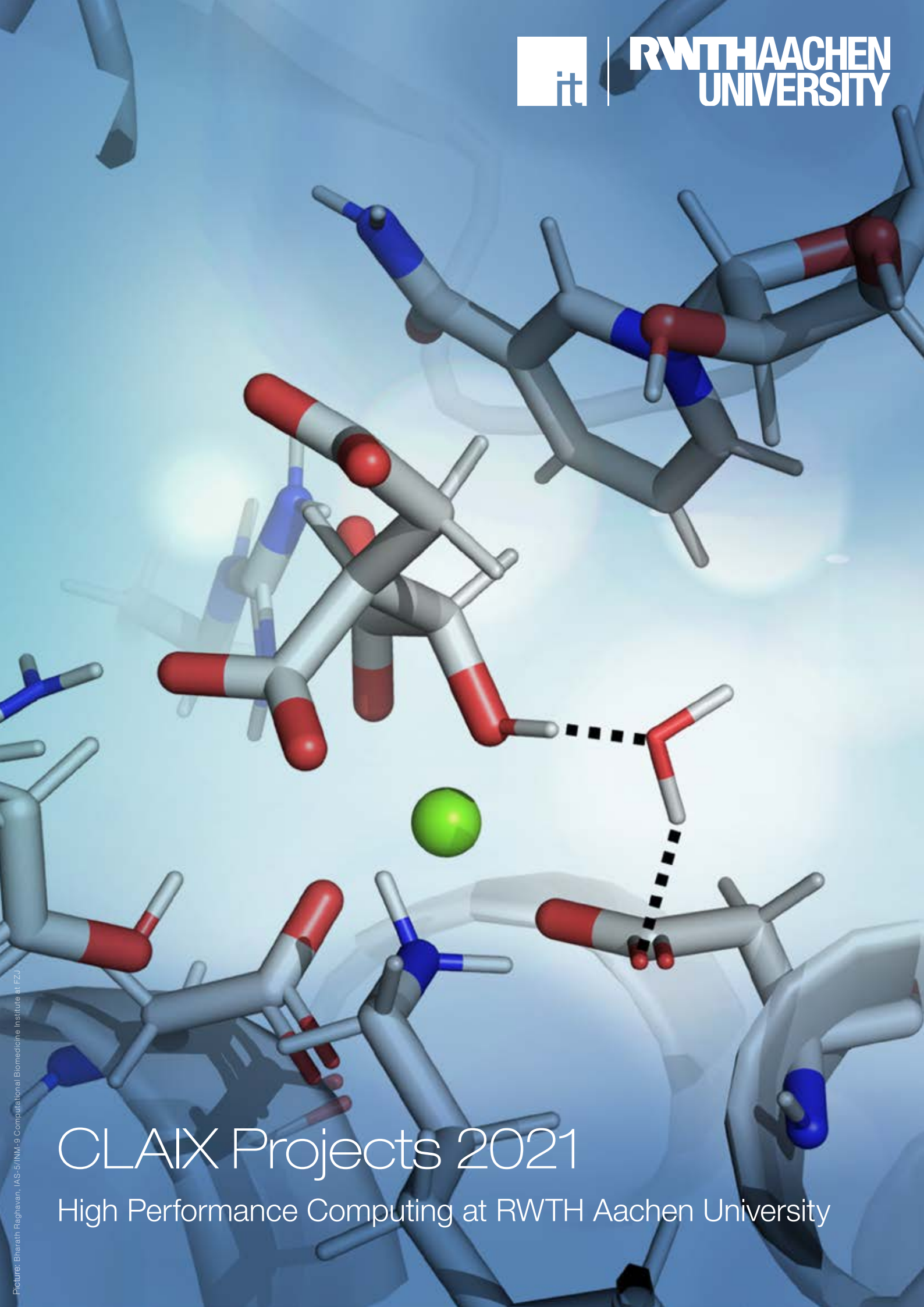

CLAIX Projects 2021

High Performance Computing at RWTH Aachen University

Picture: Bharath Raghavan, IAS-5/INM-9 Computational Biomedicine Institute at FZJ

IT Center | RWTH AACHEN UNIVERSITY

CLAIX Projects 2021

High Performance Computing at RWTH Aachen University

Imprint

IT Center
RWTH Aachen
University

Seffenter Weg 23
D-52074 Aachen

Phone: +49 241 80 24680
Fax: +49 241 80 22134

info@itc.rwth-aachen.de
www.itc.rwth-aachen.de

Editorial Design
HPC Offices,
IT Center

Aachen, August 2022

Content

90 Scientific reports | Engineering Sciences

Picture: Alexander F. Müller

Preface

Dear reader,

In the second year of the pandemic, which continued to be characterized by stagnation but also adaptation, the progress of research was a key constant. High-performance computers such as the Cluster Aix-la-Chapelle (CLAIX) help us understand global issues and solve problems, which concern us. Interesting projects ran on CLAIX in 2021 and helped to address these issues.

The project Numerical analysis of wind-induced pressure fluctuations on open volumetric receivers in solar power tower plants (SPTP) for example explores the field of solar tower power plants, where the technology of the open volumetric receiver (OVR) has proven to be very robust and efficient at experimental scales as well as at the pilot power plant in Jülich (1.5 MWel). The next step in research and development of the technology is the scale-up towards market-relevant sizes. This project investigates a reference power plant with a tower height of around 200m and a thermal receiver placed in three separate cavities facing south, north-east and north-west with a combined thermal power of around 350 MWth. The aim of this study is to simulate the wind flow around the reference plant with transient cfd simulations utilizing DES turbulence modelling (Forschungszentrum Jülich, see page 102).

The topic of data security is becoming increasingly important. The security of complex systems and networks often depends on data aggregated from several sources such as enduser devices, or industry control systems. These devices can create a vast amount of alerts, that make it hard for analysts to discern attacks from benign behavior. There exist several approaches for Intrusion Detection Systems (IDS) and Intrusion Prevention Systems (IPS) to handle these alerts, including machine learning approaches, to filter relevant output. However, such approaches raise questions on privacy, as they often include interactions with enduser systems and can be used to create user profiles or monitor user activity. Furthermore, the question arises how threats can be addressed preemptively, e.g., by leveraging public information to identify and secure vulnerable systems. The goal of the project Privacy-Preserving Machine Learning for Intrusion Detection is to research privacy-preserving machine learning approaches to several known problem domains (RWTH Aachen University, see page 132).

The figure presented on the cover of this report is an example of the project Molecular Dynamics study of mutant IDH1 for in silico drug design against neurological diseases (Forschungszentrum Jülich, see page 16).

You can find more information about these projects and also other interesting projects in this CLAIX Report 2021. We hope you enjoy reading it!

Yours sincerely,

Matthias Müller

PROF. DR. MATTHIAS MÜLLER

The HPC system at RWTH Aachen University: CLAIX

The research projects in this report represent a selection of projects using the high-performance computing system CLAIX - Cluster Aix-la-Chapelle - at RWTH Aachen University in 2019. The system is operated by the IT Center and currently consists of three parts: the Tier-2 part from the procurement phases 2016 and 2018 and the Tier-3 part from the procurement phase 2018. In 2022, as part of NHR4CES@RWTH, new fast and large-capacity storage systems will go operational and will be available from CLAIX. An extension of compute capacity is expected to go operation towards the end of that year.

CLAIX-2016
The system consists of over 600 systems with 2x Intel Xeon Broadwell processors. Specialized node types with up to 144 cores at 1 Terabyte main memory or integrated GPGPUs or NVRAM complete the system for special tasks. All nodes as well as the parallel Lustre file system with a capacity of 3 petabytes are connected with an Intel Omni-Path network at 100-GigaBit/s speed. The overall system achieves a computing power of approx. 670 TeraFlop/s.

CLAIX-2016 started test operation in November 2016 and since December 2016 the system has been available without restriction for use by computing time projects.

CLAIX-2018
CLAIX-2018 consists of over 1000 computing nodes with 2x Intel Xeon Skylake processors, each with 24 cores and 192 GB RAM. In addition, there are 48 computing nodes of identical architecture, each equipped with two NVIDIA Volta V100 GPUs (incl. NVLink) as accelerators and available for special applications such as machine learning. A high-performance Lustre-based storage system offers a file system capacity of 10 petabytes and a bandwidth of 150 gigabytes/s (read and write). For interactive work with the system, CLAIX has eight additional dialog systems that are equipped with the same CPUs but have 384 GB more RAM. All nodes are connected to an Intel Omni-Path 100 Gigabit/s network.

The Tier-3 part consists of over 220 compute nodes with identical configuration (6 of those with GPUs) and are fully integrated into the overall cluster.

CLAIX-2018 started test operation in November 2018 and since January 2019 the system has been available without restriction for use by computing time projects.

Application for Compute Time
The allocation of compute time follows the recommendations of the Gauss Alliance for the establishment of nationally coordinated application and approval procedures. Depending on the amount of compute time request, independent national and international experts assess each proposal. According to regulations of the Deutsche Forschungsgemeinschaft (DFG), the Vergabegremium (VGG) of NHR4CES, JARA-HPC or RWTH determines detailed scientific and technical criteria for the assessment of proposals for computing time.

Technical Summary

	CLAIX-2016	CLAIX-2018
# compute notes for projects	609 standard nodes + special nodes	1080 standard nodes + 221 Tier-3 std. nodes
Processor type	Intel Xeon E5-2650v4 (Broadwell-EP)	Intel Xeon Platinum 8160 (Skylake)
# cores per node	24	48
Main memory per node [GB]	192	128
Capacity of Lustre HPC filesystem	3 PB	10 PB
Bandwidth of Lustre HPC filesystem	45 GB/s	150 GB/s
Theoretical peak performance	0.53 Pflops	3.55 Pflops
LINPACK performance	0.51 PFlops	2.04 Pflops on 2014 nodes

Life Sciences

Life Sciences

Picture: Pexels

Life Sciences

Basic Biological and Medical Research | DFG 201

Molecular Dynamics study of mutant IDH1 for in silico drug design against neurological diseases

Project ID: rwth0596

EMILIANO IPPOLITI
Institute for Advanced Simulation,
Computational Biomedicine Institute
(IAS-5/INM-9), Forschungszentrum Juelich

PAOLO CARLONI
RWTH Aachen University &
Institute for Advanced Simulation,
Computational Biomedicine Institute
(IAS-5/INM-9), Forschungszentrum Juelich

MARCO DE VIVO
Senior Researcher Tenured
at Principal Investigator,
Molecular Modeling and Drug Discovery,
Italian Institute of Technology, Genova, Italy

BHARATH RAGHAVAN,
Institute for Advanced Simulation
Computational Biomedicine Institute
(IAS-5/INM-9), Forschungszentrum Juelich

Project Report

Recent research has linked the occurrence of mutations on the Isocitrate Dehydrogenase enzyme (IDH1) to some cancers like low grade glioma, glioblastoma and acute myeloid leukaemia (AML). This has been found to be due to the production of the molecules 2-hydroxyglutarate (2-HG) in abnormal quantities by the mutant IDH1 (mut-IDH1).

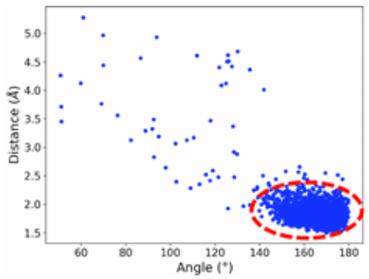

Wild-type IDH1 (wt-IDH1) catalyzes the normal reaction converting isocitrate (ICT) to α-ketoglutarate (αKG) as part of the TCA cycle in glucose metabolism. They are predominantly found in mitochondria and cytoplasm. Mutations on certain amino acids residues of this protein cause it to lose this ability, but results in a 'new gain of function' allowing it to catalyze the conversion of αKG to 2-HG. This neomorphic reaction leads to the buildup of abnormal levels of 2-HG in the body, and has been linked with tumorigenesis leading to glioma and AML. Thus, mutant IDH1 (mut-IDH1) could be a potential drug target to treat these diseases. Indeed, many pharmaceutical companies have potential drug candidates in clinical trial stage of development. Although inhibitors have been identified, there is disagreement over the exact catalytic mechanism of the neomorphic reaction. This has impeded a more scientific design of drug candidates. Thus, our aim is to elucidate the mechanism of the neomorphic reaction catalyzed by mut-IDH1 through computational methods in order to aid future drug design efforts.

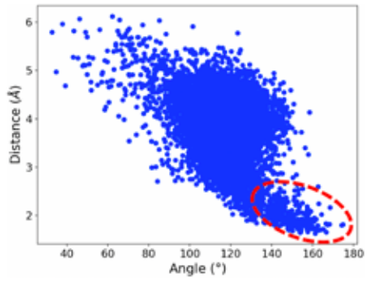

We planned to do this in two steps, 1) by applying classical Molecular Dynamics (MD) simulations to study the ligand-protein interaction in the wild-type and mutant; and 2) based on frames extracted from the MD simulations, exploit our newly developed MiMiC QM/MM interface to study the transition state and shed light on mechanism of the neomorphic reaction. This project covered the first step, i.e., using MD to study the Michaelis complex of the enzyme-ligand complex as a precursor to the transition state.

In the simulation of wt-IDH1, we observed a water-aspartate pair interacting with the α-alcoholic hydrogen of ICT as shown in Figure 1a. The plot in Figure 1b shows that at many points in the simulation, the distance and angle of interaction between the alcohol of ICT and the water molecule bound to the aspartate residue Asp 252 exists in the region consistent with hydrogen bonding. This is important because the initiating step of the catalysis is the abstraction of proton from the alcohol of ICT by a base. The hydrogen bond observed between water and the α-alcohol in our simulations suggests that the water-Asp 252 pair could potentially act as the base.

In the case of mut-IDH1, we observed the tyrosine residue Tyr 139 closely interacting with the α-ketone group of αKG as shown in Figure 2a. Similar to Figure 1b, the plot in Figure 2b shows that at many points the simulation exists in the region where the distance and angle of interaction between Tyr 139 and the ketone group of aKG are consistent with hydrogen

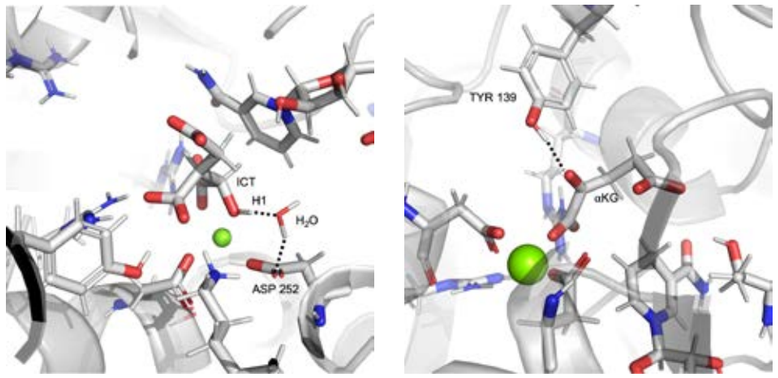

bonding. In a mirror image of the wt-IDH1 catalysis, the initiating step of the mut-IDH1 catalysis is the protonation of the carbon and oxygen atoms involved in the α-ketone bond of αKG. An acid is required to donate a proton to the oxygen atom. From the interaction observed in the MD simulations, Tyr 139 could potentially act as the acid to protonate the ketonic oxygen and drive the reaction forward.

These interesting results on the Michaelis complex and potential acid/base candidates in the IDH1 catalysis will be investigated further in our upcoming QM/MM studies.

Selected national and international cooperations

- MICHELE PARRINELLO, Laboratory of Atomistic Simulations, Italian Institute of Technology, Genova, Italy
- LAURA CANCEDDA, Local Micro-environment and Brain Development Team, Neuroscience and Brain Technology Department, Italian Institute of Technology, Genova, Italy
- BERND NEUMAIER, Institute for Neuroscience and Medicine-5 (INM-5), Forschungszentrum Juelich

Life Sciences

Basic Biological and Medical Research | DFG 201

Molecular dynamics of the SLC26 family of ion channels and transporters

Project ID: jara0177

PIERSILVIO LONGO
Institute of Biological Information Processing (IBI-1), Forschungszentrum Jülich, Germany

JAN-PHILIPP MACHTENS
Institute of Biological Information Processing (IBI-1), Forschungszentrum Jülich, Germany, and Institute of Clinical Pharmacology, Uniklinik RWTH Aachen, Germany

Project Report

Membrane proteins of the Solute Carrier family 26 (SLC26) include functionally versatile anion transporters and channels found in all kingdoms of life. The human genome encodes ten functional homologs, several of which are causally associated with severe human diseases, such as diarrhea, ulcerative colitis, asthma, skeletal malformation, brain edema, or deafness. Although disease conditions and organ-specific expression profiles of SLC26 members substantiate the high physiological and pathophysiological importance of these proteins, fundamental principles of function, regulation, and role in cell and organ physiology have thus far remained unaddressed or poorly understood.

Progress has been slowed by missing structural information at the molecular level and lack of suitable model systems at the physiological level. The determination of the structural architecture of SLC26 proteins by X-ray crystallography [1] represents a major breakthrough that now enables scrutinizing this protein family at unprecedented spatiotemporal resolution using state-of-the-art biomolecular dynamics simulations [2].

SLC26 proteins include secondary active anion exchangers, isoforms that mediate channel-like anion transport, and the voltage-driven motor protein prestin (SLC26A5). Substrates of SLC26 transporters include chloride, bicarbonate, iodide, sulfate, and oxalate. So far, the molecular underpinnings of the functional diversity of transport mechanisms, as well as the basis of substrate selectivity are unknown [3]. We will investigate the molecular mechanisms of substrate binding as well as thermodynamically coupled and uncoupled anion transport by SLC26 proteins using high-performance computational biology methods, including molecular modeling, docking, and extensive all-atom molecular dynamics (MD) simulations.

An X-ray crystal structure of the SLC26 homolog from the bacterium Deinococcus geothermalis, a α-fumarate symporter termed SLC26Dg, revealed the detailed molecular architecture of the SLC26 family [1]. The SLC26Dg structure consists of 14 transmembrane α-helices (TM) arranged in two structurally similar intertwined halves with opposite orientation, referred to as a 7-TM inverted repeat fold (7TMIR), and shows an inward-facing substrate-free monomeric conformation. The structure can be decomposed into two subdomains: a compact core domain shielded on one side by a gate domain. The core domain is assumed to mediate substrate binding, while the gate domain is assumed to mediate protomer interaction to form SLC26 dimers [1].

The comparison of the SLC26Dg structure with structurally related transporter families suggests an elevator transport mechanism, which involves a translationalrotational rigid-body movement of a mobile domain relative to a static dimerization domain [4, 5]. Recently, a cryo-EM structure of murine SLC26A9 has been published, which confirms these structural insights and demonstrates a conserved protein fold in the SLC26 family [6].

In the current funding period, we used extensive all-atom MD simulations, in combination with enhanced sampling techniques and Markov state modeling, to investigate the transport mechanism of human SLC26A9.

References

[1] Eric R Geertsma, Yung-Ning Chang, Farooque R Shaik, Yvonne Neldner, Els Pardon, Jan Steyaert, and Raimund Dutzler, Structure of a prokaryotic fumarate transporter reveals the architecture of the SLC26 family, Nature Structural & Molecular Biology, 22, no. 10, 803–808, 2015.

[2] Carsten Kutzner, David A. K¨opfer, Jan-Philipp Machtens, Bert L. de Groot, Chen Song, and Ulrich Zachariae, Insights into the function of ion channels by computational electrophysiology simulations, Biochimica et Biophysica Acta (BBA) - Biomembranes, 1858, no. 7, 1741–1752, 2016.

[3] Ehud Ohana, Dongki Yang, Nikolay Shcheynikov, and Shmuel Muallem, Diverse transport modes by the solute carrier 26 family of anion transporters, The Journal of Physiology, 587, no. 10, 2179–2185, 2009.

[4] Yung-Ning Chang and Eric R. Geertsma, The novel class of seven transmembrane segment inverted repeat carriers, Biological Chemistry, 398, no. 2, 2017.

[5] Xinzhe Yu, Guanghui Yang, Chuangye Yan, Javier L Baylon, Jing Jiang, He Fan, Guifeng Lu, Kazuya Hasegawa, Hideo Okumura, Tingliang Wang, Emad Tajkhorshid, Shuo Li, and Nieng Yan, Dimeric structure of the uracil:proton symporter UraA provides mechanistic insights into the SLC4/23/26 transporters, Cell Research, 27, no. 8, 1020–1033, 2017.

[6] Justin DWalter, Marta Sawicka, and Raimund Dutzler, Cryo-EM structures and functional characterization of murine Slc26a9 reveal mechanism of uncoupled chloride transport, eLife, 8, 2019.

Selected national and international cooperations

This project is part of the DFG Research Unit FOR 5046 Integrated analysis of epithelial SLC26 anion transporters - from molecular structure to pathophysiology.

Collaborations

- PROF. DOMINIK OLIVER, Institute of Physiology and Pathophysiology, Philipps-Universität Marburg, Germany

Publications

- KOSTRITSKII AY, ALLEVA C, CÖNEN S, MACHTENS JP.
  g elpot: A Tool for Quantifying Biomolecular Electrostatics from Molecular Dynamics Trajectories, Journal of Chemical Theory and Computation, 17, no. 5, 3157–3167, 2021
- KOSTRITSKII AY, MACHTENS JP.
  Molecular mechanisms of ion conduction and ion selectivity in TMEM16 lipid scramblases, Nature Communications, 12, no. 1, 2021

Life Sciences

Basic Biological and Medical Research | DFG 201

The Mechanics of Brain Folding

Project ID: rwth0399

LUCAS DA COSTA CAMPOS,
Institute of Neuroscience and Medicine (INM-1), Forschungszentrum Jülich, Germany
and Institute for Anatomy I
Heinrich-Heine-University Düsseldorf
Germany

JENS ELGETI,
Institute of Biological Information Processing (IBI-5), Forschungszentrum Jülich, Germany

SVENJA CASPERS,
Institute of Neuroscience and Medicine (INM-1), Forschungszentrum Jülich
Germany
Institute for Anatomy I
Heinrich-Heine-University Düsseldorf
Germany
and JARA-BRAIN, Jülich-Aachen Research Alliance, Germany

Project Report

The overarching objective of this project is to better understand the mechanism by which mammalian brains obtain their folded landscape. This folding is highly stereotyped within each species, with misfolding in humans being associated with epilepsy, seizures, cerebral palsy, among many other issues. We perform finite element simulations, where the brain is modelled as a perfect nonlinear elastic divided into two regions: an outer growing region, modelling the brain cortex, and an inner non-growing region, modelling the brain white matter.

The current step of the project closely builds upon our previous reports, where we studied the influences of cortical thickness on folding of the mammalian brain. Those simulations were performed using the quasistatic approximation, an approach often used in the literature (1). While prevalent, the validity of such an approach has not been thoroughly studied in the literature. Thus, in this stage of the work we focused on both new results and methodological validation. Our objectives were four folded:

1. Check that the simulations performed previously in the quasistatic regime were consistent by comparing them with dynamical simulations growing very slowly;
2. Study the interplay between fast growth and high cortical thickness in brain folding;
3. Study the effect of growth inhomogeneities in the folding landscape;
4. Study the interplay between the cortical thickness inhomogeneities (see previous report) and growth inhomogeneities.

To accomplish these objectives, the simulation software used previously was re-designed into a simulation library of growing materials, JuFold.

For the first objective, we simulated systems with constant cortical thickness growing at various rates. We observed that the folding wavenumber is consistent between dynamical systems growing very slowly and the simulations in the quasistatic regime. However, as growth speed is increased, the obtained wavenumbers diverged, with these systems folding into a higher wavenumber right after buckling, followed by a period of relaxation. We also observed that these systems had a wider range in their frequency spectrum.

In the second objective, we expanded the phase space by also varying the cortical thickness of each system. We found that thick cortices lead to further overestimation in wavenumber, compounding with the effects of fast growth.

We revisited the results from the previous project, where cortical thickness was investigated as one of the drivers of folding. We resimulated a specific thickness profile using different growth rates and compared them to the results obtained from using the quasistatic approximation. While rough folding profile was similar between the two methods -- folding concentrates at the thinnest point of the cortex, and decreases from there --, a few key differences were observed. Due to the effects found in the previous objectives, the folding of the thicker regions depends strongly on the growth rate, yielding a larger number of sulci and gyri pairs the faster the cortex grows. We employed energy minimization algorithms to show these new configurations were remakably stable.

Differences in local growth rate have also been associated with complex folding landscapes. We investigate their effects by augmenting our system with an inhomogeneous growth profile in an otherwise homogeneous cortex. We observed the emergence of localised folding, similar to the previous project. However, this folding was less complex than that with inhomogeneous thickness, with folding concentrated in the regions of fast growth, while being mostly inhibited in other regions.

Finally, the two types of inhomogeneities were combined into a single system, in a complementary fashion. Namely, a higher growth rate, which is predicted to result in a large wavenumber, was applied to the thicker regions, where a low wavenumber is instead expected; vice-versa for the thinner regions. We found that the effects of the two inhomogeneity kinds were mutually exclusive, not additive. We observed that the systems either folded in the regions of thin cortices, or around the region of fast growth, but not in between, and most importantly, not in both regions at the same time.

The results of this step in our project and the detailed descrition of JuFold were publised as part of the PhD Thesis “The Physics of Brain Folding”. Articles with similar content are under preparation to be published in peer-reviewed journals.

References

(1) BUDDAY, STEINMANN, and KUHL, ‘Secondary Instabilities Modulate Cortical Complexity in the Mammalian Brain’; Xu et al., ‘Axons Pull on the Brain, But Tension Does Not Drive Cortical Folding’; Bayly et al., ‘A Cortical Folding Model Incorporating Stress-Dependent Growth Explains Gyral Wavelengths and Stress Patterns in the Developing Brain’; Holland et al., ‘Symmetry Breaking in Wrinkling Patterns’; Costa Campos et al., ‘The Role of Thickness Inhomogeneities in Hierarchical Cortical Folding’.

Publications

- The Physics of Brain Folding. da Costa Campos, Lucas. PhD thesis (Köln, 2021)
- The role of thickness inhomogeneities in hierarchical cortical folding. Da Costa Campos et al., Neuroimage. https://doi.org/10.1016/j.neuroimage.2021.117779
- JuFold: A framework for simulation of brain folding. da Costa Campos et al. (In preparation)
- The interplay between cortical inhomogeneities: A simulation study. da Costa Campos et al (In preparation)

Life Sciences

Basic Biological and Medical Research | DFG 201

Understanding the Effect of Guanidinylation of Human YB-1 Protein on Its Interactions with the NOTCH-3 Receptor

Project ID: rwth0565

BATUHAN KAV
BASTIAN AGGELER
BIRGIT STRODEL
Institute of Biological Information Processing, Structural Biochemistry (IBI-7), Forschungszentrum Jülich, Germany

Project Report

Systemic lupus erythematosus (SLE) is an autoimmune disease which causes widespread inflammation and organ damage in the affected tissues. Recently, it has been discovered that the human box protein YB-1, which binds to the transmembrane receptor Notch-3, is increased in patients with active SLE. It has been further found that the YB-1 protein bears two mutations resulting from the guanidylation of Lys54 and Lys58 in the evolutionarily conserved cold-shock-domain (CSD). These mutations have been demonstrated to activate the Notch-3 signaling and delay the development of lupus nephritis, which is a common and life-threatening manifestation of SLE. Furthermore, although to a lesser extent, two additional guanidylations at the positions Lys64 and Lys81 have been identified in patients to have possible effects on the Notch-3 activation. Consequently, the Notch-3 activation through doubly mutated YB-1 may be a promising approach in the treatment of SLE patients. However, the molecular mechanisms behind Notch-3 activation by YB-1 and the effect of the mutations is not clear. In this project, we employ molecular dynamics (MD) simulations and protein-protein docking to elucidate the molecular mechanisms that could be responsible for the increased Notch-3 activation by YB-1.

The human box protein YB-1 consists of 324 amino acids. The N-terminal domain (residues 1-50) is rich in alanine and proline, residues 51-129 correspond to the evolutionary conserved cold-shock domain consisting of 5 antiparallel β-strands packed into a β-barrel, and the disordered C-terminal domain (residues 130-324). The Notch-3 receptor is a single-pass transmembrane protein. The extracellular domain consists of 34 epidermal growth factor-like repeat (EGFr) domains, which are ~40 amino acid long modular protein subunits, and is involved in the binding of ligands. The EGFr domains 18-19 are flexible, while domains 21-23 (calcium binding sites) are more rigid and elongated in structure. The negative regulatory region (NRR) follows the EGFr domains and keeps the receptor in an auto-inhibited state. Based on various signaling assays and protein-protein docking, it has been recently found that the YB-1 binds to the EGF repeats 20-23. Furthermore, it has been proposed that the binding of YB-1 to EGFr 20-23 alters the conformation of the negative regulatory domain of the Notch-3 receptor, which transduces the signal from the ligand binding extracellular EGF domain to the intracellular domain. However, the molecular mechanism behind this signal transduction is not clear.

We aimed at answering following questions: 1) How do the double guanidylations at the positions Lys54/Lys58 (YB-1$G_{54/58}$) and Lys64/Lys81 (YB-1$G_{64/81}$) affect the structure of the YB-1 protein? 2) How do these mutations affect the binding of YB-1 to EGFr? 3) How stable are the different YB-1/EGFr complexes?

In the first phase of this project we obtained ≈15 μs long trajectories for the YB-1 and YB-1$G_{54/58}$. Our analysis showed that both proteins have stable secondary structures around the CSD domain and the mutations do not alter the local secondary structure. The only exception we observed was between the residues 105-115, which resulted in a reduced β-sheet propensity for the YB-1$G_{54/58}$. By calculating the solvent accessible surface area, we found that the Lys58 mutation is more exposed to the solvent compared to the wild-type residue. We further found that the double guanidinylation makes the CSD domain more exposed to the solvent, which could facilitate its interactions with the EGFr. On the other hand, we did not observe any significant changes for the YB-1$G_{64/81}$ mutant due to the Lys64/Lys81 mutations.

We then investigated the effect of the guanidinylation on the interactions between the YB-1 variants and EGFr proteins using protein-protein docking. Protein-protein docking is a set of algorithms that tries to find possible interactions between two structures, similar to solving a jigsaw puzzle. Yet, it is important to note that different docking software can result in somewhat different predictions and the docking results should generally be further investigated via MD simulations. We used two three different docking software to obtain a set of common interaction pairs between the YB-1($G_{54/58}$) and EGFr. We further visually analyzed the docked structures to find common interaction sites, where we focused on the complexes that featured direct interactions between the EGFr and the mutation sites. Our analysis yielded five distinct complexes per YB-1 and YB-1$G_{54/58}$, resulting as a consensus prediction by the three docking programs. Among these complexes, we observed that the YB-1$G_{54/58}$/EGFr complexes had generally better docking scores compared to YB-1, which suggests that the YB-1$G_{54/58}$/EGFr complexes are more stable. With these docked structures, we ran 100 ns of MD simulations to assess their stability. On that timescale, all complexes of both YB-1 and YB-1$G_{54/58}$ are stable, providing further trust in the docking predictions.

In summary, we have investigated the structure of the YB-1, YB-1$G_{54/58}$, and YB-1$G_{64/81}$ proteins using all-atom MD simulations. Our results showed that the secondary structure of the YB-1$G_{54/58}$ has a reduced tendency to form β-sheets, whereas YB-1$G_{64/81}$ did not show any differences from the wild-type YB-1 structure. Our docking results, supported via MD simulations, did not reveal significant differences between the YB-1/EGFr and YB-1$G_{54/58}$/EGFr complexes; however, the complexes involving YB-1$G_{54/58}$ seem to involve stronger binding based on the binding free energy. Our current conclusion is that the double guanidinylation on the YB-1 protein does not significantly alter its interactions with the Notch-3 receptor. On the other hand, most often only subtle changes in protein-protein interactions can lead to chronic diseases in the long run.

Selected national and international cooperations

- THOMAS RAUEN, Uniklinik RWTH Aachen, Germany
- UFE RAFFETSEDER, Uniklinik RWTH Aachen, Germany

Basic Biological and Medical Research | DFG 201

Improved Diagnostics of Respiratory Flows Using a Lattice-Boltzmann Method and Machine Learning Techniques

Project ID: jara0203
ANDREAS LINTERMANN
Jülich Supercomputing Centre,
Forschungszentrum Jülich, Germany

MARIO RÜTTGERS, MORITZ WALDMANN,
Institute of Aerodynamics and Chair of Fluid Mechanics, RWTH Aachen University

Project Report

1 Abstract

Numerical methods have the potential to support and improve classical clinical diagnostics. They enable to investigate a patients' condition in a detail that in vivo diagnostics cannot provide. The continuously increasing computing power of high-performance computing (HPC) systems has led to new and highly efficient numerical methods to simulate more and more complex physical phenomena. In the last few years, this trend is accelerated by the penetration of machine learning (ML) into the realm of computational fluid dynamics (CFD). Such algorithms are capable of providing rapid feedback to the scientist/user in some cases even faster and more accurate than numerical methods. They are well suited to automate processes and to automatically extract important features from large amounts of data, frequently produced by numerical simulations. The success of ML algorithms depends, however, on the quality of the training data, i.e., in the end it is essential to focus on the continuous hand-in-hand advancement of both ML and simulation methods. It is the objective of the research projects CFD and ML approaches for improved diagnostics in rhinology (AM-SIT) and Multi-physics model of the nasal airflow (MMNA) to develop new numerical methods intelligently combining CFD and ML techniques for rhinology, and to bring those to clinical application.

2 Scientific Work accomplished and results obtained

The simulations that have been performed in 2021 are based on a thermal lattice-Boltzmann (TLB) and a level-set (LS) method. They operate on hierarchical unstructured Cartesian meshes. The TLB, as well as the LS methods, are part of the simulation framework multiphysics Aerodynamisches Institut Aachen (m-AIA), jointly developed by the Institute of Aerodynamics and Chair of Fluid Mechanics (AIA), RWTH Aachen University, and the SDL Highly Scalable Fluids & Solids Engineering (SDL FSE), Jülich Supercomputing Centre (JSC)

2.1 AM-SIT

CFD simulations have the disadvantage that they usually start from an equilibrium state and need time to reach a fully developed and/or converged state. Therefore, it was studied how flow field approximations generated by Convolutional Neural Networks (CNN) help to overcome this initialization period. The training data (flow simulations for 40 nasal cavities) used for the study was generated on CLAIX using m-AIA. The training itself was done on the GPU partition of JURECA-DC. The large domain size of the highly resolved simulations necessitates to distribute a CNN to multiple GPUs and use patches of the domain as training data. In more detail, an encoder-decoder type fully connected CNN is split to have the encoder branch executed on a single GPU, and the three decoder branches to be distributed across three further GPUs. The decoder branches predict particle probability distributions functions (PPDFs), which are necessary to compute the macroscopic flow variables. The encoder branch takes the Cartesian coordinates of a cell, the distance of a cell to the next boundary, or PPDFs at their boundaries as input. At the moment, the training of the CNN is still ongoing.

2.2 MMNA

2.2.1 Virtual surgery using the TLB-LS approach

To test the virtual surgery environment based on the TLB and LS method, a simplified test case is used. A three-dimensional stenotic pipe is chosen to model a nasal cavity with a constriction. During the virtual surgery the stenosis of the pipe was fully removed. That is, the stenotic pipe is simulated for 300,000 iterations to obtain a converged steady state. Based on this solution, the modification of the geometry, which took another 200,000 iterations, is initiated. The simulation outcome before and during the modification is in good agreement with steady state simulations using m-AIA and literature findings.

The virtual surgery in the nasal cavity uses the same simulation methods and wall boundary condition as the stenotic pipe case. At the pharynx a volumetric flow rate of $\dot{V}$ =250ml/s was prescribed. The grid resolution (0.1 mm) is finer than the spatial resolution of the CT data (0.34 mm,0.34 mm,0.75 mm) and resolves all relevant flow features. Again, a steady state simulation for the pre-surgical geometry was performed before the geometry modification was made. During the modification phase, a bone spur was removed, and the deviated septum was straightened. The results show a decreased respiratory resistance after the surgery [2].

2.2.2 Comparison of simulative and RL-based results

The virtual surgery approach proposed in Sec. 2.2.1 was further developed using a reinforcement learning (RL) algorithm to optimize the geometry of a channel with a constriction based on the pressure loss and the heating of the fluid. Since these two parameters have competitive goals, it was expected, that an optimal constriction can be found where the pressure drop is minimized while the heating of the fluid is maximized. The simulations are conducted on 2 nodes of CLAIX. To analyze the behavior of the RL algorithm, a number of 3,400 simulations using m-AIA were conducted, in which the size of the constriction of the channel was continuously increased. From the simulation outcome, a correlation between pressure loss/heating and the size of the constriction was derived. This correlation was defined as the reference solution and compared to the simulation outcome of the RL. The performance of the agent is evaluated in terms of the averaged size of the predicted optimal constriction at each batch. At 69 batches (1,450 simulations using the RL), the agent misses the reference solution by only 0.1%. From here on the error remains below 0.1% for the rest of the training [3]. This study is currently extended to 3D flows

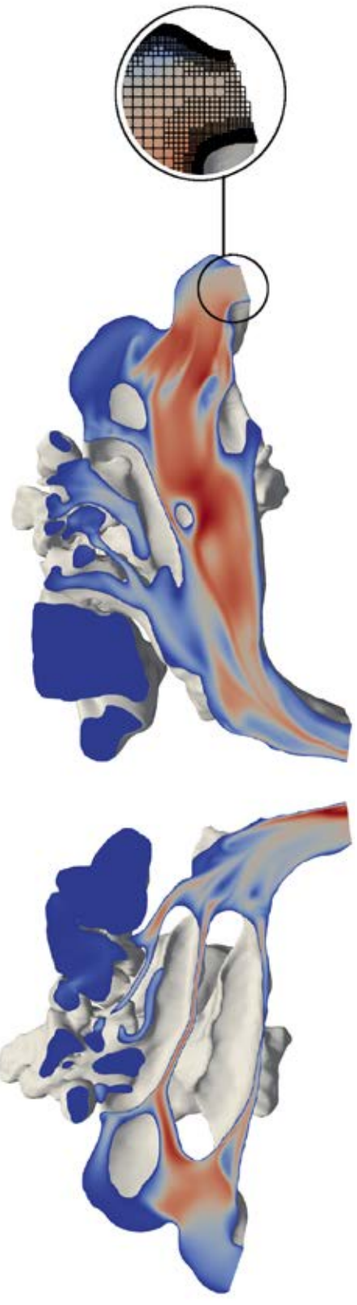

Selected conference participations

- MARIO RÜTTGERS, Machine-Learning-Based Control of Perturbed and Heated Channel Flows, ISC High Performance 2021, Frankfurt (online), Germany, June 24 – July 2, 2021
- MORITZ WALDMANN, Implementation of a Lattice Boltzmann method for the analysis of langding-gear noise on GPU based HPC Systems, 2nd high-fidelity industrial les/dns symposium (HiFiLed), Toulouse (online), France, September 22-24, 2021

Publications and References

[1] RÜTTGERS M, WALDMANN M, SCHRÖDER W, LINTERMANN A. A machine-learning-based method for automatizing lattice-Boltzmann simulations of respiratory flows, Applied intelligence (2022), doi:10.1007/s10489-021-02808-2

[2] WALDMANN M, RÜTTGERS M, LINTERMANN A, SCHRÖDER W. Virtual Surgeries of Nasal Cavities Using a Coupled Lattice-Boltzmann–Level-Set Approach, ASME Journal of Medical Diagnostics 5(3) (2022), doi:10.1115/1.4054042

[3] RÜTTGERS M, WALDMANN M, SCHRÖDER W, LINTERMANN A. Machine-Learning-Based Control of Perturbed and Heated Channel Flows, High Performance Computing / Jagode, Heike (Editor) ISC High Performance 2021 (2021), doi:10.1007/978-3-030-90539-2_1

[4] ALJAWAD H, RÜTTGERS M, LINTERMANN A, SCHRÖDER, W, LEE KC. Effects of the Nasal Cavity Complexity on the Pharyngeal Airway Fluid Mechanics: A Computational Study, Journal of digital imaging 34 (2021), doi:10.1007/s10278-021-00501-x

Life Sciences

Basic Biological and Medical Research | DFG 201

Impact of pH and voltage in Mice HCN channel's gating: mechanistic insights from metadynamics simulations

Project ID: rwth0605

PAOLO CARLONI
Department of Physics,
RWTH Aachen University
Institute for Neuroscience and Medicine
Computational Biomedicine (INM-9) and
Institute for Advanced Simulation (IAS-5),
Forschungszentrum Jülich, Germany

MARC SPEHR
Department of Biology,
RWTH Aachen University

EMILIANO IPPOLITI,
Institute for Neuroscience and Medicine
Computational Biomedicine (INM-9),
Forschungszentrum Jülich, Germany

ALEJANDRO GIORGETTI
Department of Biotechnology,
University of Verona, Italy
Institute for Neuroscience and Medicine
Computational Biomedicine (INM-9) and
Institute for Advanced Simulation (IAS-5),
Forschungszentrum Jülich, Germany

SOMAYEH ASGHARPOUR
Department of Physics,
RWTH Aachen University
Institute for Neuroscience and Medicine
Computational Biomedicine (INM-9) and
Institute for Advanced Simulation (IAS-5),
Forschungszentrum Jülich, Germany

Project Report

Hyperpolarization-activated Cyclic Nucleotide-gated (HCN) channels are key mediators of synaptic weight regulation, dendritic integration, filtering, gain control as well as neuronal and network oscillations. They conduct the I_h current. HCN's highly diverse functions render I_h an important target for multisensory computation. Recently, one of us (Marc Spehr) identified a novel mechanism of mouse HCN channel regulation (Cichy et al, 2015). He found that extracellular acidification acts as a potential ion current activation, suggesting I_h -dependent sensory gain control in social chemosignaling.

In this project we have used advanced enhanced sampling simulations (specifically metadynamics, see below for details) to predict, for the first time, the free energy landscape associated with gating of HCN channels and production of I_h current. This is the first step towards the characterization of the effect of pH on mouse HCN channel gating. Our calculations were based on experimental structural information and used the CHARMM36 force field. We also performed MD simulations (details below) to investigate the effect of pH on the structural determinants of the protein.

The perspective here is to introduce the effect of pH in the simulations, to predict the impact of the latter on the free energy landscape associated with channel gating. This will quantify in an unprecedented manner the effect of pH on HCN function and provide a molecular basis for the effect of acidification on this important class of ion channels.

MD simulations

We setup two Mice HCN2 systems (UniProtKB – O88703 (HCN2-MOUSE)) (uniprot.org/uniprot/O88703), one at pH=2 and the other at pH=7 (size: ~ 284,378 atoms, including TIP3 water, POPC bilayer, Na^+ and Cl^- ions). We performed 400ns-long plain MD simulations for both systems. Then, we added a hyperpolarized membrane potential of -50 mv/nm to check the system's response to the electric field and we extended each simulation for additional 150 ns. Fig. 1 shows our MD initial model.

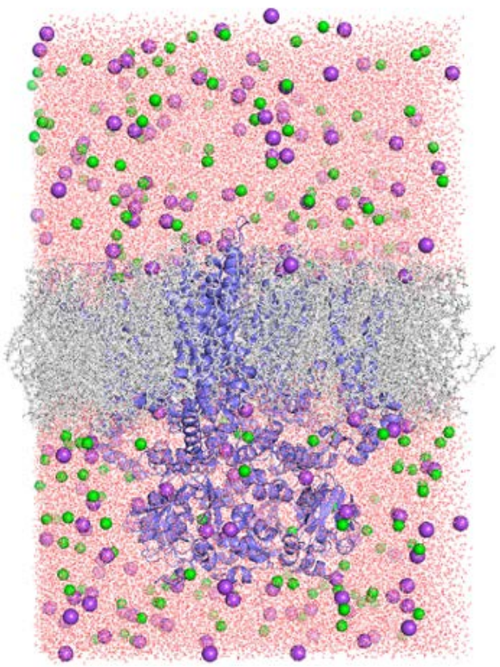

Fig. 1 – Initial setup of the MD simulation box

The two systems at pH=2 and pH=7 were compared in terms of their electrostatic surface, residue-residue interactions and hydrogen bond networks.

Metadynamics simulations

Metadynamics predicts the free energy landscape as a function of a small set of collective variables (CVs) able to describe all the relevant slow modes of the activation process, as a function of the atomic coordinates. Here we used a CV based on the coordination numbers associated with the translational motion of two arginine residues found to play an important role for the gating (Kasimova et al, 2019). We also used a pathway CV approach. This approach can be employed only if the initial and final states of the system are known. The procedure is to define a path that connects the initial and final states to each other by a number of reference frames in between. The approach allows obtaining a free energy landscape with respect to the progression along this path (first CV) and the distance from the path (second CV). By defining a path of 10 reference structures, we were able to identify a meaningful free energy landscape associated with the channel opening process as shown in Fig. 2.

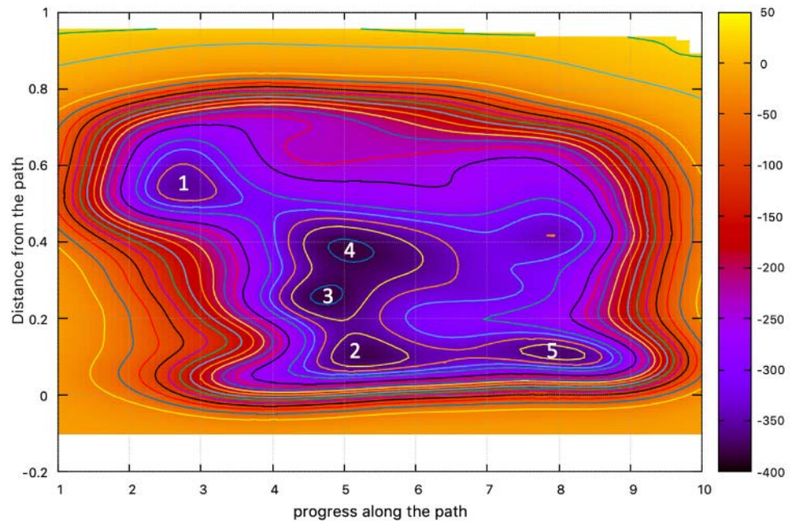

Fig. 2 – Free energy landscape as a function of the progress along the path and the distance from the path. The number identified the different free energy minima associated to the different (meta)stable configurations involved in the channel opening process.

References

- KASIMOVA MA ET AL. "Helix Breaking Transition in the S4 of HCN Channel is Critical for Hyperpolarization-Dependent Gating". In: elife 8 (2019).
- CICHY A ET AL. "Extracellular pH Regulates Excitability of Vomeronasal Sensory Neurons". In: Journal of Neuroscience 35(9) (2015), pp. 4025–4039.

Life Sciences

Basic Biological and Medical Research | DFG 201

Molecular dynamics simulations of P2X receptors

Project ID: jara0180

JAN-PHILIPP MACHTENS
SASKIA CÖNEN
Institute of Biological Information Processing (IBI-1), Forschungszentrum Jülich, Germany, and Institute of Clinical Pharmacology, Uniklinik RWTH Aachen, Germany

RALF HAUSMANN
LINHAN CHENG
Institute of Clinical Pharmacology, Uniklinik RWTH Aachen, Germany

Project Report

The family of P2X receptors are membrane proteins that are involved in important physiological processes in various species including humans. They belong to the class of ligand-gated ion channels and are activated by extracellular adenosine triphosphate (ATP) [1]. The subtypes named $P2X_1$ to $P2X_7$ assemble in homo- or heterotrimeric complexes and are permeable to mono- or divalent cations.

Mansoor et al. recently determined high-resolution X-ray crystal structures of the human $P2X_3$ receptor in three assumed conformational states: open, desensitized, and apo-resting [2]. These structures illuminated major conformational changes between ATP-free and -bound states and revealed a particular unexpected feature, the cytoplasmic cap, a complex structure dynamically formed by the N- and C-terminal intracellular domains in the open state [2]. However, the molecular mechanisms that link ATP (un)binding to opening/closing of the ion channel, the mechanisms of ion permeation and selectivity, and of receptor desensitization are still unclear. While application of extracellular ATP activates P2X receptors and opens the ion pore, prolonged presence of ATP leads to pore re-closure, a process called desensitization.

We demonstrated that the cytoplasmic cap markedly stabilizes the transmembrane domains in the open state, thereby preventing pore closure. We proposed that $P2X_3$ receptor desensitization is a three-step process, characterized by an initial fast detachment and unfolding of the C-terminal domains and a subsequent slow disassembly of the N-terminus. This process is accompanied by conformational changes of the transmembrane domains, which lead to pore closure.

All-atom molecular dynamics simulations based on the $hP2X_3$ structures were used to investigate conformational changes and pore closure during receptor desensitization and to identify molecular determinants of these processes. All simulations are designed to be directly compared with electrophysiological experiments in our laboratories, thus enabling insights into $P2X_3$ function at atomic resolution with direct experimental validation.

References

[1] Burnstock G, Kennedy C. “P2X receptors in health and disease”, in: Advances in Pharmacology, pp.333–372. Elsevier, 2011.

[2] Mansoor SE, Lü W, Oosterheert W, Shekhar M, Tajkhorshid E, Gouaux E. X-ray structures define human P2X3 receptor gating cycle and antagonist action, Nature, 538, no. 7623, 66–71, 2016.

Selected national and international cooperations

- FRITZ MARKWARDT, Julius-Bernstein-Institut für Physiologie, Martin-Luther-Universität Halle-Wittenberg, Halle, Germany
- RALF SCHMID, University of Leicester, Leicester, UK

Publications

- KOSTRITSKII AY, ALLEVA C, CÖNEN S, MACHTENS JP. g_elpot: A Tool for Quantifying Biomolecular Electrostatics from Molecular Dynamics Trajectories. Journal of Chemical Theory and Computation, 17(5), 3157-3167.

Natural Sciences

Picture: Pexels

Natural Sciences

Molecular Chemistry | DFG 301

In silico design and development of green catalysts for polymerization reactions - ab initio molecular dynamics (AIMD) simulations in condensed phase

Project ID: rwth0635

VERONICA GRÜNTZIG,
CAT Catalytic center ITMC,
RWTH Aachen University

MARTIN MACHAT,
Covestro Deutschland AG

MOJGAN HESHMAT,
CAT Catalytic center ITMC,
RWTH Aachen University

Project Report

The research activities at the CAT Catalytic Center, Institute of Technical and Macromolecular Chemistry (ITMC), focus on the development of novel catalysts for polymer synthesis via sustainable routes as well as for chemical depolymerization of plastics. [1-2] The CAT Catalytic Center is a joint project between Covestro Company and RWTH to generate and develop sustainable catalysts and chemical processes. To this end, extensive understanding of the state-of-the-art catalytic systems and molecular processes involving in polymerization reactions is of great importance. Modeling of homogeneous and heterogeneous catalysis of polymerization reactions with complex interactions and the reaction path sampling in explicit solvent using molecular dynamics simulations leading to development of new sustainable catalysts is our main research objective in this project. Utilizing HPC facilities of the RWTH, we have elucidated and identified the key-steps and critical structural parameters of the proper catalysts for the three projects that are defined below. To this end, we have performed molecular dynamics simulations as well as the static DFT calculations to investigate basis set convergence for a series of DFT functionals (both hybrid and nonhybrid). B3LYP-D3 and PBE-D3 functional in combination with 6-311g** and DZVP basis sets for static and molecular dynamics calculations, respectively, have given the most satisfactory results compared to the experimental and former computational studies. [3-4]

Project description

Ring opening polymerization (ROP) of propylene oxide (PO) to polyols: The main goal of this project is to design new sustainable and environmentally friendly catalysts for the reaction of ROP of propylene oxide (Figure 1) that could replace the cobalt from the DMC (Di Metal Cyanide) catalyst, which is the state-of-the-art catalyst for this reaction. [5-6] To this end, details of the reaction including substrate-catalyst interactions, mechanism and energetics of the initiation and propagation steps of polymerization reaction, and possible reaction pathways, the activation phase of the DMC(Co-Zn) catalyst, and the role of surrounding complexing agent as well as nucleophile were investigated.

Figure 1. Polymerization of propylene oxide.

DreamResourceConti project - Resource-efficient production of CO_2-containing surface-active materials - ROP of carbonates to linear Polyethercarbonates polyols:

The „DreamResourceConti“ project is intended to increase the degree of technological maturity by optimizing the technology and increasing the production scale. The project partners want to develop a continuous production process and extend the use of CO_2 to additional areas of application. The use of CO_2 as an additional component for surface-active materials in this regard broadens the raw material base for many applications. In addition, the greenhouse gas CO_2 is recycled via chemical incorporation into the material, which is an important step on the way to a functioning, climate-friendly circular economy. In this context, CAT Catalytic Center is contributing with detailed computational analysis of the applied catalytic technology in order to understand and further fine-tune the respective catalytic process.

For „DreamResourceConti“, two academic partners and one company join forces. In addition to application-oriented technical development, this cooperation also brings advantages for the analysis of results. The cooperation promotes understanding through the intensive characterization and analysis of the novel substances. In addition, environmental and technological-economic assessments make it easier to assess the potential of this innovative technology. The major goal of the project is production of linear Polyethrercarbonates polyols throughout catalyzed ROP (Figure 2) of carbonates. To this end, detailed mechanisms of the ROP and CO_2-release reactions have been investigated computationally and the key-steps, structural factors and catalyst characteristics are identified and evaluated in comparison to the experimentally studied catalysts.

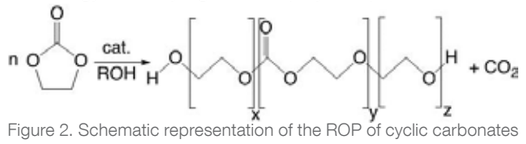

Figure 2. Schematic representation of the ROP of cyclic carbonates to generate PEC polyol.

Turning CO/CO_2-containing industrial process gas into valuable building blocks for the polyurethane industry - C4PUR project: Transforming the chemical industry from finite fossil to renewable carbon resources displays one of the major challenges of the 21st century. At the same time the steel industry needs to reduce the CO_2 emissions of the blast furnaces to decrease its environmental impact. Turning this lose–lose into a win–win situation is the basic concept of the EU-funded Carbon4PUR project. The project tackles a first concept of how the carbon content of blast furnace gas (BFG), a CO/CO_2-containing process gas from steel production, could be utilized in a sequence of selective chemical conversion steps to produce high value intermediates for the polymer industry. In this context, CAT Catalytic Center is contributing with the development of novel catalysts at the chemical heart of the developed chemical technology. The aim of this project is double carbonylation of PO to synthesize succinic anhydride (Figure 3) in the presence of an appropriate homogeneous catalyst. With the aim of the computational studies we in detail evaluated the interactions between various components in the reaction environment including substrates, catalyst and solvent.

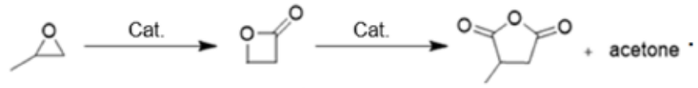

Figure 3. Double carbonylation of the PO, the reaction is viable in the presence of catalyst.

References

[1] LEITNER W, ET AL., Chem. Ing. Tech., 2018, 90, 1504-1512.
[2] GHATTAS G, ET AL., Chem. Commun., 2018, 90, 1504-1512.
[3] HESHMAT M, J. Phys. Chem. C, 2020, 124, 10951-10960.
[4] HESHMAT M, ET AL., J. Phys. Chem. A, 2020, 124, 6399-6410.
[5] ALMORA-BARRIOS N, ET AL., Chem. Ing. Tech, 2015, 7, 928 –-935.
[6] LAWNICZAK-JABLONSKA K, J. Phys. Conference Series, 2016, 712, 012062.

Selected conference participations

- MOJGAN HESHMAT, MARTIN MACHAT, In silico design of novel catalysts for ROP of carbonates, DreamResourceConti meeting Covestro AG, Aachen, Germany, February 19, 2021 (online)
- MOJGAN HESHMAT, MARTIN MACHAT, Catalyzed ROP of carbonates: insights and perspectives, Advisory Board Meeting, CAT Catalytic Center, Aachen, Germany, June 10, 2021 (online)
- MOJGAN HESHMAT, Catalyzed propoxylation of the PO: insights from molecular dynamics simulations, Covestro, Aachen, Germany, July 08, 2021 (online)
- MOJGAN HESHMAT, MARTIN MACHAT, In silico design of novel catalysts for ROP of carbonates, DreamResourceConti meeting Covestro, Aachen, Germany, October 07, 2021 (online)

Selected national and international cooperations

- OLGA LINKER AND MARTIN MACHAT, Covestro Deutschland AG

Natural Sciences

Molecular Chemistry | DFG 301

Computational studies of reactivities in organic and organometallic transformations

Project ID: jara0091
FRANZISKA SCHOENEBECK, THERESA SPERGER, ÁNGEL L. MUDARRA, CHRISTIAN D.-T. NIELSEN, ABDURRAHMAN TURKSOY, SAMIR BOUAYAD-GERVAIS, FILIP OPINCAL, AVETIK GEVONDIAN, DANIEL HUPPERICH, SEBASTIAN WELLIG, JULIAN HÜFFEL, ULADZISLAVA DABRANSKAYA,
Institute of Organic Chemistry, RWTH Aachen University

Project Report

Our research is focused on gaining a fundamental understanding of reactivity by the interplay of computational investigations and experiments. In particular, using computations to establish key features of the underlying reactivity aids in experimental design of novel catalysts and transformations.

In the current reporting period, we have explored competing radical pathways in the activation of aryl halides with Pd(0) to account for detrimental side reactions, as well as the reactivity of Pd nanoparticles as an alternative and often unaccounted for catalytically active species during cross-coupling reactions.

We have continued our long-standing interest in metal(I) species and studied the electronic structure of a variety of open-shell metal(I) monomers, including Pd(I), Ni(I) and Co(I). We have also extended our efforts to elucidate the mechanism of the Hiyama transmetalation in particular with respect to observed solvent effects and also commenced an investigation on similar processes in corresponding nickel-based systems where our calculations could account for experimentally observed ligand effects.

Furthermore, we could address the divergent reactivity of diazonium salts and diazoethers in Stille and Suzuki cross-coupling showing that transmetalation at a Pd(II)-alkoxy complex is the likely cause for the pronounced difference in reactivity.[1] We have also explored the reactivity of diazonium salts under gold/light catalysis and photoredox catalysis.[2] Notably, the calculations could provide an explanation for a competing decomposition pathway and encouraged our search for a mechanistic alternative to overcome it.

Lastly, we have also studied purely organic reactivity in the mechanism of the chemoselective ipso-halogenation of aryl germanes.[3]

References

[1] SANHUEZA IA, KLAUCK FJR, SENOL E, KEAVENEY ST, SPERGER T, Schoenebeck F, 'Base-Free Cross-Couplings of Aryl Diazonium Salts in Methanol: PdII-Alkoxy as Reactivity-Controlling Intermediate'
Angew. Chem. Int. Ed. 2021, 10.1002/anie.202014842.

[2] SHERBORNE GJ, GEVONDIAN AG, FUNES-ARDOIZ I, DAHIYA A, FRICKE C, Schoenebeck F, 'Modular and Selective Arylation of Aryl Germanes (C–GeEt3) over C–Bpin, C–SiR3 and Halogens Enabled by Light-Activated Gold Catalysis',
Angew. Chem. Int. Ed. 2020, 59, 15543-15548.

[3] FRICKE C, DECKERS K, SCHOENEBECK F., Orthogonal Stability and Reactivity of Aryl Germanes Enables Rapid and Selective (Multi)Halogenations', Angew. Chem. Int. Ed. 2020, 59, 18717-18722.

Selected honors, prizes and awards

- FRANZISKA SCHOENEBECK, ERC Consolidator Grant (2020-2025)
- FRANZISKA SCHOENEBECK, Klung-Wilhelmy-Wissenschafts-Preis 2020, awarded in 2021, Berlin, Germany

Selected conference participations

- FRANZISKA SCHOENEBECK, Streitwieser Lecture 2021, UC Berkeley, USA

Selected national and international cooperations

- TOM ROVIS, Columbia University, New York, USA
- ERIC CARREIRA, ETH Zürich, Zürich, Schweiz
- JOHN MURPHY, University of Strathclyde, Glasgow, UK

Publications

- HUEFFEL JA, SPERGER T, FUNES-ARDOIZ I, WARD JS, RISSANEN K, SCHOENEBECK F. Accelerated dinuclear palladium catalyst identification through unsupervised machine learning, Science 2021, 374, 1134-1140.
- NIELSEN CDT, ZIVKOVIC FG, SCHOENEBECK F. Synthesis of N-CF3 Alkynamides and Derivatives Enabled by Ni-Catalyzed Alkynylation of N-CF3 Carbamoyl Fluorides, J. Am. Chem. Soc. 2021, 143, 13029-13033.
- GUVEN S, KUNDU G, WESSELS A, WARD JS, RISSANEN K, SCHOENEBECK F. Selective Synthesis of Z-Silyl Enol Ethers via Ni-Catalyzed Remote Functionalization of Ketones, J. AM. CHEM. SOC. 2021, 143, 8375-8380.
- SHEN Y, FUNES-ARDOIZ I, SCHOENEBECK F, ROVIS T. Site-Selective α-C–H Functionalization of Trialkylamines via Reversible Hydrogen Atom Transfer Catalysis, J. Am. Chem. Soc. 2021, 143, 18952-18959.
- SELMANI A, SCHOENEBECK F. Transition-Metal-Free, Formal C–H Germylation of Arenes and Styrenes via Dibenzothiophenium Salts, Org. Lett. 2021, 23, 4779-4784.

Molecular Chemistry | DFG 301

Exploring the synergistic power of bimetallic metal catalysts for selective bond manipulations and value-adding transformations: a combined experimental & computational approach

Project ID: rwth0636
FRANZISKA SCHOENEBECK,
SEBASTIAN WELLIG,
Institute of Organic Chemistry,
RWTH Aachen University

Project Report

The activation of carbon dioxide CO_2 by non-precious nickel has become an efficient and sustainable procedure for the synthesis of carboxylates. A popular approach is reductive carboxylation to convert organohalides into carboxylates under addition of a reducing agent like zinc or manganese.

Ni^{I}-species have been commonly proposed at the heart of catalytic cycles for CO_2 functionalization. Yet, mechanistic studies to support this claim are scarce. We therefore conducted a broad theoretical investigation using density functional theory (DFT) to verify and rationalize the supposed superiority of Ni^{I}. Moreover, we wanted to gain insight into potential ligand effects. The commonly proposed inner and outer sphere mechanisms were initially considered as possible carboxylation pathways. The latter had been proposed to only proceed with alkyl moieties.

However, during the course of our investigation we found a second type of outer sphere mechanism for arenes forming a Meisenheimer complex in the transition state.

We first set out to compute exemplary systems reported in literature in order to validate our approach. At that point only two ligands had been reported to show stoichiometric reactivity towards CO_2 with isolated Ni^{I}-alkyl species: *t*Bu-Xantphos and phenMes2 (2,9-dimesitylphenanthroline). For both systems we computed feasible barriers, but a switch in mechanism. While $phenMes_2$ preferred the inner sphere mechanism, tBu-Xantphos preferred the outer sphere mechanism in accordance with the mechanistic proposals in the respective publications. For *t*Bu-Xantphos, in addition the Ni^{I}-alkyl complexes also alkynyl and aryl complexes have been reported as well, but neither showed reactivity towards CO_2. Our calculations were consistent with these findings, as we found prohibitively high barriers for both cases.

We proceeded with calculating a variety of Ni^{I}- and Ni^{II}-alkyl and -aryl spices and evaluated their reactivity towards CO_2. Both the ligand and oxidation state were observed to have a crucial role for the preference of the mechanism: While we found that Ni^{I} complexes exhibited a preference for the inner-sphere mechanism, the outer-sphere mechanism was preferred for Ni^{II}. In general, we observed high barriers for outer sphere mechanisms, which indicates that they can only proceed at elevated temperatures. *t*Bu-Xantphos appears to have a privileged role in promoting an outer sphere mechanism that proceeds at room temperature. The inner- sphere mechanism, on the other hand, was tentatively more sensitive towards the choice of the ligand.

We concluded that systems that proceed via inner-sphere mechanism should be preferred as they generally possessed lower barriers. Due to the tendency of Ni^{I} to prefer the inner sphere mechanism, it is easier to select a suitable ligand, while for Ni^{II} one must find a ligand to switch the innate preference of the outer-sphere mechanism. We believe that these results will be of great interest to the community and enable a more rational design of suitable ligands for the activation of CO_2 with nickel complexes.

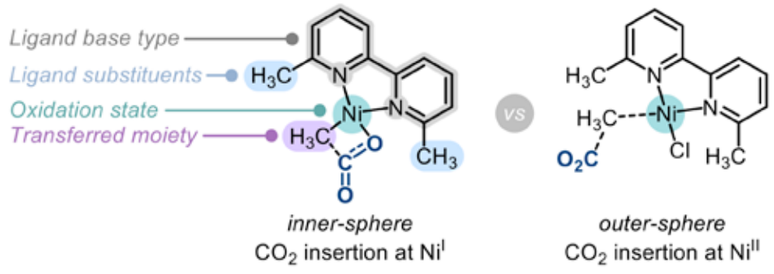

References

[1] SANHUEZA IA, KLAUCK FJR, SENOL E, KEAVENEY ST, SPERGER T, SCHOENEBECK F, ‘
Base-Free Cross-Couplings of Aryl Diazonium Salts in Methanol: PdII-Alkoxy as Reactivity-Controlling Intermediate’
Angew. Chem. Int. Ed. 2021, 10.1002/anie.202014842.

[2] SHERBORNE GJ, GEVONDIAN AG, FUNES-ARDOIZ I, DAHIYA A, FRICKE C, SCHOENEBECK F,
‘Modular and Selective Arylation of Aryl Germanes (C–GeEt3) over C–Bpin, C–SiR3 and Halogens Enabled by Light-Activated Gold Catalysis’,
Angew. Chem. Int. Ed. 2020, 59, 15543-15548.

[3] FRICKE C, DECKERS K, SCHOENEBECK F.,
‘Orthogonal Stability and Reactivity of Aryl Germanes Enables Rapid and Selective (Multi)Halogenations’,
Angew. Chem. Int. Ed. 2020, 59, 18717-18722.

Selected honors, prizes and awards

- FRANZISKA SCHOENEBECK, Streitwieser Lecture 2021, UC Berkeley, USA
- SEBASTIAN WELLIG, FSC CrA Meeting, August 2021, online

Natural Sciences

Molecular Chemistry | DFG 301

Computational evaluation and catalyst screening of the electrocatalytic reduction of CO_2 with low valent rhodium complexes

Project ID: rwth0609

MARKUS HÖLSCHER, ANNE-CHRISTINE KICK, Institute for Technical and Macromolecular Chemistry (ITMC), RWTH Aachen University

Project Report

The computational reproduction of experimental reduction potentials for 15 complexes of the type $[Rh(dxpx)_2]NTf_2$ using two different approaches is summarized in Figure 1. Application of a direct thermodynamic cycle for the reduction reaction (model A, Figure 1, above) leads to a good approximation of the trends observed with experimental reduction potentials.

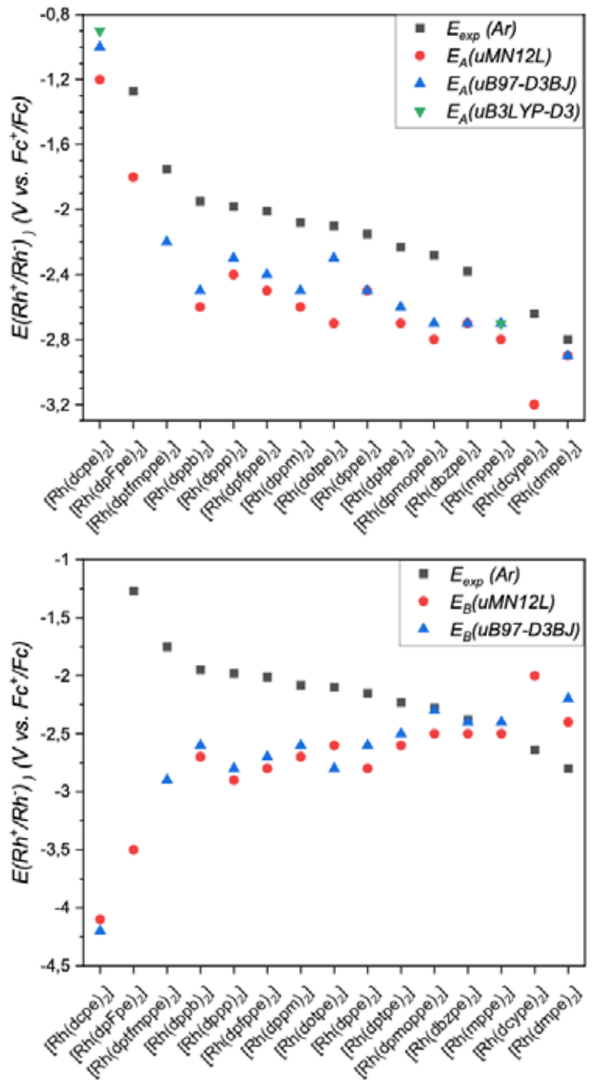

Figure 1: Summary of the calculated potentials for the reduction of the respective Rh^I-complexes to the Rh^{-I}-complexes. Above: Computation with model A using direct thermodynamic cycles. Below: Computation with model B using an isodesmic reaction.

The reduction potentials for the Rh^I/Rh^{-I} couples calculated with different density functionals are in accordance with each other and they constantly underestimate experimental values by 460 mV on average for uMN12L and 350 mV for uB97-D3BJ. Only the calculated reduction potentials of $[Rh(dptpe)_2]NTf_2$ deviate for different density functionals, which might be due to conformational differences in the optimized geometry for each functional.

It is noteworthy, that the application of an isodesmic reaction (oxidation of sodium naphthalide, model B, Figure 1, below) with a known experimental potential does not give an appropriate description of the reduction potentials observed in corresponding cyclic voltammogram measurements since the effect of electronic variations in ligand structure is not modeled adequately. In fact, the exact opposite trend for the reduction potentials in comparison with experimentally determined potentials is depicted with model B.

With regard to using DFT as a design tool, computationally designed catalyst structures have been under investigation subsequently. Therefore, the reduction potentials for phosphinine type rhodium complexes have been calculated using the previously mentioned model A. The results indicate that the electrocatalytic CO_2-reduction using these novel catalysts will proceed at a considerably lower overpotentials of -1.2 V vs. Fc^+/Fc. Chemical control experiments are in work.

Investigation of the reaction mechanism opened up more than the four originally proposed reaction pathways also considering reduction events for the catalytic intermediates. Applying the calculation of reduction potentials, some of these pathways could already be ruled out.

However, due to the risen number of structures involved in the reaction mechanism not all intermediates and transition states could successfully be localized. The results obtained so far suggest that the reduction of $[Rh(dppe)_2]^+$ to the catalytically active $[Rh(dppe)_2]^-$ complex is the most energy demanding step in the electroreduction of CO_2.

Natural Sciences

Molecular Chemistry | DFG 301

Computational evaluation and catalyst screening of the catalytic reduction of CO_2 to methanol via an indirect formate ester route with manganese complexes

Project ID: rwth0698

MARKUS HÖLSCHER,
DAVID KUSS,
Institute for Technical and Macromolecular Chemistry (ITMC), RWTH Aachen University

Project Report

Recently our group developed experimental procedures for the usage of different C1-surrogates like CO and methanol as ß-methylation agents for alcohols.[1] To guide the development of a process that enables as well the use of CO_2 in this type of reaction, a computational screening of different catalyst structures and suitable alcohols were performed. Therefore a cascade reaction was envisioned to first hydrogenate CO_2 to MeOH[2] and subsequently use the MeOH in the ß-methylation.

To maximize the generated amount of CO_2 in the first step, the thermodynamic energy profile for various alcohols were investigated (Figure 1). Based on the experimental evidence, the relevant reaction steps were assumed to be the formation of a formate resting state at the Mn-Pincer catalyst (1), esterification of the bound formate ligand to a formate ester (2) and subsequent hydrogenation of the ester species (3).

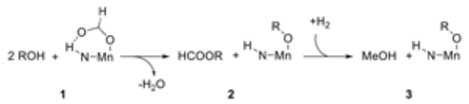

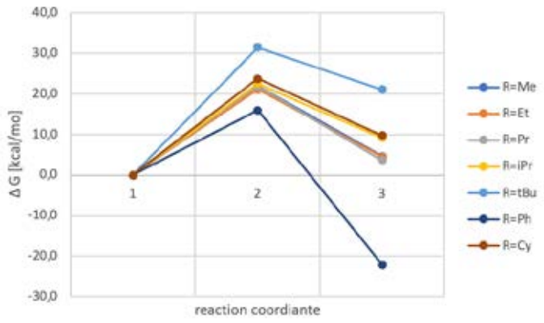

Figure 1: Thermodynamic profile for the three relevant reaction steps in the hydrogenation of CO2 to MeOH with different alcohols assisting in the esterification (PBE0-D3BJ/def2-TZVP/IEF-PCM(SMD=MeOH).

The analysis showed that especially electron withdrawing groups like the phenyl substituent are beneficial to decrease the thermodynamic stability of the ester intermediate and activate it for further hydrogenation with respect to the catalyst structure

To integrate also kinetic aspects of the mechanism, a simplified reaction mechanism with the most relevant minima and transition states for hydrogen activation (TS-I-II and TS II-III),

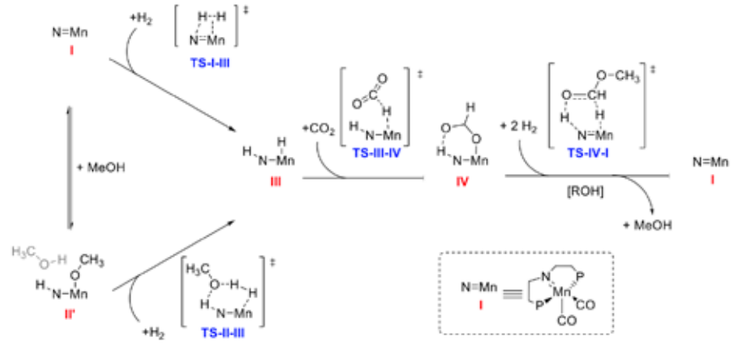

CO_2 hydrogenation (TS-III-IV) and formate ester hydrogenation (TS-IV-I) was calculated for different catalyst modifications (Figure 2). It turns out that the most stable structure is the formate complex III

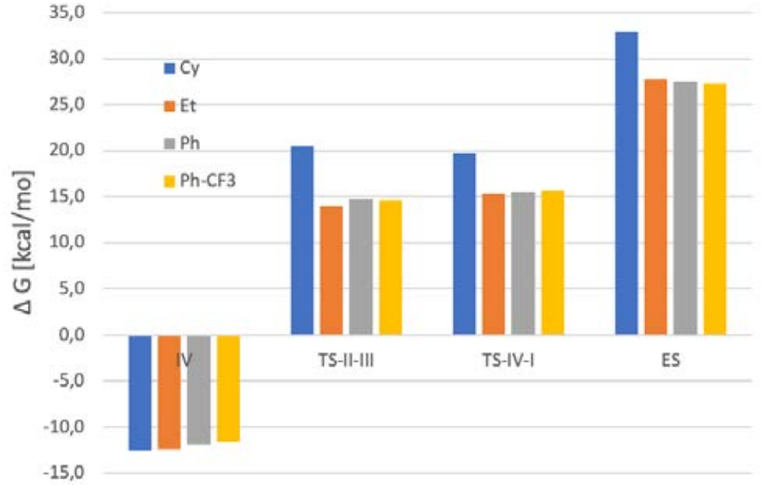

Figure 2:Simplified mechanism for the hydrogenation of CO_2 to methanol with Manganese Pincer complexes (PBE0-D3BJ/def2-TZVP).

Therefore we could identify a new electron withdrawing derivative of the Mn-Pincer catalyst that is promising for experimental applications within the ß-methylation of preferably aromatic alcohols.

References

[1] KAITHAL A, VAN BONN P, HÖLSCHER M, LEITNER W, Angew. Chem. Int. Ed. 2020, 59, 215-220.
[2] SHERBORNE GJ, GEVONDIAN AG, FUNES-ARDOIZ I, DAHIYA A, FRICKE C, SCHOENEBECK F, Chem. Sci. 2021, 12, 976-982.
[3] KUSS DA, HÖLSCHER M, LEITNER W, ChemCatChem 2021, 13, 3319-3323.

Selected honors, prizes and awards

- DAVID KUSS, Hydrogenation of CO2 to Methanol with Mn-PNP-Pincer Complexes in the Presence of Lewis Acids: the Formate Resting State Unleashed, online, 54. Jahrestreffen Deutscher Katalytiker, March 16 - 19, 2021

Natural Sciences

Chemical Solid State and Surface Research | DFG 302

Ab-initio study of composition, structure and conductivity in interstitial oxygen conductors

Project ID: jara0156

STEFFEN NEITZEL-GRIESHAMMER,
Institute of Physical Chemistry,
RWTH Aachen University
TIM SCHULTZE,
Helmholtz Institute Münster:
Ionics in Energy Storage (IEK-12)
Forschungszentrum Jülich, Germany

Project Report

Ceramic oxygen ion conductors are important electrolytes in solid oxide fuel cells and high temperature batteries. The transport of ions in these materials can occur by vacancies - as in stabilized zirconia and doped ceria - or interstitials, as in melilite and apatite structures. In this project, oxygen ion migration in melilites and apatites was investigated by means of density functional theory (DFT) calculations. In previous reporting periods, the migration of ions in melilite-structured $La_{1+x}Sr_{1-x}Ga_3O_{7+x/2}$ and apatite-structured $La_{10-x}Sr_ySi_6O_{27-3/2x+y}$ was identified. Tetragonal melilites exhibit a layered structure of alternating layers of La/Sr-cations and GaO_4-tetraheder that form interconnected pentagonal rings. Interstitials are located in the centers of these rings and migration between the rings occurs by an cooperative interstitialcy mechanism. In hexagonal apatites, the transport occurs mainly along the c-axis in oxygen ion containing channels by a combination of interstitial and interstitialcy motion.

For both materials, the migration barriers and site energies depend on the specific ionic surrounding of the moving ions, thus influencing the overall transport properties. Based on the calculated results, a model to describe the individual barriers in subsequent Monte Carlo simulations was created.

In the current reporting period, the focus was shifted to clarify the impact of different compositions on the transport properties. Melilites of general composition $A_{1+x}B_{1-x}Ga_3O_{7+x/2}$ with varying A-cations (A = La, Nd, Ce, Pr, Sm) and B-cations (B = Mg, Ca, Sr, Ba) were considered.

Different arrangements in supercells with composition $A_{18}B_{14}Ga_{48}O_{113}$, comprising one oxygen interstitial ion, were calculated. For each combination of *A*- and *B*-cation, one cation distribution was selected in order to limit the computational demand and the position of the interstitial was varied, thus probing the energy changes due to the change in the local environment of the interstitial. The resulting relative energies vary in a range of more than 1 eV revealing the strong dependence of the site energy on the local cation environment. This scattering is especially pronounced for Mg-containing compositions but low for Sr-containing materials. As strong scattering of the energy landscape is usually unfavourable for long range transport, Sr-containing compositions are thus favourable to achieve high ionic conductivities. In contrast, Mg-containing compounds show strong distortions and these compositions were disregarded in the subsequent analysis of the migration barriers.

Migration energies were calculated for eight representative cation distributions for all of the 15 remaining A/B-combinations. The averaged barriers for each cation combination are given in Table 1. Again, the migration barriers scatter over a wide range of energies and the averaged values were calculated for comparison. Among the considered A/B-combinations the lowest barriers are found for La/Sr followed by further combinations of Ca and Sr with Sm and La. These combinations will be the main focus of further investigations.

	Sm^{3+} (0.958 Å)	Nd^{3+} (0.983 Å)	Pr^{3+} (0.99 Å)	Ce^{3+} (1.01 Å)	La^{3+} (1.032 Å)
Ca^{2+} (1.00 Å)	0.34	0.34	0.34	0.34	0.34
Sr^{2+} (1.18 Å)	0.34	0.34	0.34	0.34	0.34
Ba^{2+} (1.35 Å)	0.34	0.34	0.34	0.34	0.34

Table 1: Averaged Migration barriers for different cation combinations.

Apatites of the general composition $La_{10-x}B_xSi_6O_{26\pm\delta}$ show high ionic conductivity along the c-direction, especially for La-rich compositions and Sr-containing compositions such as $La_8Sr_2Si_6O_{26}$. Previous calculations demonstrated the low activation barrier and fast interstitial transport inside the channels along the c-axis. Nevertheless, the rate limiting process is the transport in the a/b-plane between the channels.

Here we investigated the effect of doping of the Si-sites on the migration barriers in the a/b-plane. Therefore, barriers in supercells with composition $La_{24}Sr_6Si_{17}XO_{79}$ (X = Al, Ga, Ge, Fe, In, Mg) were calculated where the dopant ion X is along the migration path.

During the migration, the oxygen interstitial moves from the channel to a SiO_4 tetrahedron forming a new SiO_5 polyhedron. Subsequently, the ion moves to the next SiO_4 tetrahedron and into the adjacent channel.

The results show that the dopant does not lower the migration barrier for the oxygen ion to exit or enter the La-tunnel but can lower the migration barrier for the migration between two SiO_4 tetrahedrons from 0.2 eV to 0.1 eV. While the migration barrier for exiting and entering the La-tunnel is not significantly affected, the migration between SiO_4 polyhedrons is favored. Thus, only a slight effect on the transport behavior is expected due to doping of the Si-sites. Further investigations will focus on the effect of substitution of La/Sr-ions along the migration pathway.

Chemical Solid State and Surface Research | DFG 302

Ionic conductivity of NASICON materials from first principles

Project ID: rwth0445

STEFFEN NEITZEL-GRIESHAMMER,
Institute of Physical Chemistry,
RWTH Aachen University

JUDITH SCHÜTT,
Helmholtz Institute Münster:
Ionics in Energy Storage (IEK-12),
Forschungszentrum Jülich, Germany

Project Report

Ionic conductivity is a key property of electrolytes for solid state batteries. NASICON materials with the general composition AMM'$(PO_4)_3$ are attracting attention as solid state electrolytes, as they show high ionic conductivities as well as stability and their compositional diversity leads to many possible applications. The term NASICON (Na Super Ionic Conductors) was originally coined for doped $NaZr_2(PO_4)_3$ (NZP). Previous studies have shown that highest Na-ion conductivities are achieved by doping Sc for Zr and Si for P in $Na_{1+x+y}Zr_{2-x}Sc_xP_{3-y}Si_yO_{12}$ which introduces Na-ions on regular lattice sites in the cell. The NASICON structure exhibits rhombohedral symmetry ($R\bar{3}c$) at room temperature, except for the range of $1.8 \leq x \leq 2.2$, where it shows monoclinic distortion (C2/c). The skeleton of corner-sharing PO_4 tetrahedra and ZrO_6 octahedra provides a network of three-dimensional pathways for the monovalent ions. Sodium ions migrate collectively from Na1 position onto Na2 or Na3 position and vice versa through bottlenecks formed by ZrO_6 octahedra and PO_4 tetrahedra edges.

By means of Density Functional Theory (DFT) calculations, we refined our pair interaction energy model which describes the influence of the local cation occupation of each sodium site in $Na_{1+x}Zr_2Si_xP_{3-x}O_{12}$ (x = 1, 2) (see last report). In addition, migration energies of different pathways defined by their migration angle were calculated using Climbing Images Nudged Elastic Band (CI-NEB) and interpolated between those of $Na_{1+x}Zr_2SixP_{3-x}O_{12}$ with x = 0 and x = 3. The migration energy decreases with doping fraction as increasing sodium ion concentration increases coulombic repulsion and promotes more correlated jumps. Due to substitution of P^{5+} ions with larger Si^{4+} ions, the bottleneck enlarges, which facilitates the sodium ion migration. In addition, the migration energy decreases with increasing angle due to less steric hindrance. Based on DFT results, we performed subsequent KMC simulations to investigate the influence of local site energies and migration pathways on the ionic conductivity of $Na_{1+x}Zr_2Si_xP_{3-x}O_{12}$ (x = 0.2 - 2.8) at T = 300 - 573 K. The results of rhombohedral structure are depicted in Figure 1a. The simulation shows a maximum of ionic conductivity at x=2.5-2.8 in accordance with experimental studies.

The migration energy decreases with increasing doping fraction and angle of pathway leading to high conductivity at high doping fraction. However, at very high x, the conductivity decreases due to insufficient vacant sodium sites for migration. At low temperature (T < 450 K) conductivity decreases between $1 \leq x \leq 2$ since sodium ions are trapped in low energy states formed by the introduced silicon ions. Activation energies are obtained according to Arrhenius equation. The maximum in activation energy appears at x = 1.0 as shown in Figure 1b. Due to the trapping effect of sodium ions, the activation energy increases at low doping fraction.

However, migration energy decrease at high doping fraction because of the percolation of sodium ion between energetical favorable silicon rich positions. In addition, migration energies decrease with x leading to higher activation energies at small doping fraction. Our study reveals that not only the migration pathway, coulombic sodium-sodium repulsion, and bottleneck enlargement but also the trapping/percolation effects of sodium ions caused by introduced silicon ions need to be considered to explain the maximum of ionic conductivity at high doping fractions.

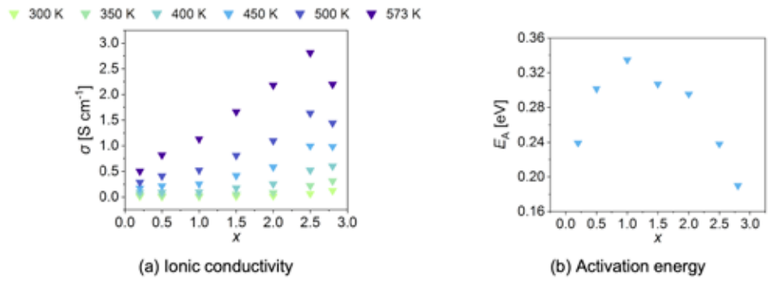

Figure 1. (a) Conductivity σ of rhombohedral $Na_{1+x}Zr_2Si_xP_{3-x}O_{12}$ structure in dependence of doping fraction x=0.2-2.8 at temperature T = 300 - 573 K. (b) Activation energies of $Na_{1+x}Zr_2Si_xP_{3-x}O_{12}$ (x=0.2-2.8) obtained from Arrhenius plot of KMC simulations.

Furthermore, the influence of different M cations on the structure and sodium ion migration in monoclinic and rhombohedral cells with composition $Na_{1+x}M_2Si_xP_{3-x}O_{12}$ (M = Si, Ni, Ge, Cr, V, Ti, Mo, W, Nb, Sn, Hf, Zr, Pb, Ce, U) with x = 0 and x = 3 were investigated by DFT calculations. The volume increases with increasing radius of M cation and doping fraction in agreement with literature. In addition, migration pathways of sodium ions have been calculated by CI-NEB method. The results confirm that the bottleneck size depends on the volume of the cell and influences the migration mechanism. Results of compositions with x = 3 reveal that sodium ions migrate by an interstitial mechanism in cells that contain small M cations (r ≤ 0.68 Å). In cells with intermediate M cations (r = 0.69 Å), sodium ions migrate by an interstitialcy mechanism. In cells with large M cations (r ≥ 0.71 Å) an additional Na1/2 site is involved which is located between Na1 and Na2 sites and was already reported in lithium ion NASICON structures. In cells with x = 0 ions migrate always via an interstitialcy mechanism and again in cells with big M cations the Na1/2 site is involved. According to our previous results of the composition $Na_{1+x}M_2Si_xP_{3-x}O_{12}$, the 180° pathway is energetically most favorable, and the 80° pathway is energetically less favorable. Migration energies are lower in compositions with x = 0 than in compositions with x = 3. In addition, interstitialcy mechanism is energetically more favorable than interstitial mechanism.

Selected honors, prizes and awards

- JUDITH SCHÜTT, JSPS short-term fellowship, Japan Society for the Promotion of Science, Japan

Selected conference participations

- JUDITH SCHÜTT, Multi-Scale Modelling & Physical Chemistry of Colloids, Bunsen-Tagung 2021, Regensburg, Germany (online), May, 10-12, 2021

Selected national and international cooperations

- MASANOBU NAKAYAMA, Nagoya Institute of Technology, Japan

Natural Sciences

Chemical Solid State and Surface Research | DFG 302

Understanding the aggregation of sickle hemoglobin and identification of aggregation inhibitors

Project ID: rwth0518

BIRGIT STRODEL
OLAGUNJU MARYAM
Institute of Biological Information Processing, Structural Biochemistry (IBI-7), Forschungszentrum Jülich, Germany

OLUJIDE O. OLUBIYI,
Department of Pharmaceutical and Medicinal Chemistry, Afe Babalola University, Ado-Ekiti, Nigeria

Project Report

Sickle cell diseases (SCD) is an inherited blood disorder resulting from a single point mutation in the beta-globin gene involving the substitution of glutamic acid at the sixth position of the β-globin chain of the hemoglobin molecule to valine (E6V). The protein molecule that is found in the red blood cells of humans is called haemoglobin. In manifestation, SCD represents a symptom complex that involves dehydration of the E6 to V6 mutated hemoglobin, which is called sickle hemoglobin or hemoglobin S (HbS), and elevated 2,3-diphosphoglycerate (2,3-DPG) levels whose interaction with hemoglobin reduces HbS solubility and promotes polymerization, also called sickling. This ultimately leads to hampered O_2 binding and transport, impaired erythrocyte morphology and interaction with endothelial surfaces, premature erythrocyte rupture and anemia, painful vaso-occlusive crisis, a general poor health, and, in many cases, death.

Until very recently, there were only two medicines that have been approved for the treatment of SCD, hydroxyurea and L-glutamine, and they are not effective for everyone. The main aim of this project is to identify small molecules and peptides able to bind to HbS and thereby inhibit its aggregation.

We focused our attention on existing drugs with possible drug repurposing for the treatment of SCD in mind, natural products, which exhibit a wide range of pharmacophores and a high degree of stereochemistry creating a great source of possible hits, as well as peptides as they turned out to be promising candidates for blocking the detrimental protein–protein interactions in other protein aggregation diseases. In this project we employed a rational approach towards the discovery of aggregation inhibitors by considering and modulating the physicochemical forces driving HbS aggregation. To this end, we have to first understand the polymerization of HbS. It should be noted that both HbA (present in individuals without sickling) and HbS form linear aggregates involving the formation of axial contacts between Hb molecules. Only in the case of HbS, these linear aggregates grow into double filaments, facilitated by lateral βV6–β'F85/β'L88/β'A70 contacts (where the prime indicates that F85, L88, and A70 belong to another hemoglobin than V6).

We first explored the dynamics and stability of HbS as a monomer (which consists of four polypeptide chains) and dimer using all-atom molecular dynamics (MD) simulations. Furthermore, we unraveled the aggregation process based on MD simulations, which was done at the coarse-grained level given the size of the system. The dimers formed during this aggregation process were investigated in detail by converting them back to the atomistic level, testing their stability by MD simulations, and revealing their protein-protein contacts. The MD simulations indeed revealed that βV6–β'F85/β'L88/β'A70 contacts are very crucial to HbS aggregation, in addition to nearby electrostatic interactions that were newly determined by our study.

This was followed by employing a computer aided drug design (CADD) approach in search of compounds that are capable of inhibiting the aggregation of HbS. Using molecular docking, we screened a library containing more than 65,000 small molecules (natural products, FDA-approved and non-FDA approved drugs) and a library of 1,000 D-enantiomeric decapeptides against different HbS structures. The best binding small molecules and peptides were identified based on the binding affinities obtained from docking and the distance between the docked ligands or peptides and the Val6 binding-site residues. The top 100 small molecules and top 61 peptides were further investigated by testing the stability of the HbS-ligand/peptide complexes using atomistic MD simulations. The simulations were initially carried out for 20 ns for each of the 161 complexes. Using various quantities such as the root mean square deviation of the ligand, the distance between ligand and the binding site, logP values, and interaction energies between the compounds and the binding site residues, we assessed the stability of the ligands or peptides in the binding sites. 59 of the 100 compounds from the small molecule library and 21 out of the 61 D-peptides that fulfilled the cutoffs indicating complex stability were then extended to 100 ns. Following the 100 ns simulations, 19 ligands and 9 peptides were identified that fulfilled the chosen stability criteria.

An additional analysis using ADME predictions, which identifies compounds that are likely to efficiently penetrate the gastro-intestinal epithelial barrier and the plasma membrane, was applied, further narrowing down the 19 ligands to 16 which will be further tested experimentally for their prospective HbS-aggregation inhibitory capabilities. These experiments are currently ongoing by our collaboration partner, Dr. Cyril-Olutayo, in Nigeria.

Selected national and international cooperations

- MOJISOLA CYRIL-OLUTAYO, Faculty of Pharmacy, Obafemi Awolowo University Ile-Ife, Nigeria

Natural Sciences

Chemical Solid State and Surface Research | DFG 302

Analyzing the Polaron Migration Mechanism

Project ID: rwth0526

JOHN P. ARNOLD,
MANFRED MARTIN,
Institute of Physical Chemistry,
RWTH Aachen University

Project Report

Reduced ceria ($CeO_{2-\delta}$) has been the subject of many studies due to its promising applications within environmental and energy technologies. [1] This can be explained by the relatively high ionic and electronic conductivity at medium temperatures. The electronic conductivity is created by moving polarons. In this project period we conducted an in-depth analysis of the polaron migration via ab inito calculations.

In the first step we calculated the polaron migration with the nudged elastic band (NEB) method within the density functional theory with the Hubbard correction (DFT+U) framework and fitted our results with the Marcus model for electron transfer reactions (see figure 1).[2] Our study shows that the migration is well described with the Marcus model and we obtain a migration barrier of 0.18 eV and an attempt frequency of 1.10 * 10^{13} Hz. The Marcus model predicts that at the polaron transition state one may observe two electronic states – an electronic ground and excited state. Within density of states (DOS) calculations we were indeed able to see two polaron states. However, the energetic difference between the states is vastly greater than predicted by the Marcus fit.

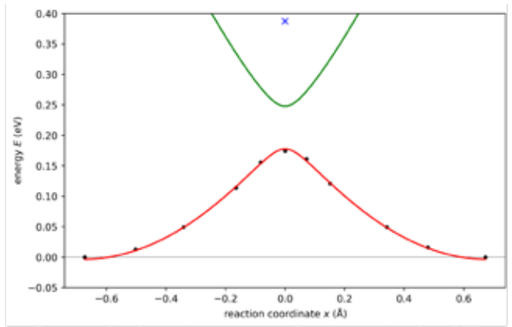

Energy profile of the polaron migration. Energies obtained from DFT are shown as black dots and as a blue cross for the elctronic ground and excited state, respectively. The fits from Marcus theory are shown as red and green lines.

In order to examine the transition more thoroughly, we ran DFT simulations with hybrid functionals. This method introduces two parameters which need to be set, namely the screening parameter μ and the fraction of exact exchange from Hartree-Fock theory α. Although, the parameters α and μ have established values which work well for structural properties in many solids, electronic properties may need a more thorough choice.

For example Du et al. suggested a value of α=0.15 to achieve good agreement between the experimental and computational band gap for ceria.[3] In addition, it has been shown by Kweon et al. in bismuth vanadate that the polaron migration barrier varies with the value of α.[4] For this reason, we conducted parameter variation simulation, in which we looked at the influence of the α setting on the polaron migration barrier and localization energy.

Indeed, we find a strong, almost linear connection for both the migration barrier and localization energy and α. Choosing a value below α=0.20 leads to negative migration barriers, which means that the polaron is more stable to two ceria sites than on one alone. At a value below α=0.10 the polaron no longer forms at all. Therefore, a value of at least α=0.25 is necessary. We are currently working with a method which includes the satisfaction of Koopmans theorem to determine the correct α value.

We also conducted simulations for the concerted migration between oxygen vacancies and polarons. For this, we simultaneously moved a vacancy and a polaron. We find that the migration is 0.1 eV lower than for the lone oxygen vacancy jump when the polaron is initially in first or second-nearest neighbor position. The reason behind the lowered migration barriers is that the polaron first jumps towards the vacancy before the latter reaches its transition point. The defect pair can thus be viewed as a vehicle with an effective charge of -1. Because of this lowered charge the migration is more easily achieved. This result is consistent with experiments by Park et al. where a coupled migration is predicted. [5]

References

[1] KHARTON VV, et al. : Ceria-based materials for solid oxide fuel cells. J. Mater. Sci. 36, 1105–1117 (2001).

[2] MARCUS RA, Sutin N. Electron transfers in chemistry and biology. BBA Reviews On Bioenergetics 811, 265–322 (1985).

[3] DU D, et al. : Screened hybrid functionals applied to ceria: Effect of Fock exchange, Phys. Rev. B 97, 23-37 (2018).

[4] KWEON KE, et al. : Electron small polarons and their transport in bismuth vanadate: a first principles study, PCCP 17 (1), 256–260 (2015).

[5] PARK WS, et al. : Onsager Transport Coefficients of Mixed Ionic Electronic Conduction in CeO2-δ, ECS Trans. 13 (26), 327–336 (2008).

Natural Sciences

Chemical Solid State and Surface Research | DFG 302

Mechanistic Investigations of the Direct Decomposition of Nitric Oxide on Platinum-Doped Graphene Model Surfaces

Project ID: rwth0577

NINA M. SACKERS,
Institute of Technical and Macromolecular Chemistry, RWTH Aachen University

PHILIPPE SAUTET,
Department of Chemical and Biomolecular Engineering, UCLA, USA

REGINA PALKOVITS,
Institute of Technical and Macromolecular Chemistry, RWTH Aachen University

Project Report

In this project, the direct decomposition of NO to N_2 and O_2 was investigated on a platinum-doped model catalyst. The catalyst model surface was described by single-layered graphene. The 2D periodic structure calculations were performed using VASP.

The direct cleavage of the NO bond can be excluded since this reaction step requires an enormous activation barrier of e.g. more than 600 kJ mol^{-1} on a dinuclear Pt center in neighboring double vacancies of graphene (Fig. 1, d). Therefore, two different pathways via the $(NO)_2$ dimer were examined. In both cases, the adsorbed $(NO)_2$ undergoes two N-O bond cleavages to N_2O and subsequently N_2 as well as one O adsorbate each.

A reaction of an adsorbed oxygen atom with another NO molecule can lead to NO_2, which can form O_2 and NO with another O adsorbate (Pathway I). Alternatively, a direct recombination of the adsorbed oxygen atoms is feasible, if both N-O bond cleavages took place on the same catalyst center (Pathway II). Both pathways were calculated in the singlet and triplet state to account for the most stable spin state of each intermediate.

On a dinuclear Pt center, the NO decomposition according to Pathway I proceeds via a very stable intermediate that has NO_2 and O bound to the same Pt atom. Due to repulsion with NO_2, the O adsorbate interacts with a carbon atom from the graphene support. This highly stable intermediate leads to very high overall activation barriers (energetic span, ES) of 361 and 334 kJ mol^{-1} for the singlet and triplet cycle, respectively.

In contrast, if the two generated O atoms are each adsorbed to one of the neighboring Pt centers and are directly recombined, the particularly stable NO_2 intermediate can be circumvented (Pathway II). This decreases the ES for Pathway II to 331 and 319 kJ mol^{-1} in the singlet and triplet state. Despite the high ESs for both reaction sequences, Pathway II is slightly more likely.

Pathway II was used to investigate the influence of a modification of the catalyst model. For this purpose, single-atom catalyst models with Pt in different vacancy sizes were compared (Fig. 1, a-c). On single atoms, the adsorbates experience repulsion and therefore interact with the carbon support. This interaction leads to a significant stabilization for Pt/DG. Compared to Pt_2/DG in the same type of vacancy, the ESs differ only slightly

with a reduction of up to 20 kJ mol^{-1}. On Pt/SG and Pt/TG, the substrate-support interactions are significantly less favorable. This can be explained by the electronic structure of Pt surrounded by four or three carbon atoms. Since the interactions of the adsorbates with the carbon support are weaker and the relative energies of the other stationary points are in a similar energy range as for Pt/DG, the ES decreases for both the singlet and triplet cycles on Pt/SG and Pt/TG. Consequently, the activation barrier of the NO decomposition can be tailored by modification of the catalyst model.

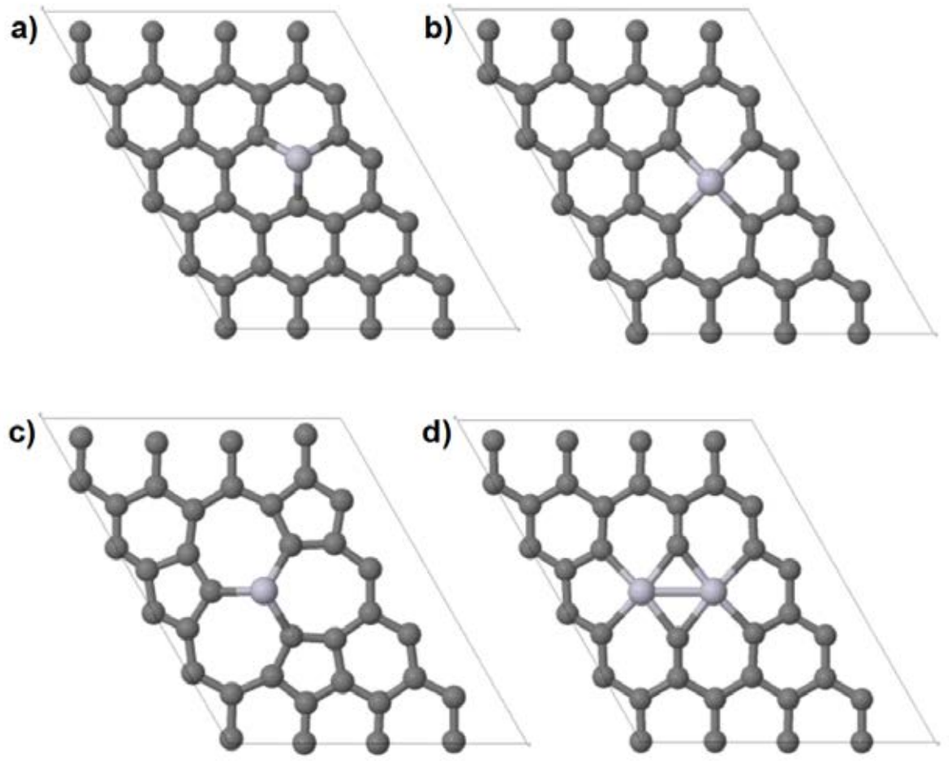

Fig. 1. Unit cells of graphene based catalyst models doped with Pt. a) Pt/SG, b) Pt/DG, c) Pt/TG, d) Pt_2/DG. Color code: dark gray = C, light gray = Pt.

Selected national and international cooperations

· PHILIPPE SAUTET, Department of Chemical and Biomolecular Engineering, UCLA, USA

Chemical Solid State and Surface Research | DFG 302

Computational studies of field-dependent oxygen migration in crystalline and amorphous fluorite structured oxides

Project ID: rwth0656

DENNIS KEMP,
ROGER A. DE SOUZA,
Institute of Physical Chemistry,
RWTH Aachen University

Project Report

Fluorite structured oxides like HfO_2 or CeO_2 are used in a variety of applications, e.g. as an insulator material in Resistive Random Access Memory (ReRAM) or as electrolyte material in Solid Oxide Fuel Cells (SOFC). One important, common aspect of these applications is that ion transport occurs in presence of an electric field. Usually, these electric fields are negligibly small but under certain conditions, e.g. nm-thin layers of the material and/or high applied voltages, large electric fields may exist. Such high field strengths can lead to a non-linear increase in the ionic mobility u_{ion} and subsequently to increases in the ionic conductivity σ_{ion} by orders of magnitude.

In this project, we focused on one very important representative of the fluorite oxides: Gd substituted CeO_2 (GDC), $Ce_{1-y}Gd_yO_{2-y/2}$. This material is a promising candidate as electrolyte material in Intermediate Temperature Solid Oxide Fuel Cells (IT-SOFC). The idea of IT-SOFC is a reduction of the operating temperature to slow down the degradation of materials and to save costs. However, this is at the expense of the ionic conductivity of the electrolyte and it is therefore crucial to increase its conductivity in other ways.

The aim of this project was to find out under which conditions field-dependent ion transport can be observed in GDC and to be able to describe this field dependence mathematically. Another aspect was the influence of the distribution of Gd substituents on the (field-dependent) ionic conductivity. Classical synthesis routes of these electrolyte materials are associated with high temperatures and thus it can be assumed that the Gd cations are mobile during this time and reach an equilibrium distribution. We have compared these with random ones to find the optimal distribution.

To generate the equilibrium distributions, we conducted Metropolis Monte Carlo (MMC) simulations with three different Gd concentrations (y = 2, 10 and 20%) and used cells with randomly distributed Gd as a comparison. Subsequently, we performed temperature- and field-dependent molecular dynamics (MD) simulations with all six systems and extracted oxide-ion mobilities u_O (E,T,y).

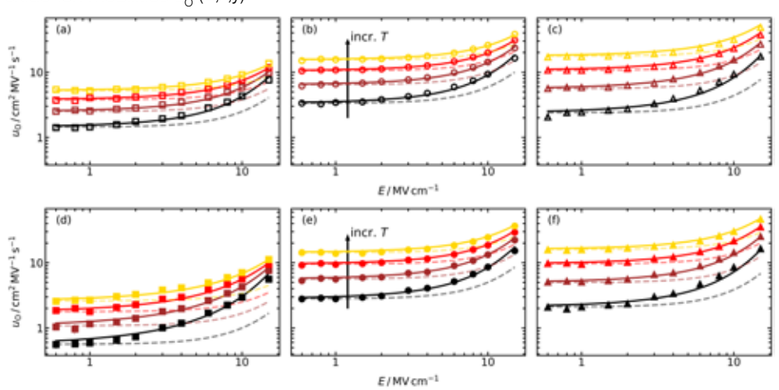

Figure 1: Field-dependent oxide-ion mobilities u_O extracted from molecular dynamics simulations at four different temperatures (T/K =1400;1600;1800;2000) for (a, d) GDC2, (b, e) GDC10 and (c, f) GDC20. The Gd distribution in (a-c) was random, whereas in (d-f) the equilibrium distributions were employed. The solid lines are fits to our improved model and for comparison the standard model is shown as transparent dashed lines.

In Fig. 1, u_O (T) is plotted in a double-logarithmic plot as a function of the field strength E. As expected, a field-independent mobility is observed at low E and a non-linear increase at high E. The classical model for the description of field-dependent mobilities (dashed lines in Fig. 1) is not able to describe the data, since this was derived for a simple model system without defect–defect interactions. We augmented this model with an additional, empirically derived term that allowed us to describe all u_O (E,T,y) data in this study (solid lines in Fig. 1).

The new derived model and the successful description of u_O (E,T,y) allowed us further to extrapolate uO to a typical working temperature of IT-SOFCs and convert them to ionic conductivities σ. The resulting field-dependent σ are shown in Fig. 2 with the required thickness of a hypothetical thin-film to achieve the corresponding electric field strength E if a voltage of 1 V is applied. Two important points crystallize from this figure: (i) for all three Gd concentrations the random distribution of Gd leads to a higher conductivity than the equilibrium distribution and (ii) for thin-films with thicknesses of less than 8 nm field-dependent ion transport is predicted.

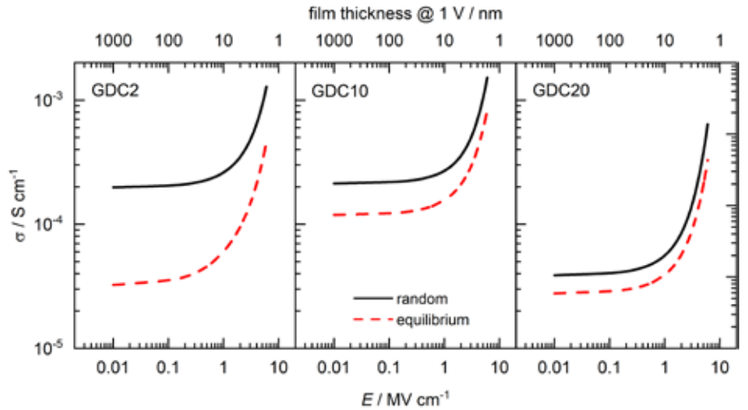

Figure 2: Predicted field-dependent ionic conductivities σ at T = 700 K for all three concentrations with random as well as equilibrium distributions of Gd. The corresponding thickness of a hypothetical thin film at an applied voltage of 1 V is shown on the top abscissa axis.

All results shown here will be published in 2022.

The second part of the project intended to study the field-dependent ion transport in amorphous fluorite oxides was not successful. Unfortunately, we observed that the amorphous structures were not stable under these conditions and it was not possible to extract ion mobilities.

Natural Sciences

Chemical Solid State and Surface Research | DFG 302

Investigating structural and chemical differences of the SARS-CoV-2 Mpro binding site before and after covalent bond formation with ligands: enabling efficient and accurate virtual screening campaigns.

Project ID: rwth0725

AGATA KRANJC PIETRUCCI,
EMILIANO IPPOLITI,
Institute of Neuroscience and Medicine (INM-9)/ Institute for Advanced Simulation (IAS-5)
Forschungszentrum Jülich, Germany

HIEN THI THU LAI,
Key Laboratory for Multiscale Simulation of Complex Systems,
VNU University of Science,
Vietnam National University, Hanoi, Vietnam

Project Report

The severe acute respiratory syndrome coronavirus 2 (SARS-CoV-2) caused a worldwide COVID-19 epidemic and triggered an urgent need to search for appropriate treatments to control the spread of infection and to treat sick people. SARS-CoV-2 carries on its surface spike-like projections; these spikes enable the fusion between viral and host membranes and are essential for the beginning of the COVID-19 infection. Once entered in the cell, the virus starts to replicate.

For a successful viral replication, the viral pp1a and pp1ab polyproteins must be cleaved into individual functional proteins. The SARS-CoV-2 main protease (Mpro) is the enzyme that ensures such cleavage. Inhibiting SARS-CoV-2 Mpro enzymatic activity can cause viral death. Thus, SARS-CoV-2 Mpro represents an attractive drug target for development of anti-covid-19 compounds and indeed many inhibitors (mostly covalently bound to the protein) have been identified.

Here, as a first step towards the investigation of the protein with new binders, we investigated the structural rearrangements of SARS-CoV-2 Mpro before and after binding of its covalent inhibitors 11a and 11b, using molecular dynamics (MD) simulations based on the AMBER99SB-ILDN forcefield [1] to describe protein and ions and TIP3P forcefield [2] for water molecules. Both the complex with the covalent bond formed or not were investigated. We analyzed as well the conformation of the ligands and the impact of different charge models used to describe the ligands during the MD simulations (RESP [3] and AM1-BCC [4]).

We found that (i) Mpro monomers A & B in complex with covalently bound ligands 11a/b show less or smaller conformational changes than when the ligands are non-covalently bound; (ii) We observe that the Mpro monomers A and B, despite being homodimeric behave differently during the MD simulations as well as the ligands bound to them. This points out that they are asymmetric, as it was observed already experimentally [5]. (iii) The stability of 11a/b ligands bound to the Mpro protein is affected not only by weather or not they have a covalent bond with the Cys145 catalytic residue, but also by the charge model used to describe the ligands in the MD simulations; With RESP, the ligands are more stable in the binding pocket than with AM1-BCCl. (iv) 11a ligand is more stably bound than 11b ligand according to our MD simulation results.

This is in line with the experimental data [6] (v) In the covalent systems Cys145 residue is covalently bound to the ligands and His41 residue retains always interactions with the cyclohexyl group of the ligand 11a or with the 3-fluorophenyl group of the ligand 11b, regardless of the monomer and of the charge model used. In the non-covalent systems Cys145 residue interacts most of the time with the aldehyde group of the ligands and His41 residue retains the same interactions with the ligands as in the covalent systems.

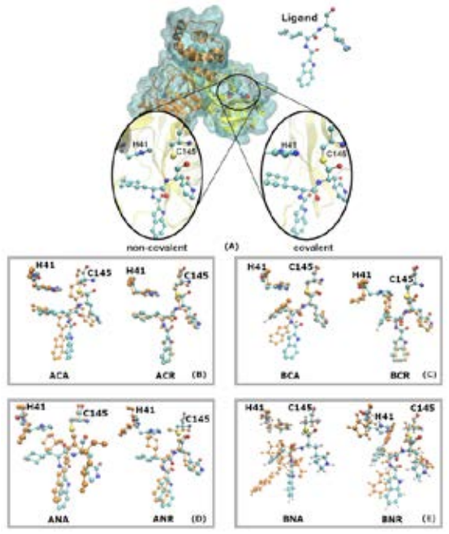

Figure 1:
(A) The 3D structure of SARS-CoV-2 main protease (Mpro) dimer (monomer A is shown in yellow and monomer B in orange color). In zoom out of the catalytic site are shown non-covalently and covalently bound ligands and the two key residues of the catalytic dyad Cys145 and His41.

(B-E) Configurations of the 11a / b ligands and of the two catalytic residues (His41 and Cys145) before (in cyan ball-and-stick representation) and after (in orange ball-and-stick representation) 400ns of the MD simulation time in the eight independent Mpro systems named according to the code: XYZ (X – the ligand name, 11a – A or 11b – B; Y – covalently – C or non-covalently – N bound; and Z – the charge model used, RESP – R or AM1-BCC – A). Color codes used for atoms: C – cyan, N – blue, O – red, S – yellow and F – pink.

References

[1] PONDER JW, CASE DA. Force fields for protein simulations. Advances in protein chemistry, 66 (2003) 27.

[2] JORGENSEN WL, CHANDRASEKHAR J, MADURA JD, IMPEY RW, KLEIN ML. Comparison of simple potential functions for simulating liquid water. The Journal of chemical physics, 79 (1983) 926-935.

[3] BAYLY CI, CIEPLAK P, CORNELL W, KOLLMAN PA. A well-behaved electrostatic potential based method using charge restraints for deriving atomic charges: the resp model. The Journal of Physical Chemistry , 97 (1993) 10269-10280.

[4] JAKALIAN A, BUSH BL, JACK DB, BAYLY CI. Fast, efficient generation of high-quality atomic charges. am1-bcc model: I. method. Journal of computational chemistry , 21 (2000) 132-146.

[5] IIDA S, FUKUNISHI Y. Asymmetric dynamics of dimeric sars-cov-2 and sars-cov main proteases in an apo form: Molecular dynamics study on fluctuations of active site, catalytic dyad, and hydration water. BBA Advances, p. 100016, 2021.

[6] DAI W, ZHANG B, JIANG XM, SU H, LI J, ZHAO Y, XIE, JIN Z, PENG J, LIU F, LI C. Structure-based design of antiviral drug candidates targeting the SARS-CoV-2 main protease. Science, 368 (2020) 1331-1335.

Selected Conference Participations

- HIEN T. T. LAI, Investigating structural differences of the SARS-CoV-2 Mpro binding site before and after covalent bond formation with ligands: enabling efficient and accurate virtual screening campaigns, the 46th Vietnam conference of Theoretical Physics, Hanoi, Vietnam, October 4-6, 2021
- HIEN T. T. LAI, The thermodynamic features of SARS-CoV-2 Spike and Mpro structures for virtual screening phytocompounds against SARS-CoV-2,Workshop “Research on COVID-19 in Vietnam”, Hochiminh city, Vietnam, October 15-16, 2021
- HIEN T. T. LAI, Molecular mechanism of interactions of some potential compounds tar geting SARS -CoV-2 main protease, Sakura Science Workshop at Ibaraki University 2021 (SSWIU 2021), Sakura, Japan, October 28-29, November 11-12, 2021

Natural Sciences

Chemical Solid State and Surface Research | DFG 302

Investigation of the surface of the cathode material $LiCoO_2$

Project ID: rwth0542

STEFFEN NEITZEL-GRIESHAMMER,
Institute of Pyhsical Chemistry (IPC),
Forschungszentrum Jülich, Germany

KATHRIN NIESWIEC,
Institute of Physical Chemistry,
RWTH Aachen University

PIOTR KOWALSKI,
Institute of Energy and Climate Research:
Nuclear Waste Management and Reactor Safety (IEK-6) & Theory and Computation of Energy Materials (IEK-13),

Project Report

$LiCoO_2$ is an important cathode material in lithium ion batteries. For the performance of the cell and the ageing behavior, not only the bulk properties but also the interfacial properties and the interaction with the liquid electrolyte are important. In this project we performed density functional theory calculations to study the surface of $LiCoO_2$ and the interaction between the surface and dissolved species in the liquid electrolyte. Calculations were performed by means of the DFT+U approach with the PBEsol xc-functional with additional dispersion correction.

Three non-polar surfaces were considered: the $(10\bar{1}0)$, $(11\bar{2}0)$, and $(10\bar{1}4)$ surface. The $(10\bar{1}4)$ surface was estimated to be the most stable one in agreement with previous results. Symmetric slabs of the surfaces were constructed and the slab thickness and height of the vacuum region were varied. Considering the convergence behavior and the computation time, a slab thickness of 16 Å with a vacuum height of 60 Å was chosen for subsequent calculations.

A critical issue is the correct description of the electronic ground-state for the surface that is described by an intermediate spin state for the $(10\bar{1}4)$ surface. The effective U-value in the DFT+U approach and the number of unpaired electrons was varied and the localization of electrons and the total energy was monitored. For subsequent calculations the values were fixed to 3 eV and 8, respectively. Figure 1 shows a symmetric slab of the $(10\bar{1}4)$ surface with the magnetization density of unpaired electrons at the surface cobalt ions.

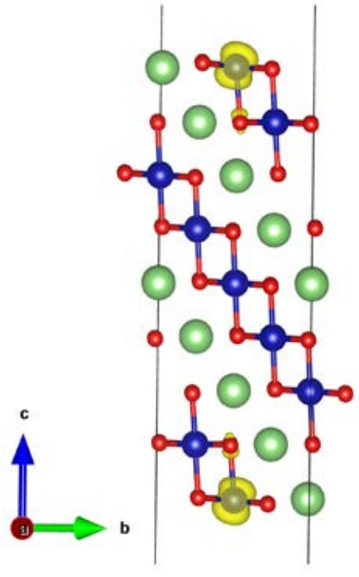

Figure 1: Symmetric slab of the $(10\bar{1}4)$ surface with cobalt ions in blue, oxygen ions in red, and lithium ions in green. The magnetization density of unpaired electrons at the surface cobalt ions is shown.

Three typical molecules of the electrolyte solvent were considered, namely dimethyl carbonate (DMC), ethylene carbonate (EC), and propylene carbonate (PC). Isolated molecules were calculated as reference. Subsequently, the distance from the surface and the orientation were varied. Figure 2 shows the energy depending on the molecule – surface distance for one specific orientation of DMC, EC, and PC. For each of the molecules, two regions can be identified. When starting at a large molecular – surface separation, decreasing the distance leads to a slight decrease of the relative energy.

This is the non-adsorbed region, where surface and molecule are essentially independent and experience only weak interaction. At a certain point, around 2 Å to 5 Å depending on the type of molecule, the energy drops considerably due to the adsorption of the molecule at the surface. This change can also be observed in the structure of the molecule/slab ensemble as depicted in Figure 2.

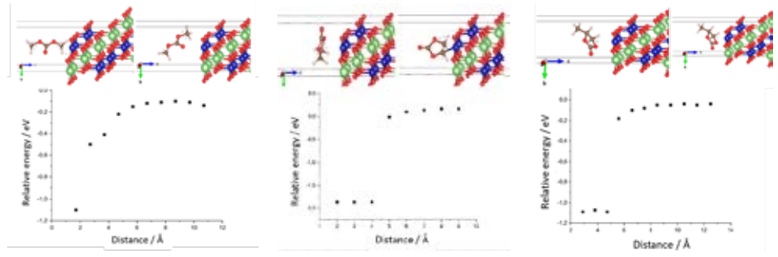

Figure 2: Structure and relative energy for a LiCoO2 surface close to DMC (left), EC (center) or PC (right). The structures represent the non-adsorbed (left) and adsorbed (right) case.

The calculations showed that the strength of the interaction in the adsorbed case depends on the orientation of the molecule. The strongest bonding between the molecule and the surface is found for the interaction of the carbonyl oxygen with the surface cobalt ions and the interaction of hydrogen atoms with the surface oxygen ions.

The major issues in the calculation of the surfaces and the interactions with the molecules are the modelling of the electronic ground-state corresponding to the intermediate or high spin states and the preservation of the symmetry of the cell.

In future calculations we will continue the calculation of the surface interactions, taking into account additional molecules and orientations. In addition, implicit solvation models will be applied for a more realistic representation of the liquid electrolyte.

Chemical Solid State and Surface Research | DFG 302

Quantum chemistry of functional chalcogenides for phase-change memories and other applications

Project ID: jara0033
JAN HEMPELMANN,
PETER C. MÜLLER, DR. DAVID SCHNIEDERS, RALF STOFFEL, RICHARD DRONSKOWSKI,
Chair of Solid-State and Quantum Chemistry,
RWTH Aachen University

Project Report

The project dealt with chalcogenide functional materials for storage-class memory. We utilized large-scale atomistic simulations based on density-functional theory (DFT) to model stabilities of solids and surfaces, investigate electronic properties, and perform chemical-bonding analysis. By calculating pristine surfaces, surface oxidation, and ligand-covered terminations, this project has matured to include new concepts to understand the electronic properties of phase-change materials (PCMs) and to introduce new materials for future applications. Furthermore, this project keeps making important contributions to the collaborative research center CRC 917 “Nanoswitches”.

Notwithstanding these goals, our project is grounded on fundamental research. DFT studies in the pseudo-binary chalcogenide systems GeTe–GeSe and Sb_2Te_3–Sb_2Se_3 were carried out, highlighting the one-and two-dimensional chalcogenide defect chemistry, aiming to both understand the overall bonding and to predict their influence on relevant material applications. In 2021, we published two papers on novel quantum chemical descriptors for PCMs developed here. The crystal orbital bond index (COBI) and the projected force constants (pFC) allow to access information both from an orbital and a thermochemical basis. Knowledge of both is invaluable to understand the chemical bonding of PCMs being the basis for their unusually characteristics but also aids in the search for improved PCMs. Future studies will combine both descriptors to achieve a more complete picture of the bonding nature of these unusual functional materials.

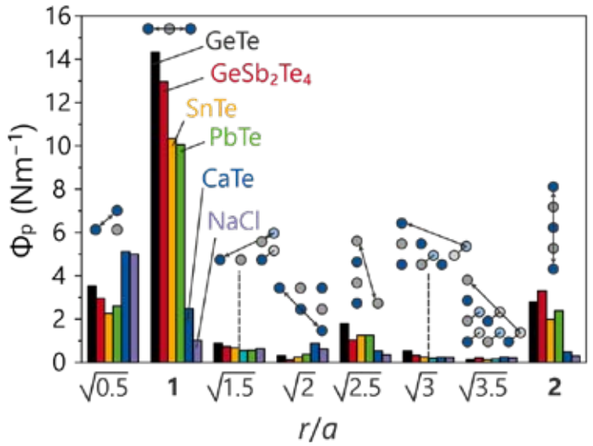

Projected force constants in various IV–VI tellurides, as well as CaTe and NaCl for reasons of comparison; the unusual long-range force constants are exclusively found in all IV–VI compounds; see J. Hempelmann et al., Adv. Mater. 2021, 33, 2100163.

Publications

[1] MÜLLER PC, ERTURAL C, HEMPELMANN J, DRONSKOWSKI R
Crystal Orbital Bond Index: Covalent Bond Orders in Solids,
J. Phys. Chem. C 2021, 125, 7959–7970.

[2] HEMPELMANN J, MÜLLER PC, KONZE PM, STOFFEL RP, STEINBERG S, DRONSKOWSKI R Long-Range Forces in Rock-Salt-Type Tellurides and How they Mirror the Underlying Chemical Bonding,
Adv. Mater. 2021, 33, 2100163.

Condensed Matter Physics | DFG 307

Understanding spin-orbital physics in correlated systems

Project ID: jara0213
J. MUSSHOFF,
X-J. ZHANG,
Forschungszentrum Jülich, Germany

E. PAVARINI,
RWTH Aachen University and Forschungszentrum Jülich, Germany

Project Report

The results obtained have been published as part of the articles summarized below.

Solving the many-body problem in materials

In this article we reviewed methodological and computational advances as well as key applications on superconducting, orbitally ordered and spin-orbit controlled strongly-correlated materials. [Riv. Nuovo Cimento, Springer-Nature (2021)]

Incommensurate magnetic structures and ferromagnetism in cuprates

In this work we performed a systematic study of static and dynamical magnetic properties of the t–t′ Hubbard model in a parameter regime relevant for high-temperature superconducting cuprates. Our results show that large t′/t suppresses incommensurate features and eventually lead to ferromagnetic instabilities for sufficiently large hole doping x. [Phys. Rev. B 103, 075136 (2021)]

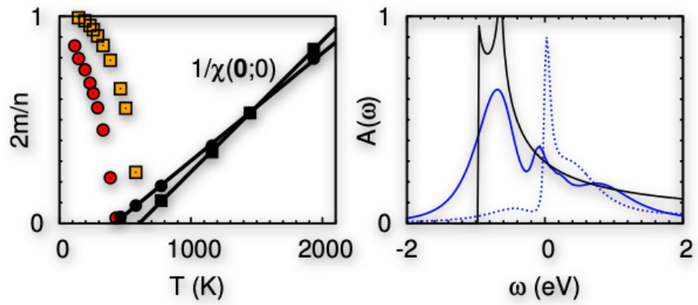

Broken orbital symmetry in $LaTiO_3$ and $YTiO_3$

The nature of broken orbital symmetry phases in correlated transition-metal compounds is strongly debated. For the paradigmatic e_g systems $KCuF_3$ and $LaMnO_3$, it has been shown that the electronic Kugel-Khomskii mechanism alone is not sufficient to drive the orbital-ordering transition up to the high temperatures at which it is experimentally observed. In the case of t_{2g} compounds, however, the role played by the superexchange interaction remains unclear. Here we investigate this question for two representative systems, the $3d^1$ Mott insulators $LaTiO_3$ and $YTiO_3$. In this work we show that the Kugel'-Khomskii superexchange transition temperature T_{KK} is unexpectedly large, comparable to the value for the eg fluoride $KCuF_3$. By deriving the general form of the orbital superexchange Hamiltonian for the t_{2g}^1 configuration, we show that the $GdFeO_3$-type distortion plays a key part in enhancing T_{KK} to about 300 K. Still, orbital ordering above 300 K can be ascribed only to the presence of a static crystal-field splitting. [Phys. Rev. B 102, 035113 (2020)]

Other relevant publications:

- Autumn School on Correlated Electrons:
  Eva Pavarini and Erik Koch (eds.)
- Simulating Correlations on Computers
  Modeling and Simulation, Vol. 11
- Verlag des Forschungszentrum Jülich, 2021
  ISBN 978-3-95806-529-1
- Permanent Link https://juser.fz-juelich.de/record/896709

Natural Sciences

Condensed Matter Physics | DFG 307

Materials for topological quantum computing from first principles

Project ID: jara0191

PHILIPP RÜSSMANN,
JOHANNES WASMER,
STEFAN BLÜGEL,
Peter Grünberg Institut and Institute for Advanced Simulation (PGI-1/IAS-1
Forschungszentrum Jülich GmbH, Germany

RUBEL MOZUMDER,
Heinrich-Heine-Universität Düsseldorf, Germany

Project Report

Within the project we develop and apply first-principles methods based on density functional theory (DFT). We use DFT to describe the electronic structure of materials and heterostructures of materials that are believed to be the building blocks for topologically protected qubits. In heterostructures of topological insulators, magnetic materials and superconductors, a topologically nontrivial superconductor can be realized by design. These materials are believed to host Majorana zero modes whose unconventional exchange statistics can be used to encode the quantum information needed to realize qubits. The appeal to pursue this direction lies in the fact that Majorana-based qubits are intrinsically protected by their topological nature and it is believed that these qubits are then less prone to errors and decoherence than today's existing qubit technologies. In order to realize topological qubits, insights into the microscopic electronic structure at the atomic interfaces is required. Simulations with DFT have the predictive power and can provide these unique insights which can help in understanding the material challenges and finding ways to optimize the complicated interfaces between superconducting, magnetic and topological materials.

We have recently extended the open source JuKKR code package to incorporate superconductivity via the Bogoliubov-de Gennes (BdG) formalism [Phys. Rev. B 105, 125143 (2022)]. The JuKKR code is an implementation of DFT and implements the Korringa-Kohn-Rostoker Green function method (KKR) that is based on multiple scattering theory. We are constantly improving the implementation and extend the functionalities of the JuKKR package. For instance, a particular strength of the KKR method is its ability to describe impurities and imperfections in crystals on the basis of the coherent potential approximation or by directly solving the Dyson equation in a real-space cluster around a defect or impurity. Such ab-initio impurity embedding calculations will be able to shed light onto the influence of disorder at the interface of heterostructures intended as platforms for Majorana qubits.

The typical size of the superconducting gap lies in the meV range which is a very small energy scale and resolving, for instance, the size of the superconducting gap in the superconducting density of states, requires much larger numerical cutoffs than usual in normal state calculations. Consequently, running KKR-BdG simulations need to use more computational resources than usual DFT calculations. A significant amount of the allotted computing time went into the development, verification and application of the KKR-BdG method. Ultimately, this led to a publication that describes the method and applies the KKR-BdG method to the s-wave superconductor niobium both in the bulk bcc crystal structure and in its (110) surfaces [Phys. Rev. B 105, 125143 (2022)]. Niobium is an important superconducting material that is widely used also in the currently much pursued research towards Majorana platforms. Building up on this research, further calculations involving, for example, a heterostructure of Nb and a topological insulator are on the way.

Apart from investigating superconducting heterostructures with the newly developed KKR-BdG technique we explored magnetically doped topological insulators that can realize the long-sought quantum anomalous Hall insulator phase. The topic of the master thesis of Rubel Mozumder was to study co-doping of different magnetic impurities embedded into the topological insulator Sb_2Te_3. He studied a large number of dimers of substitutional transition-metal defects in Sb_2Te_3 and calculated the resulting exchange interactions among the magnetic atoms. This information can be mapped onto the classical Heisenberg model that allows to describe the magnetic ordering and the critical temperature of these materials. Both are vital information in the quest for a stable quantum anomalous Hall phase. We will be able to study the magnetic ordering using our newly developed AiiDA-Spirit plugin that connects the Spirit spin-dynamics simulation software to the AiiDA infrastructure for automation and high-throughput calculations [Frontiers in Materials 9, 825043 (2022)].

Furthermore we explored the use of machine learning techniques with the ultimate goal of developing a surrogate machine learning model that is able to accelerate DFT calculations. In DFT an iterative procedure is used to refine the charge density or potential from an initial guess for the starting point until the converged solution is found. For complex systems this can require hundreds of steps until the procedure converges which evidently requires a large amount of computational resources. The topic of the master thesis of Johannes Wasmer was to investigate the use of machine learning to accelerate the DFT iteration scheme. During his work he created a large database of ab-initio impurity embedding calculations and he then investigated different ways to featurize the crystal structure information to make it machine-learnable. The generated database of converged calculations will be used in the future to train a machine learning surrogate model that is able to predict better starting points for the DFT calculations. This has to potential to significantly accelerate DFT calculations in the future if much fewer iterations are required to arrive at the converged solution.

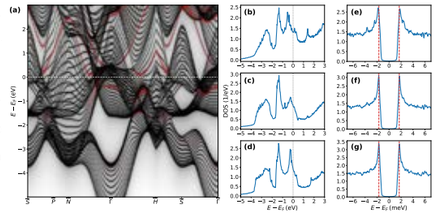

Selected conference participations

- P. RÜSSMANN, D. ANTOGNINI SILVA, ML4Q conference, online, Germany, February 24-26, 2021
- P. RÜSSMANN, R. MOZUMDER, J. WASMER, Virtual Materials Design workshop, online, Germany, July 20-21, 2021
- P. RÜSSMANN, D. ANTOGNINI SILVA, ML4Q Students' & Postdocs' Retreat, Oberlahr, Germany, August 26-28, 2021
- P. RÜSSMANN, D. ANTOGNINI SILVA, M. HEMMATI, J. WASMER, DPG Tagung Sektion Kondensierte Materie, online, Germany, September 27 – October 1, 2021
- P. RÜSSMANN, M. HEMMATI, D. ANTOGNINI SILVA, SPP1666 Young researcher work shop, Munich, Germany, October 6-8, 2021

Selected national and international cooperations

- XIANKUI WEI, Ernst-Ruska Centre (ER-C-2), Forschungszentrum Jülich GmbH, Germany
- KENTA HAGIWARA, Momentum microscopy group of C. Tusche, Peter Grünberg Institut (PGI-6), Forschungszentrum Jülich GmbH, Germany
- LUKASZ PLUCZINSKI, Peter Grünberg Institut (PGI-6), Forschungszentrum Jülich GmbH, Germany
- VLADIMIR HINKOV, Experimental Physics IV, Würzburg University, Germany
- TOM G. SAUNDERSON, Institute of Physics, Johannes Gutenberg-Universität Mainz, Germany
- MARTIN GRADHAND, HH Wills Physics Laboratory, University of Bristol, United Kingdom

Publications

- RÜSSMANN P, MAVROPOULOS P, BLÜGEL S. Ab Initio Theory of Fourier-Transformed Quasiparticle Interference Maps and Application to the Topological Insulator Bi2Te3, 2021, physica status solidi B 258, 2000031.
- RÜSSMANN P, BERTOLDO F, BLÜGEL S. The AiiDA-KKR plugin and its application to high-throughput impurity embedding into a topological insulator, 2021, npj Comput Mater 7, 13.
- WASMER J. Development of a surrogate machine learning model for the acceleration of density functional calculations with the Korringa-Kohn-Rostoker method, 2021, Master thesis, RWTH Aachen University
- MOZUMDER R. Design of magnetic interactions in doped topological insulators, 2021, Master thesis, HHU Düsseldorf

Natural Sciences

Condensed Matter Physics | DFG 307

Ab-initio study of defects in phase-change materials

Project ID: jara0210

RICCARDO MAZZARELLO,
YAZHI XU,
VALENTIN EVANG,
PETER SCHMITZ,
Institute for Theoretical Solid State Physics,
RWTH Aachen University

PROF. DR. MATTHIAS WUTTIG,
I. Institute of Physics (IA),
RWTH Aachen University

Project Report

We carried out two main projects using the computational resources from JARA0210. Both projects were devoted to the study of point defects in chalcogenide materials.

The first project focused on GeSbTe alloys, an important family of phase-change materials (PCMs) employed in optical discs (such as rewritable Blu-Ray discs) and non-volatile, electronic memory devices (phase-change memories) [i-iii]. Theoretically, crystalline GeSbTe compounds are predicted to be small-gap semiconductors, but in experiment they show p-type conduction due to self-doping.

However, the very defect types responsible for this effect have not been entirely identified. We carried out an ab-initio study of point defects and their formation energies in $GeSb_2Te_4$ and $Ge_2Sb_2Te_5$. Our simulations indicate that Ge_{Sb} is the most important defect to explain p-doping in the hexagonal structure of these alloys, contrary to previous work claiming that V_{Ge} or Sb_{Te} are the dominant defects. The results of this project have recently been published in Materials Science in Semiconductor Processing.

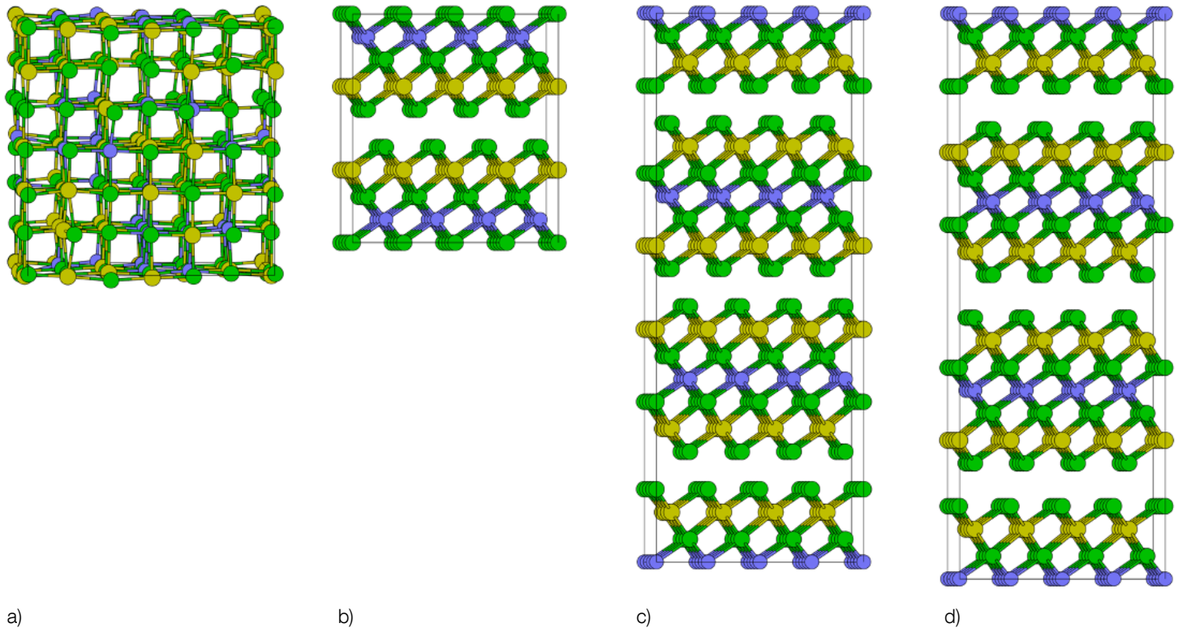

Figure 1. Supercells of (a) an exemplary cubic $GeSb_2Te_4$ model, (b) hexagonal Ge_2Sb2Te_5, (c) hexagonal $GeSb_2Te_4$, (d) ordered cubic $GeSb_2Te_4$. Blue, yellow and green balls denote Ge, Sb, and Te atoms respectively. Figure adapted from Ref. [1].

Project 2 was devoted to the investigation of the charge-carrier transition from n-type to p-type observed experimentally in PbSbTe alloys as a function of the annealing temperature. This transition occurs in the rocksalt-like phase due to the increasing structural order induced by annealing. We showed that the Fermi energy shifts from the tail of the conduction band to the valence band because different levels of overall structural disorder lead to different predominant types of native point defects. This view was confirmed by our computational study of point defects, revealing a transition from excess cations and Sb_{Pb} for high levels of disorder to Pb_{Sb} prevailing for low disorder. We have recently submitted to Advanced Materials a paper about this project, in which our simulations have been combined with experiments performed in the group of Prof. M. Wuttig.

References

[i] RAOUX S, WEŁNIC W, IELMINI D. Chem. Rev. 110, 240 (2010)

[ii] ZHANG W, MAZZARELLO R, WUTTIG M, MA E. Nat. Rev. Mater. 4, 150 (2019)

[iii] CHOE J. Intel 3D XPoint Memory Die Removed from Intel Optane PCM (Phase Change Memory), https://www.techinsights.com/blog/intel-3d-xpoint-memory-die-removed-intel-optanetm-pcmphase-change-memory/ (accessed: October 2020)

National and international cooperations

- WEI ZHANG, Xi'an Jiaotong University, Xi'an, China
- MARCO BERNASCONI, University of Milano-Bicocca, Milan, Italy

Publications

- EVANG V, MAZZARELLO R. "Point defects in disordered and stable GeSbTe phase-change materials", Mat. Sci. Semicond. Proc. 133, 105948 (2021)

Natural Sciences

Condensed Matter Physics | DFG 307

Novel Quantum Monte Carlo Approches to Competing Orders in Quantum Magnets

Project ID: jara0216

NILS CACI,
STEFAN WESSEL,
LUKAS WEBER,
Institute for Theoretical Solid State Physics
RWTH Aachen University

Project Report

In our project, we contributed to the understanding of the physics of various quantum magnetic materials by providing unbiased quantum Monte Carlo simulations. Below, we summarize some of our findings. In particular, we provided extensive quantum Monte Carlo simulations in order to explore the thermodynamic behavior of a basic quantum spin model for $BaNi_2V_2O_8$, a material that features Berezinskii-Kosterlitz-Thouless critical behavior due to its essential two-dimensional and anisotropic magnetic character.

These simulations were performed in close correspondence to inelastic neutron scattering experiments, in order to identify the different temperature regimes in this material in terms of the dominant scaling behavior. We were able to identify a basic quantum spin model on a distorted honeycomb lattice along with a dominant single-ion anisotropy term that accounts well for the experimental scattering and thermodynamics data while still avoiding the quantum Monte Carlo sign problem and which can thus be studied on comparably large system sizes in order to systematically explore the thermodynamic limit behavior that is important to reach in order to compare to the experimental data.

Moreover, we contributed quantum Monte Carlo data on a previously proposed XXZ model for the quantum magnetism observed in the coupled-ladder spin-1/2 planar antiferromagnet $C_9H_{18}N_2CuBr_4$. In more detail, we performed our simulations in close correspondence to inelastic neutron scattering experiments performed on this material under high pressure, for which a pressure-induced quantum phase transition is observed from an antiferromagnetic phase into a non-magnetic state that exhibits signatures of spin fractionalization. By comparing the experimental data to the more conventional findings obtained from quantum Monte Carlo for the previously established quantum spin model for this compound under ambient pressure, we were able to demonstrate that the critical behavior and the nature of the high-pressure phase in this compound cannot be captured by a conventional order-to-disorder mechanism within the conventional theoretical description of this material. Our combined experimental and computational work therefore calls for an extended modeling of the high-pressure regime of this material in future theoretical investigations in order to fully clarify the nature of the unconventional high pressure findings.

Furthermore, we reported on a combined experimental and theoretical study of several systems, including the prominent magnetic compound $SrCu_2(BO_3)_2$ that realizes the Shastry-Sutherland model geometry, in which we identify a quantum magnetic analogue to the critical point of water. In all cases, we observe, in distinct difference to the case of water however, two prominent lines of maxima in the specific heat within the plane spanned by temperature and a further control parameter, such as pressure or a coupling ratio.

These lines of maxima meet near the thermal critical point, which itself is the termination point of a line of first-order thermal phase transitions that emanates from an underlying quantum first-order transition point, which in all cases separates two distinct ground state phases: a magnetic phase and a non-magnetic, quantum-paramagnetic regime, arising from the geometric frustration. By combining the experimental investigations with quantum Monte Carlo and tensor network calculations, we were able to thus identify a common underlying mechanism behind this phenomena.

Selected national and international cooperations

- JOHANNES REUTER, Helmholtz-Zentrum Berlin für Materialien und Energie, Berlin, Germany
- BELLA LAKE, Helmholtz-Zentrum Berlin für Materialien und Energie, Berlin, Germany
- TAO HONG, Neutron Scattering Division, Oak Ridge National Laboratory, Oak Ridge, Tennessee, USA
- Kai P. Schmidt, Universität Erlangen-Nürnberg, Germany
- Frederic Mila, Ecole Polytechnique Fédérale de Lausanne (EPFL), Lausanne, Switzerland

Publications

- KLYUSHINA ES, REUTHER J, WEBER L, ISLAM ATMN, LORD JS, KLEMKE B, MANSSON M, WESSEL S, LAKE B. Signatures for Berezinskii-Kosterlitz-Thouless critical behaviour in the planar antiferromagnet $BaNi_2V_2O_8$, Phys. Rev. B 104, 064402 (2021), Editors Suggestion.
- LARREA JIMENEZ J, CRONE SPG, FOGH E, ZAYED ME, LORTZ R, POMJAKUSHINA E, CONDER K, LÄUCHLI AM, WEBER L, WESSEL S, HONECKER A, NORMAND B, RÜEGG CH, CORBOZ P, RONNOW HM, MILA F. A quantum magnetic analogue to the critical point of water, Nature 592, 370 (2021).
- SCHULER M, HESSELMANN S, WHITSITT S, LANG TC, WESSEL S, LÄUCHLI A. Torus Spectroscopy of the Gross-Neveu-Yukawa Quantum Field Theory: Free Dirac versus Chiral-Ising Fixed Point, Phys. Rev. B 103, 125128 (2021).
- DOHM V, WESSEL S. Exact Critical Casimir Amplitude of Anisotropic Systems from Conformal Field Theory and Self-Similarity of Finite-Size Scaling Functions in d≥2 Dimensions, Phys. Rev. Lett. 126, 060601 (2021).
- DOHM V, WESSEL S, KALTHOFF B, SELKE W, Multiparameter universality and conformal field theory for confined systems: test by Monte Carlo simulations, J. Phys. A: Math. Theor. 54, 23LT01 (2021).
- WEBER L, WESSEL S. Spin versus bond correlations along dangling edges of quantum critical magnets, Phys. Rev. B 103, L020406 (2021).

Natural Sciences

Condensed Matter Physics | DFG 307

Novel Materials by Design: The Treasure Map Approach

Project ID: rwth0662

MATTHIAS WUTTIG,
I. Institute of Physics (IA),
RWTH Aachen University

RICCARDO MAZZARELLO,
Department of Physics,
Sapienza University of Rome, Italy

YAZHI XU,
Institute for Theoretical
Solid State Physics,
RWTH Aachen University

CARL-FRIEDRICH SCHÖN,
I. Institute of Physics (IA),
RWTH Aachen University

JEAN-FELIX DUSHIMINEZA,
I. Institute of Physics (IA),
RWTH Aachen University

Project Report

This project had the target to investigate three sub-projects: The first one was regarding so-called strange metals. Most metallic materials can be described by the so called Fermi-liquid theory, a theory of weakly correlated Fermions. Sometimes even the free electron gas approach is sufficient to deduce characteristics of metallic materials. Nevertheless, as electron-electron correlations increase, these approaches fail to describe a set of materials, which are still metallic.

This group of metals is called bad-metals or Non-Fermi-liquid metals, which exhibit a deviating temperature dependence of the resistivity compared to ordinary metals. Normally, at low temperature a square dependence of the resistivity on temperature is expected. The concept of metavalent bonding (MVB) and the corresponding 2d-map of materials has shown to be a promising frame work for explaining and predicting material properties. Hence, embedding strange metals in this framework can complement and expand the recent research on this material group. We have investigated a variety of strange metals, mainly GaPt, GaPd, AlPd and AlPt in respect to their quantum chemical bonding descriptors and orbital occupations. Interestingly, these materials show a rather unexpected and striking similarity to metavalent solids. This is also supported by experimental findings such as an unconventional bond rupture as observed by atom probe tomography. We have already written major parts of a manuscript to describe and explain those findings. Yet, there is still an ongoing investigation of the optical properties that has to be finalized before the manuscript can be completed and submitted.

The second sub-project was focused on Materials bonded by d-electrons. The orbitals relevant for bonding of the materials investigated thus far are almost all so called p-orbitals. However, many compounds are bonded by d-electrons, hence it is crucial for the next development step of the bonding map to include d-orbital bonded systems as well. First tests of this material group has shown that they do seem to follow a different distribution pattern on the map, compared to the p-orbital bonded systems. We have calculated a set of d-bonded systems (also tying in to sub-project 1) in order to understand these differences. These investigations are continued in the subsequent project p0020115.

The third sub-project investigated the compound family of the $M_{n+1}A_{Xn}$ phases (short: MAX phases), where M is a transition metal, A an A group element and X is either C or N (n=1,2,3). MAX phases exhibit an extraordinary set of properties, namely high stiffness, good damage tolerance, thermal shock resistance, corrosion resistance, good thermal and electrical conductivity, while also being machinable. In cooperation with Prof. Jochen Schneider, an expert on MAX phases, we have employed ES and ET to analyze and characterize said MAX phases to further understand the underlying physics causing their special combination of properties.

These investigations nicely explain the unconventional bonding in the MAX phases and demonstrate that the binding mechanism involved is indeed both a combination of metallic and iono-covalent bonding. Systematic trends are observed and can be explained upon changing the transition metal as well as the X atom. Such studies could be employed to predict property trends and identify phases with interesting properties.

Furthermore, we have utilized the allocated compute time to support several projects, leading to the publications listed below.

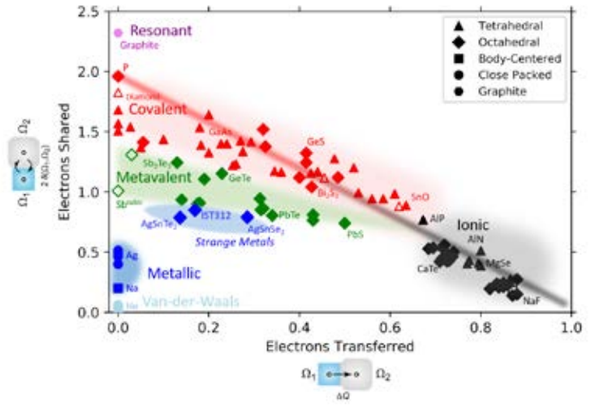

Figure 1: Map based on quantum-chemical calculations performed within this project. Upon determination of the sharing and transfer of electrons between adjacent atoms and the corresponding material properties we can distinguish three fundamental bonding mechanisms (metallic, covalent and ionic bonding) and can identify a novel fourth bonding mechanism, i.e. 'metavalent bonding'. Furthermore, the so-called group of "Strange Metals" (which still belong to the general group of metals, including In_3SbTe_2) are located right below the metavalent region.

Selected conference participations

- Colloquium TUM München, Metavalent Bonding in Solids: Provocation or Promise? January 2021
- Colloquium University Johannesburg, Metavalent Bonding in Solids: Provocation or Promise? June 2021
- Invited Talk, MRS India, Crystallization and Vitrification Kinetics by Design: The Role of Chemical Bonding, December 2021

Selected national and international cooperations

- JEAN-YVES RATY Physics of Solids, Interfaces and Nanostructures, University of Liège, Belgium
- CLAUDIA FELSER, MPI Dresden
- RICARDO LOBO, ESPCI Paris
- CARLO GATTI, CNR Milano
- CHRISTOPHE BICHARA, CiNaM Marseille

Publications

- HESSLER A ET AL, In_3SbTe_2 as a programmable nanophotonics material platform for the infrared, Nature Communications 12, 924 (2021)
- RATY JY ET AL, How to identify Lone Pairs, van der Waals gaps and Metavalent bonding using charge and pair density methods: From Elemental Chalcogens to Lead Chalcogenides and Phase Change Materials, Physica Status Solidi – RRL 15, 2000534 (2021)
- GUARNERI L ET AL, Metavalent Bonding in Crystalline Solids: How does it collapse? Advanced Materials 33, 2102356 (2021)
- Wuttig M et al, Halide Perovskites: Advanced Photovoltaic Materials Empowered by a Unique Bonding Mechanism, Advanced Functional Materials, Early View, 2110166 (2021)
- Persch C et al., The Role of Chemical Bonding to Design Crystallization and Vitrification Kinetics, Nature Communications 12, 4978 (2021)

Natural Sciences

Particles, Nuclei and Fields | DFG 309

Higher order QCD predictions for top quark physics at the LHC

Project ID: rwth0414

HUANYU BI,
TERRY GENERET,
JONATHAN HERMANN,
PHILIPP MUELLENDER, J
ASMINA NASUFI,
MARCO NIGGETIEDT,
MICHELE LUPATTELLI,
MINOS REINARTZ,
DANIEL STREMMER,
MALGORZATA WOREK,
Institute for Theoretical Particle Physics and Cosmology, RWTH Aachen University

Project Report

The goal of the project was to provide state-of-the-art theoretical predictions for a broad class of processes that involve top quark pair production and top quark pair production with an additional final state. High precision theoretical prediction at next-to-next-to-leading order and next-to-leading order in the strong coupling constant, which we have obtained in this project are of immense relevance for the top quark physics studies at the CERN

Large Hadron Collider (LHC) Run III as well as for the High-Luminosity Large Hadron Collider (HL-LHC). They will additionally impact future comparisons with experimental data. Very important applications in top-quark physics are a high-precision determination of the top-quark mass, strong coupling constant extraction, the determination of the gluon distribution function and gauge boson coupling determination. Thus, it is necessary to explore all possible associated production of top-quark pairs. Furthermore, various New Physics scenarios can be tested with the help of top quark signatures. Given such rich phenomenological applications it is essential to describe all features of tt and tt + X process as accurately as possible on the theory side in order to either deepen our understanding of the Standard Model (SM) or maximise the sensitivity to deviations from it.

Selected conference participations

MALGORZATA WOREK:

- (High Precision SM) Collider phenomenology, Annual meeting of the CRC TRR 257, RWTH Aachen University, (online) plenary talk, May 26 - 28, 2021
- Theoretical aspects of top-quark physics, 9th Annual Large Hadron Collider Physics conference (LHCP2021), (online) plenary talk, June 07 - 12, 2021
- Off-shell ttbb @ LHC with HELAC-NLO, LHC Higgs Working Group, WG1 fall meeting, (online) plenary talk, October 05, 2021
- Theoretical overview on top quark physics, 11th International Workshop on the CKM Unitarity Triangle (CKM2021), University of Melbourne, Australia, (online) plenary talk, November 22-26, 2021

MICHELE LUPATTELLI:

- NLO QCD corrections for off-shell ttbb, 15th International Symposium on Radiative Corrections: Applications of Quantum Field Theory to Phenomenology, FSU, Tallahasse, FL, USA, (online) plenary talk, May 17-21, 2021
- Full off-shell predictions and b-jet definitions for ttbb at NLO in QCD, 14th International Workshop on Top Quark Physics, Michigan, USA, (online) poster, September 13–17, 2021

JASMINA NASUFI:

- ttW at NLO in QCD: Full off-shell effects and precision observables, 14th International Workshop on Top Quark Physics, Michigan, USA, (online) poster, September 13–17, 2021

JONATHAN HERMANN:

- On the exclusion limits in tt+DM searches at the LHC, 14th International Workshop on Top Quark Physics, Michigan, USA, (online) talk in Young Scientist Forum, September 13–17, 2021

TERRY GENERET:

- Top-pair events with B-hadrons at the LHC, 14th International Workshop on Top Quark Physics, Michigan, USA, (online) talk in Young Scientist Forum, September 13–17, 2021

Selected national and international cooperations

- GIUSEPPE BEVILACQUA,
  ELKH-DE Particle Physics Research Group, University of Debrecen, Hungary
- FERNANDO FEBRES CORDERO,
  Physics Department, Florida State University, Tallahassee, USA
- HERIBERTUS BAYU HARTANTO,
  Cavendish Laboratory, University of Cambridge, Cambridge, UK
- MANFRED KRAUS,
  Physics Department, Florida State University, Tallahassee, USA
- LAURA REINA,
  Physics Department, Florida State University, Tallahassee, USA

Publications

- BEVILACQUA G, BI HY, HARTANTO HB, KRAUS M, NASUFI J, WOREK M. NLO QCD corrections to off-shell ttW production at the LHC: Correlations and Asymmetries, Published in: Eur. Phys. J. C 81 (2021) 7, 675
- BEVILACQUA G, BI HY, HARTANTO HB, KRAUS M, LUPATTELLI M, WOREK M. ttbb at the LHC: On the size of corrections and b-jet definitions, Published in: JHEP 08 (2021) 008
- HERMANNA J, WOREK M. The impact of top-quark modelling on the exclusion limits in tt + DM searches at the LHC, Published in: Eur. Phys. J. C 81 (2021) 11, 1029
- CZAKON M, HARLANDER RV, KLAPPERT J, NIGGETIEDT M. Exact top-quark mass dependence in hadronic Higgs production, Published in: Phys. Rev. Lett. 127 (2021) 16, 162002

Natural Sciences

Particles, Nuclei and Fields | DFG 309

Development of a Nuclear Archaeology Toolbox

Project ID: rwth0572

MALTE GÖTTSCHE,
BENJAMIN JUNG,
LUKAS RADEMACHER,
ANTONIO FIGUEROA
Nuclear Verification and Disarmament Group,
RWTH Aachen University

CHRISTOPHER FICHTLSCHERER,
Institute for Peace Research and Security Policy (IFSH),
University of Hamburg, Germany

KATJA ERMERT,
Nuclear Verification and Disarmament Group,
RWTH Aachen University

Project Report

Nuclear archaeology focuses on reconstructing the operating history of nuclear facilities to estimate the amount of fissile material produced in these facilities. Such methods are intended to serve as verification tools in international arms control, non-proliferation and disarmament agreements. While proof-of-concept studies have demonstrated the potential of nuclear archaeology techniques, further research and development is necessary to create a comprehensive set of tools for a robust verification mechanism.

This compute project falls under the scope of a larger research project, titled A German Nuclear Archaeology Laboratory: Reconstructing the Nuclear Past to Enable a Nuclear-weapon-free future. A prime target for nuclear archaeology applications is presented by nuclear reactors because they produce plutonium, a fissile material that can be used to build nuclear weapons. To reconstruct the operating history, measurements of isotopic evidence are used to solve an inverse problem, i.e., to infer the operation parameters of the reactor that created the evidence.

Under this project, two different techniques for nuclear archaeology with reactors are being studied and developed: the isotope ratio method (IRM) and reprocessing waste archaeology. Both techniques require specialized software for simulating the physical processes of nuclear reactors as well as numerical methods for solving the inverse problem. In the following, progress on both sub-projects is detailed separately.

Isotope Ratio Method

To apply IRM as a verification tool for an arms control or a non-proliferation treaty requires knowledge of as-sociated uncertainty sources and a method for assessing the uncertainty of the results of the method. IRM requires some prior information on the reactor and extensive neutron reaction data libraries, both of which come with uncertainties. We conducted a study assessing the uncertainty of plutonium estimates with IRM, which has been accepted for publication in the peer-reviewed journal Science and Global Security. In this study, we demonstrated a quasi-Monte Carlo approach to uncertainty propagation and performed a global sensitivity analysis to identify uncertainty sources with a large impact on the overall uncertainty. Both samplingbased analyses required repeating reactor simulations many times with different input parameters. The results show that neutron reaction data uncertainties can have a significant impact on the results of IRM, contrary to previous, independent studies which have neglected these uncertainties.

Reprocessing Waste Archaeology

Using reprocessing waste to infer reactor operating histories is a concept still under development as part of the abovementioned research project. Isotopic evidence is collected from the radioactive waste and a probabilistic Bayesian inference framework is used to reconstruct parameters of the operating history. To use the Bayesian inference framework, surrogate models are required for computing the composition of the dis-charged fuel. We developed a method that uses sophisticated reactor simulations to generate training data for a surrogate model. Gaussian process regression is used to train the surrogate model, which is then used for the inference step. After extensive, simulation-based testing we achieved the first validation of the Bayesian inference framework on experimental data from the Spent Fuel Isotopic Composition 2.0 Database. These results were presented at the INMM/ESARDA 2021 Joint Annual Meeting.

Selected conference participations

- BENJAMIN JUNG, Uncertainty Assessment of the Isotope Ratio Method in Nuclear Archaeology, INMM/ESARDA 2021 Joint Annual Meeting
- ANTONIO FIGUEROA, Nuclear Archaeology Based on Measurements of Reprocessing Waste: First Experimental Results, INMM/ESARDA 2021 Joint Annual Meeting

Selected national and international cooperations

- JULIEN DE TROUILLOUD DE LANVERSIN, Belfer Center for Science and International Affairs, Harvard University, USA

Publications

- FIGUEROA A, GÖTTSCHE M. Gaussian Process Regression for Surrogate Modeling of Discharged Fuel Nuclide Compositions, Annals of Nuclear Energy 156, 2021, doi:10.1016/j.anucene.2020.108085

Natural Sciences

Particles, Nuclei and Fields | DFG 309

Nuclear Lattice Simulations

Project ID: jara0015

GIANLUCA STELLIN
Helmholtz Institute
for Radiation and Nuclear Physics,
University of Bonn, Germany

ULF-G. MEISSNER,
Institute of Advanced Simulation,
Theory of strong interactions (IKP-3/IAS-4),
Forschungszentrum Jülich and HISKP,
University of Bonn, Germany

Project Report

The computational project entitled Nuclear Lattice Simulations in the year 2021 focussed on the investigation of physical observables in ^{8}Be, ^{12}C and ^{16}O in the macroscopic α-cluster framework in a finite cubic configuration space with spacing a and N points per dimension (cf. refs. [1,2,3]). In particular, the total time allocation in the ***CLAIX-2018-MPI*** resources has been devoted to the following tasks:

1) **Variational calculation of the strength parameter of the 3α Gaussian potential for ^{16}O.** The work aimed at testing the results of the same calculation performed on another workstation at the HISKP in 2017 (cf. chap. 8 of ref. [4]). The Matlab source codes, executed on CLAIX, confirmed the results for the strength parameter of the 3α potential published in ref. [4], within marginal discrepancies.

2) **Discretization effects in the energy, squared angular momentum and mean α-α separation of low-lying lattice eigenstates of ^{16}O.** As in chap. 7 of ref. [4], a series of low-lying completely symmetric eigenstates of the Hamiltonian matrix with L ≡ Na > 19.5 fm transforming as the A_1, A_2, E, T_1 and T_2 irreducible representation of the cubic group has been considered. In contrast with chap. 7 of ref. [4], the new value of the strength parameter of the 3α potential (cf. point I)) has been exploited in the Hamiltonian. The lattice eigenstates have been produced through cuda C++ codes for the GPU nodes (cf. ref. [3]). Under the above constraint on L, samples of the energy eigenstates have been obtained by varying a from 2.0 to 3.5 fm. Based also on the behaviour of the squared angular momentum with the lattice spacing, the eigenstates have been classified as the 0_1^+, 0_2^+, 1_1^-, 2_1^-, 2_1^+, 2_2^+, 3_1^-, 3_1^+ and 4_1^+ states of ^{16}O. The average values of the α-α separation have been also included in the analysis (cf. art. iii) in § D).

3) **Reduced electric and magnetic multipole transition probabilities between eigenstates of ^{16}O**. GPU codes for the calculation of transition matrix elements mediated by electric or magnetic multipole operators have been developed. From the eigenstates of the Hamiltonian, state vectors with well-defined angular momentum projection have been obtained via the unitary transformation in app. C.3 of ref. [4]. Errors in the referenced transformation tables have been spotted and removed. The transition matrix elements B(E1,$1_1^- \to 0_1^+$), B(E2, $2_1^+ \to 0_1^+$) and B(E3, $3_1^- \to 0_1^+$) have been computed at certain values of a in the interval from 2.0 and 3.5 fm. For the E2 transition, order-of-magnitude agreement with the experimental counterpart was found already at 2.8-3.0 fm. However, the obtained data are considered as preliminary results.

4) **Worldline Monte-Carlo simulations of the finite-volume analysis of the binding energy of ^{16}O.** Based on the code exploited for the computation of the energy of the ground state (g.s) of ^{16}O presented in chap. 7 of ref. [4], the g.s. energy of ^{16}O has been determined at values of N from 3 to 40. The binding energy has been extracted from the g.s. energy through eq. (4.48) in sec. 4.5.2 of ref. [4]. The estimates of the lowest energy eigenvalue have been produced from Euclidean-time extrapolations performed on datasets that consist of the same observable sampled at time intervals of different length. Concerning the direction of time, a temporal lattice spacing a_t = 0.0564 MeV^{-1}, has been set (cf. chap. 4 of ref. [4]), whereas the lattice spacing a has been fixed to 0.50 fm throughout the simulations.

5) **Boosted frames and the restoration of Galilean invariance in 2α and 3α systems.** Pre-existing Matlab codes for the diagonalization of the lattice Hamiltonian for the ^{8}Be, ^{12}C and ^{16}O nuclei as 2α, 3α and 4α systems has been modified in order to account for finite Galilean boosts applied to the center-of-mass of the system. The effects of the breaking of this symmetry (cf. ref. [5]), have been studied in the 2α case, with the perspective of applying Galilean invariance restoration terms to two-body scattering on a cubic lattice.

6) **Discretization effects in the magnetic dipole moment of the 2_1^+ and 3_1^- states of ^{12}C.** The lattice $T_2 + E$ and $A_2 + T_1 + T_2$ eigenstates at 4.5 and 5.8 MeV analysed in ref. [3] became the object for the investigation of discretization effects in the average values of the magnetic dipole moment, μ. This analysis is a part of a larger project, covering the g-factors of excited states of self-conjugate nuclei and the ones of the neighbouring nuclei with $N = Z + 1$ and $N = Z + 2$ (cf. art. ii) in § D). Fixing $L = Na > 18.5$ fm, the average values of this observable have been computed at different values of the lattice spacing. Besides, as in ref. [2], the effectiveness of the isotropic average in suppressing the finite lattice spacing artifacts has been tested. The production of the dataset for the 3_1^- state is still in progress.

Although no time allocation was dedicated in the past year to the conference paper submitted by G.S. in 2021 (cf. § 6 D) the calculation of the single and double three-dimensional Riemann sums has been carried out thanks to the CLAIX resources, including the GPU nodes. Finally, concerning the statistics of the project, in the accounting period from 1st May 2021 to present the 80 % of the total time allocation, corresponding to 2,5 million core-hours, has been consumed.

References:

[1] Lu BN, Lähde TA, Lee D, Meißner UG. Phys. Rev. D 90, 034507 (2014).
[2] Lu BN, Lähde TA, Lee D, Meißner UG. Phys. Rev. D 92, 014506 (2015).
[3] Stellin G, Elhatisari S, Meißner UG. Eur. Phys. J. A 54, 232 (2018).
[4] Stellin G. Nuclear Physics in a Finite Volume: Investigation of two-particle and α-cluster systems, Ph.D. thesis, University of Bonn (2020).
[5] Klein N, Lee D, Meißner UG, Eur. Phys. J. A 54, 233 (2018).

Selected honors, prizes and awards

- ERC Advanced Grant “Emergent complexity from strong interactions” (EXOTIC), PI: Ulf-G. Meißner, November 2021 - October 2026

Selected conference participations

- Poster presentation, Gianluca Stellin, “P-Wave Two-Body Bound and Scattering States in a Finite Volume including QED“, The 38th International Symposium on Lattice Field Theory, Lattice approaches for Nuclear, Subnuclear and Particle Physics, Zoom & Gather (online format), organized by MIT, Cambridge, Massachusetts, USA, July 26 - 30 2021
- [participation only] Lectures on scattering resonances, Espace de Structure et de réactions Nucléaires Théorique, CEA Saclay, Saint-Aubin, France, September 06 - 10, 2021
- Invited lecture, Ulf-G. Meißner, ``Molecular structures in hadron and nuclear physics,'' Deutsche Physikalische Gesellschaft, March 11, 2021
- Invited talk, Ulf-G. Meißner, ``Hadronic molecules,'' EMMI workshop on the ``Status of the XYZ states,'' Darmstadt, April 12, 2021

Selected national and international cooperations

- SERDAR ELHATISARI, Department of Physics, Faculty of Natural Sciences and Engineering, Gaziantep Islam Science and Technology University, Gaziantep, Turkey
- KARL-HEINZ SPEIDEL, Helmholtz Institut für Strahlen- und Kernphysik, University of Bonn, Bonn, Germany

Publications

- STELLIN G. Two-Fermion Bound and Scattering States in Finite Volume including QED in P-Wave and Beyond, arXiv:2110.10485, 2021 [accepted for publication by Proceedings of Science, Sissa, Trieste].

Natural Sciences

Particles, Nuclei and Fields | DFG 309

Dark Simulations: Understanding the Dark Side of Particle Physics and Cosmology

Project ID: jara0184

JULIEN LESGOURGUES,
FELIX KAHLHÖFER,
CHRISTIAN FIDLER,
JESÚS TORRADO,
Institute for Theoretical Particle Physics and Cosmology, RWTH Aachen University

DEANNA HOOPER,
Service de Physique Théorique, Université Libre de Bruxelles, Brussels, Belgium

SILVIA MANCONI,
Institute for Theoretical Particle Physics and Cosmology, RWTH Aachen University

JANINA RENK,
Oskar Klein Centre for Cosmoparticle Physics, Stockholm University, Stockholm, Sweden

NILS SCHÖNEBERG,
PATRICK STÖCKER,
Institute for Theoretical Particle Physics and Cosmology, RWTH Aachen University

CHRISTIAN PARTMANN,
Max Planck Institute for Astrophysics, Garching Germany

NIKLAS BECKER, Institute for Theoretical Physics, Johann Wolfgang Goethe-Universität, Frankfurt, Germany

JONAS EL GAMMAL,
Institute of Mathematics and Physics, University of Stavanger, Stavanger, Norway

KATHRIN NIPPEL,
Institute for Theoretical Particle Physics and Cosmology, RWTH Aachen University

Project Report

Sub-project 1: N-body simulations

The distribution of large scale structures allows for high accuracy in constraining the properties of neutrinos. Future missions such as SDSS, DESI and Euclid promise a new age of unprecedented precision in the measurement ofneutrino masses. This upcoming leap in experimental precision requires also a fundamental improvement of the theoretical predictions. The largest challenge is given by our modelling of the influence of neutrinos during their non-relativistic transition. Utilising last year's JARA grant, we developed a new numerical method to simulate the impact of massive neutrinos on structure formation that is numerically very efficient. In 2021 we made further progress. We performed new simulations to prove that an even faster method, based on a better definition of initial conditions for N-body simulations, but avoiding the post-processing of their result, works very well. We published our results in paper [2].

Sub-project 2: Machine learning in Astroparticle Physics and Cosmology

In sub-task 2.1 we focused on the speed up of Einstein-Boltzmann solvers that one can achieve by using using neural networks to predict the evolution of cosmological perturbations. We improved over a previous work (JCAP 09 (2019) 028) by training a new set of networks, with a better architecture and choice of hyperparameters. So far, the results are only available in the Master thesis of MSc. Florian Stadtmann, but we are finishing the writing of a new publication on these results.

In sub-task 2.2 we trained neural networks to predict the signal expected in AMS-02 for different models, and to assess their compatibility with observed data. This has led to a public code for the evaluation of the AMS-02 likelihood for many different models, that we presented and used in paper [3].

In sub-task 2.3 we developed a general likelihood emulator based on Gaussian Processes (GPs) to replace the many costly evaluations of the likelihood functions and cosmological codes with a single fast GP model. Our results are available in the Master thesis of MSc. Jonas El gammal. We are currently preparing a publication based on these results.

Sub-project 3: Testing non-standard Dark Matter Models

The tension between the values of the current Hubble expansion rate inferred either from local distance ladder observations or from cosmic microwave background data has recently grown beyond 5σ. The tension is by nature model-dependent: it exists in the standard cosmological model, but it could disappear in some of its extensions. We confronted different models of Dark Matter and Dark Energy against cosmological data. This amounted to many MCMC runs on the JARA cluster, to perform Bayesian parameter extraction. We were able to gather many new results on the goodness of fit of each model. We presented a comparison and a fair ranking of these theoretical solutions to the tension in a long paper [1] submitted to Physics Reports, which is now very close to being accepted for publication.

Sub-project 4: Global fits of axion-like particles

In this project, we were supposed to apply some numerical tools developed in 2020 (within the same project jara0184) to the study of axion-like particles. Instead, we applied them to the timelier case of WIMP-like particles. We contributed to the cosmological part of a global fit to laboratory plus cosmological data. Our results are published in paper [4].

Sub-project 5: Forecasts for the Euclid satellite mission

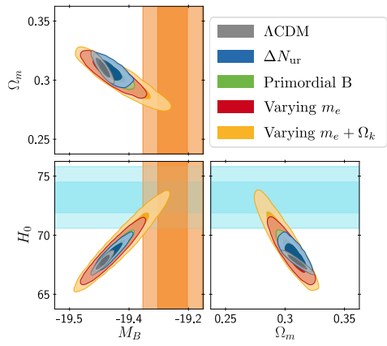

The upcoming Euclid satellite mission promises unprecedented precision in the determination of the cosmic expansion history through the observation of the clustering and lensing of distant galaxies. The scientific objective of this sub-project was to forecast the sensitivity of Euclid to several cosmological parameters, and to compare several analysis pipelines. We obtained new results and compared them successfully with those of other groups involved in the large Euclid collaboration. Thanks to this work, our analysis pipeline has been officially validated as an accurate forecasting tool within the Euclid collaboration. The results are already presented in the Master thesis of MSc. Lena Rathmann. We are currently in the process of turning them into a publication.

Selected conference participations

- J. LESGOURGUES, "Could cosmological tensions hint at non-standard DM properties?", Quarks 2021 conference, Moscow, Russia, June 22, 2021
- J. LESGOURGUES, "A fair comparison of potential Hubble-tension-solving cosmological models", GGI workshop on New Physics from the Sky, Florence, Italy, November 02, 2021
- K. NIPPEL, "Constraining dark matter annihilation with cosmic ray antiprotons using neural networks", TAUPP 2021, Valencia, Spain, September 01, 2021

Selected national and international cooperations

- V. POULIN, Montpellier University, France
- S. J. WITTE, Amsterdam University, Netherlands
- C. PARTMANN, Max Planck Institute for Astrophysics, Garching, Germany
- M. KORSMEIER, Stockholm University, Sweden

Publications

- SCHÖNEBERG N, FRANCO ABELLAN G, PEREZ SANCHEZ A, WITTE SJ, POULIN V, LESGOURGUES J. The H0 Olympics : a fair ranking of proposed models, submitted, arXiv:2107.10291
- HEUSCHLING P, PARTMANN C, FIDLER C. A minimal model for massive neutrinos in Newtonian N-body simulations, submitted, arXiv:2201.13186
- KAHLHOEFER F, KORSMEIER M, KRÄMER M, MANCONI S, NIPPEL K. Constraining dark matter annihilation with cosmic ray antiprotons using neural networks, JCAP 12 (2021) 12, 037

Natural Sciences

Particles, Nuclei and Fields | DFG 309

Deep Learning for the MADMAX Dark Matter Experiment

Project ID: rwth0583

ALEXANDER SCHMIDT,
ANDRZEJ NOVAK,
PHILIPP ALEXANDER JUNG,
TIM GRAULICH,
ERDEM ÖZ,
ALI RIAHINIA,
MAX LOHMANN,
BERNARDO ARY DOS SANTOS,
TOBIAS SEIBEL,
JAN SCHULZ,
MARVIN SCHÖFFMANN,
III. Physikalisches Institut A,
RWTH Aachen University

Project Report

The existence of Dark Matter in the Universe has been established decades ago through astronomical observations. The gravitational impact of Dark Matter can be observed in various systems, such as the rotation of galaxies. Nevertheless, the nature of Dark Matter is still unresolved. One of the most important unresolved questions of modern physics is the question what Dark Matter is made of. Several theories are able to give concincing explanations. One of the most popular theories is the theory of the Axion, which is a hypothetical elementary particle that emerges in the fundamental models of the structure of matter. Axions are being searched for in physical experiments. A promising future experimental concept to search for Dark Matter Axions is the so-called dielectric haloscope. A dielectric haloscope tries to exploit the electromagnetic interaction of axions with a strong magnetic field in order to detect axions in the galactic Dark Matter halo. In a dielectric haloscope, microwave radiation is emitted from the surfaces of dielectric disks due to axion-photon conversion at the interface between the disk and vacuum. The main function of the experiment is the resonant amplification of the electromagnetic response, which allows the resulting signal to be detected. This amplification factor is the main characterizing quantity to be studied and optimized. The amplification factor is a frequency-dependent high-dimensional quantity as it depends on the exact position of each dielectric disk within the experiment. As there can be up to 80 disks with variable thickness, the degrees of freedom are excessively large.

Simulations of the experiment can be used for sensitivity estimates as well as for constraining the experimental boundary conditions such as the required mechanical precision of the experiment. Various approaches can be used for the simulation of the experiment at different levels of detail. So-called analytical 1D methods are used in an idealised context, where the dielectric disk size is taken to be infinite and some design aspects are neglected. Actual 3D simulations are more realistic but suffer from high demands on computing resources and quickly become prohibitive, especially when optimising in a 3D simulation with a large number of disks and therefore a large number of degrees of freedom. In this computing project, we established a proof-of-principle that modern machine learning methods are able to reproduce the electromagnetic response of the experiment and can therefore speed up the simulation and reduce the required computing resources dramatically.

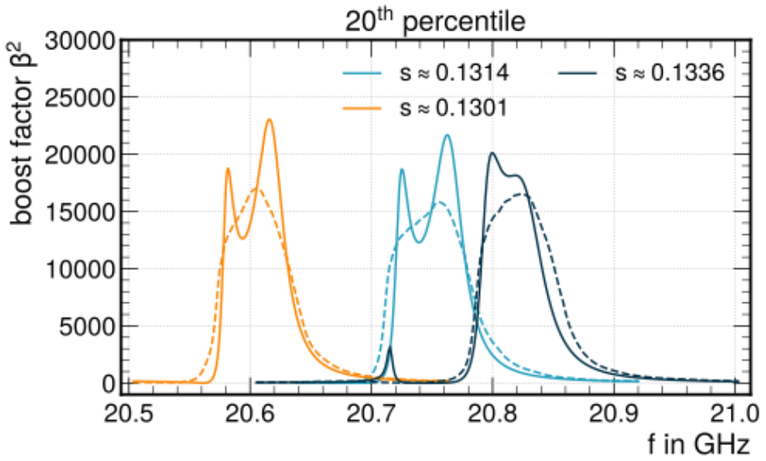

For this purpose, a convolutional neural network has been used with a 1D convolutional layerwith 128 filters with subsequent 1D max pooling, as well as flattening, followed by two dense layers with 512 nodes each and an output node. Each layer, except the last, uses batch normalization, dropout at a rate of 0.2 and PReLU as an activation function with an alpha initializer of 0.25.

For training of the network, a large dataset from analytical 1D simulations has been used. The result of the simulation is effectively the frequency-dependent amplification factor of the experiment, as explained above. The Figure below shows an example of a frequency dependent amplification factor, comparing the analytical 1D simulation (solid lines) with the output of the neural network (dashed line).

It is visible that the three important quantities, mean frequency, bandwidth and magnitude of the amplification factor are well reproduced by the neural network. This represents a successful proof-of-principle that neural networks can be used for the purpose of simulating the electromagnetic response of complex experiments, such as the planned MADMAX experiment for the search for Dark Matter particles.

Selected national and international cooperations

- Deutsches Elektronen-Synchrotron DESY, Hamburg, Germany
- Universität Hamburg, Hamburg, Germany
- University of Tübingen, Tübingen, Germany
- Max Planck Institute for Physics, Munich, Germany
- CERN, Geneva, Switzerland
- Centre de Physique des Particules de Marseille (CPPM), Marseille, France

Publications

- Master Thesis: ALEXANDER JUNG, “A novel approach to simulate axion-induced electro magnetics utilizing Deep Learning techniques in the MADMAX Experiment”
- Master Thesis: BERNARDO ARY DOS SANTOS, “Anisotropy Effects in a Dielectric Halos cope for Dark Matter Searches”
- Bachelor Thesis: ALI RIAHINIA, “Simulation of the MADMAX experiment using deep learning techniques: predicting the boost factor from disk positions”
- Bachelor Thesis: TIM GRAULICH, “A first look on possible applications of Deep Learning in MADMAX: Prediction of the disk configuration for a given Boostfactorcurve”
- Bachelor Thesis: TOBIAS SEIBEL, “Dark Matter and Deep Learning: Introduction of neural networks to three-dimensional simulation of electromagnetic waves in haloscopes”.

Natural Sciences

Particles, Nuclei and Fields | DFG 309

Computing for the CMS experiment at the CERN LHC: extension of HEP big data analysis concepts to include HPC center resources

Project ID: rwth0619

ALEXANDER SCHMIDT,
ANDREAS NOWACK,
THOMAS KRESS,
III. Physikalisches Institut B,
RWTH Aachen University

MANUEL GIFFELS,
GÜNTER QUAST,
FLORIAN VON CUBE,
Karlsruher Institut für Technologie, KIT,
Karlsruhe, Germany

ALEXANDER JUNG, III.
Physikalisches Institut A,
RWTH Aachen University

Project Report

Over the last twenty years, the CMS experiment and its partner experiment ATLAS at the Large Hadron Collider (LHC) at CERN have published more than 1,500 scientific publications which are of unique relevance for the field of Elementary Particle Physics. A highlight was the discovery of the Higgs boson, predicted more than 50 years ago, leading to the Noble Prize for physics for Peter Higgs and Francois Englert in 2013.

The Worldwide LHC Computing Grid (WLCG) is a global collaboration of computer centres. It was launched in 2002 to provide a resource to store, distribute, and analyse the data generated by the LHC. The WLCG now links over 170 centres across 41 countries. These computer centres are arranged in “Tiers”, and together serve a community of over 8,000 physicists with near real-time access to LHC data. The Grid gives users the power to easily process, analyse, and in some cases to store LHC data.

The modern particle physics experiments are characterized by an ever increasing demand for computing and storage resources. Compared to 2016, the required resources are expected to increase by a factor of 60 until 2027. The computing hardware technology itself is expected to improve only by a factor 6--10 until 2027. One possibility to mitigate this gap is the more efficient use of resources. For this purpose, the integration of resources at HPC centers and elsewhere is investigated. The use of heterogeneous and opportunistic resources within the WLCG might represent an important step towards the future of LHC computing. It is technically facilitated by adapted computing models that do not require specifically pre-installed dedicated HEP software or homogeneous operating system landscapes. Through containerization, virtualisation, as well as intelligent resource and workflow management, we are now able to distribute even large computing campaigns over a heterogeneous set of computing resources which differ in location and architecture.

It was the purpose of this project to explore the integration of heterogeneous and opportunistic resources at the RWTH Aachen HPC center into the LHC computing Grid. Modern container technology like singularity has been used to provide the expected operating system and the WLCG software and middleware necessary to execute workloads of the CMS experiment. In order to guarantee always up-to-date container images, a sophisticated toolchain has been established. The construction manual, the so-called “Dockerfile”, and all necessary build scripts are hosted in a git repository. A continuous integration workflow ensures that Docker containers are built once a day and uploaded to a Docker registry. A service hosted by CERN pulls the Docker containers and converts them into the singularity sandbox format. Those singularity sandboxes are then distributed by the CERN Virtual Machine File System (CVMFS), a http based file system, in a most scalable way.

COBalD/TARDIS, a resource meta-scheduler developed at the Karlsruhe Institute of Technology is used to dynamically extend the existing WLCG Tier-2 center towards the CLAIX HPC cluster taken into account the utilization and suitability of the CLAIX compute nodes for the current mix of workflows processed at the WLCG Tier-2. The transparent extension of the WLCG Tier-2 is achieved by using COBalD/TARDIS to submit so-called pilot jobs via a ssh connection to the CLAIX login node into the CLAIX Slurm workload manager. Those pilot jobs are placeholder jobs reserving the compute node and calling back to HTCondor batch system at the WLCG Tier-2 to fetch workload, which in that case is acting as an so-called overlay batch system. The utilization of such pilots jobs is a well-known concept used in the WLCG. It was adapted to not only reserve the compute node in this project, but also ensuring that the CMS workload runs in the expected software environment by encapsulating it inside the aforementioned singularity container. An illustration of this setup is shown in the Figure below.

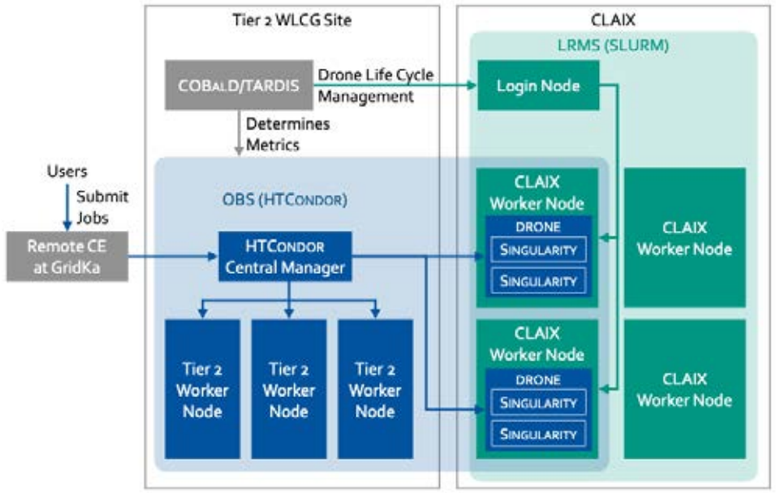

In this project the system described above has been developed and successfully deployed. In future projects, the scalability in a production scenario will be investigated.

Selected national and international cooperations

- CERN, Geneva, Switzerland
- CMS Collaboration (3100 physicists from 240 institutes in 54 countries)

Natural Sciences

Natural Sciences - Statistical Physics, Soft Matter, Biological Physics, Nonlinear Dynamics | DFG 310

Microgels at the interfaces

Project ID: bund0007

IGOR I. POTEMKIN,
DWI,
RUSTAM A. GUMEROV,
IVAN V. PORTNOV,
DWI – Leibniz-Institut für Interaktive Materialien e.V, Germany

Project Report

Within the period of the project, we have completed two tasks.
In the first and major task, we studied the monolayers of hollow microgels with a spherical cavity adsorbed at the liquid/liquid interface by large-scale dissipative particle dynamics (DPD) simulations. One liquid, named water, was always considered a good solvent, while the microgel solubility in the second liquid, named oil, was varied.

The symmetric and asymmetric cases of weak and strong differences in solubility between microgels and the liquids were considered. The effects of the cavity size on the structure, arrangement, and ordering of the microgels within the monolayer at different compression degrees have been revealed. The simulation systems contained 24 microgel particles at the interface and the total number of simulated DPD beads was over 8 millions.

The results demonstrated the important role of the cavity in the shape and volume changes of the individual microgels upon compression. In particular, the compression of the monolayer lead to the decrease of the lateral size of the microgels, accompanied by the shape transformation of the individual soft particles (a gradual change from flattened to the oblate form in respect to the interface). Moreover, unlike regular microgels, positioning of the microgels concerning the interface is determined by the solvent filling the cavity space.

The polymer concentration profiles plotted along the normal to the interface revealed a non-monotonous shape with a sharp maximum at the interface and tail towards the liquid phase, which fills the cavity. We demonstrated that the route of adsorption of hollow microgels at the liquid/liquid interface could predefine the structure of the monolayer. An important discovery is that in the symmetric case it is possible to produce a monolayer in which one part of the microgels faces the aqueous phase and the other part – the oil phase (Figure 1). Controlling the route of adsorption of hollow microgels it could be possible to predefine the structure of the monolayer. Moreover, the ratio between the microgels faced to the aqueous and oil phases can be kept constant independently of the compression degree of the monolayer.

In the second task, we studied the behavior of arborescent polymers of high generations at the liquid interface using DPD simulations (Figure 2). Initially, we constructed the polymer models based on the generation-based scheme and found that in a good solvent the mass-size dependence $R_g(M)$ of the such macromolecules is similar to the hard colloids ($R_g \sim M^{1/3}$). The results has a nice correlation with the experimental results for arborescent copolymers based on ethylene glycol methylether acrylate (EGMEA) and hydroxyl ethyl acrylate (HEA) using single electron transfer living radical polymerization (SET-LRP).

At the same time, we found that the adsorption of macromolecules to the water-toluene interface results in their strong deformations and flattening leading to an almost two-dimensional conformation (Figure 2B). The results correlated both with the tensiomentry results (Figure 2A) and with the images of atomic force microscopy at the mica surface. Overall, we demonstrated that such polymer-colloid duality of newly obtained highly branched macromolecules with molecular mass closer to microgels (but much softer) can find its application in the efficient emulsion stabilization or the obtaining of ultra-thin coatings with anti-fouling properties.

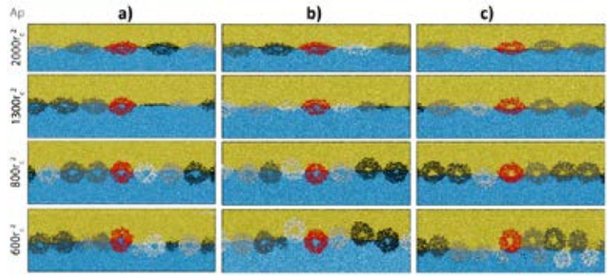

Figure 1. Side view simulation snapshots of hollow microgel monolayers at the liquid interface with hole size equal to 0.3 of a radius of swollen particle (in a solution) and different degree of compressions (measured in area per particles Ap, the smaller the Ap the stronger the compression) and at adsorption scenarios: adsorption from water (a), disproportional (b) and proportional (c) adsorption. For convenience, each microgel colored individually, and water and oil beads are respectively shown in blue and yellow.

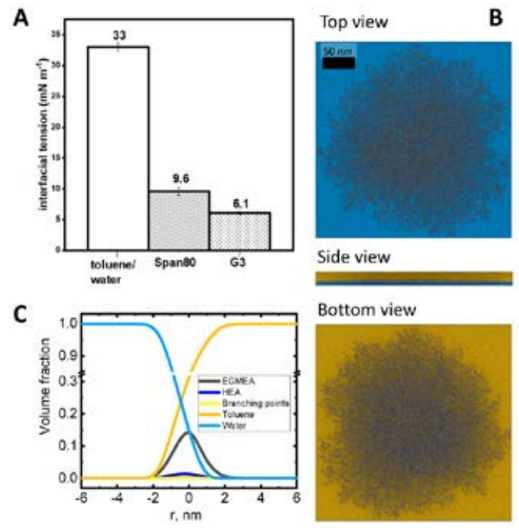

Figure 2.
A) interfacial tension between water and toluene using spinning drop method. From left to right: water and toluene before and after the addition of 1 mg*ml-1 surfactants; Span80, G3 arb. Polymer

B) Simulation snapshots of single G3 arborescent polymer at toluene/water interface at different views;

C) corresponding concentration profiles along the normal to the liquid interface.

Selected national and international cooperations

· WALTER RICHTERING, IPC, RWTH Aachen University

Natural Sciences

Natural Sciences - Statistical Physics, Soft Matter, Biological Physics, Nonlinear Dynamics | DFG 310

Structure-based drug design for the human NEET proteins: a novel target for progressive neurological diseases.

Project ID: rwth0623

PAOLO CARLONI,
Department of Physics,
RWTH Aachen University
Computational Biomedicine,
Institute of Advanced Simulation (IAS-5)
and Institute of Neuroscience and
Medicine (INM-9),
Forschungszentrum Jülich
JARA Institute: Molecular Neuroscience
and Imaging, Institute of Neuroscience
and Medicine (INM-11),
Forschungszentrum Jülich

KE ZUO,
Henri-Baptiste Marjault,
Department of Physics,
RWTH Aachen University
The Alexander Silberman Institute
of Life Science,
The Hebrew University of Jerusalem, Israel

RACHEL NECHUSHTAI,
The Alexander Silberman Institute
of Life Science,
The Hebrew University of Jerusalem, Israel

EMILIANO IPPOLITI,
Institute of Advanced Simulation (IAS-5)
and Institute of Neuroscience and
Medicine (INM-9),
Forschungszentrum Jülich

GIULIA ROSSETTI,
Institute of Advanced Simulation (IAS-5)
and Institute of Neuroscience and
Medicine INM-9,
Forschungszentrum Jülich,
Supercomputing Center (JSC),
Forschungszentrum Jülich, Germany;
Department of Neurology,
University Hospital Aachen (UKA),
RWTH Aachen University

RICCARDO CAPELLI,
Department of Applied Science
and Technology,
Politecnico di Torino, Italy

GIA LINH HOANG,
Institute of Neuroscience
and Medicine (INM-11),
Forschungszentrum Jülich, Germany

Project Report

Human NEET proteins such as mNT and NAF-1 release [2Fe-2S] clusters for their biological function. They exist in two redox states. Aberrant release is associated with many pathologies [1], such as neurodegenerative diseases [2-5] and cancer [1,6]. Thus, the human NEET proteins constitute an attractive new target for pharmaceutical intervention [2], especially for drugs that can modulate the lability of the [2Fe-2S] cluster of the NEET protein.

As a first step, we investigated the differences between the oxidized and reduced mNT in silico and in vitro. Quantum chemical calculations on all available human NEET protein structures suggest that reducing the cluster weakens the Fe–N_{His} and Fe–S_{Cys} bonds, similar to what is seen in other Fe–S proteins (e.g., ferredoxin and Rieske protein). We further show that the extra electron in the $[2Fe–2S]^{+}$ clusters of one of the NEET proteins (mNT) is localized on the His-bound iron ion, consistently with our previous spectroscopic studies. Kinetic measurements demonstrate that the mNT $[2Fe–2S]^{+}$ is released only by an increase in temperature. Thus, the reduced state of human NEET proteins [2Fe–2S] cluster is kinetically inert.

This previously unrecognized kinetic inertness of the reduced state, along with the reactivity of the oxidized state, is unique across all [2Fe–2S] proteins. Finally, using a coevolutionary analysis, along with molecular dynamics simulations, we provide insight on the observed allostery between the loop L2 and the cluster region. Specifically, we show that W75, R76, K78, K79, F82 and G85 in the latter region share similar allosteric characteristics in both redox states [7]. Next, we studied the binding of ligands towards mNT. We employed an enhanced sampling method, namely volume-based metadynamics, to predict binding poses and affinities of NEET protein ligands (including furosemide), for which the binding pose is known experimentally by X-ray crystallography.

Fig. 1 shows the binding of furosemide to mNT [8]. Our calculations provide the complete free energy landscape associated with ligand binding and they are in agreement with experimentally measured affinities. One paper has been published on this (LH. Gia, J. Goßen, R. Capelli, et al. Multiple Poses and Thermodynamics of Ligands Targeting Protein Surfaces: The Case of Furosemide Binding to mitoNEET in Aqueous Solution. Front Cell Dev Biol, 2022, in press), and another one is in preparation. We are now extending our investigation to the other important NEET protein target, namely NAF-1. This part of the work is now supported by the NHR project: p0020134.

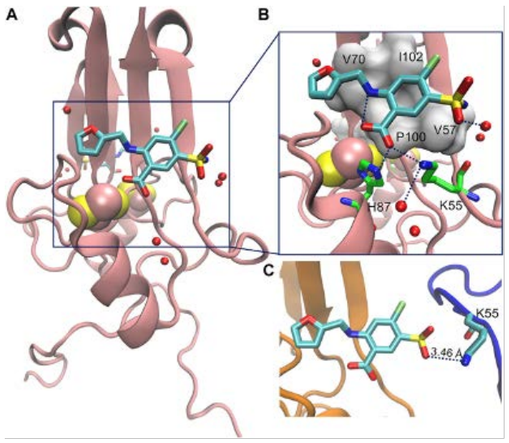

Fig. 1. (A) Crystal structure of ligand furosemide binding to mitoNEET protein at pH 7.0. (B) Close up showing furosemide-protein H-bonds/salt bridges interactions. (C) Interactions of the ligand with the protein image (in blue color) in the crystal.

References

[1] TAMIR S, PADDOCK ML, DARASH-YAHANA-BARAM M, et al. Structure-function analysis of NEET proteins uncovers their role as key regulators of iron and ROS homeostasis in health and disease, Biochim Biophys Acta, 1853 (2015) 1294-1315.

[2] GELDENHUYS WJ, YOUDIM MB, CARROLL RT, et al. The emergence of designed multiple ligands for neurodegenerative disorders, Prog Neurobiol, 94 (2011) 347-359.

[3] OKATSU K, IEMURA S, KOYANO F, et al. Mitochondrial hexokinase HKI is a novel substrate of the Parkin ubiquitin ligase, Biochem Bioph Res Co, 428 (2012) 197-202.

[4] CHEN YF, CHOU TY, LIN IH, et al. Upregulation of Cisd2 attenuates Alzheimer's related neuronal loss in mice, J Pathol, 250 (2019) 299-311.

[5] GELDENHUYS WJ, BENKOVIC SA, LIN L, et al. MitoNEET (CISD1) Knockout Mice Show Signs of Striatal Mitochondrial Dysfunction and a Parkinson's Disease Phenotype, Acs Chem Neurosci, 8 (2017) 2759-2765.

[6] DARASH-YAHANA M, POZNIAK Y, Lu M, et al. Breast cancer tumorigenicity is dependent on high expression levels of NAF-1 and the lability of its Fe-S clusters, Proc Natl Acad Sci U S A, 113 (2016) 10890-10895.

[7] ZUO K, MARJAULT HB, BREN KL, ET AL. The two redox states of the human NEET proteins' [2Fe–2S] clusters, JBIC J Biol Inorg Chem, 26 (2021) 763–774.

[8] GELDENHUYS WJ, LONG TE, SARALKAR P, et al. Crystal structure of the mitochondrial protein mitoNEET bound to a benze-sulfonide ligand, Commun Chem, 2 (2019) 77.

Selected national and international cooperations

- RACHEL NECHUSHTAI, The Alexander Silberman Institute of Life Science, The Hebrew University of Jerusalem, Jerusalem, Israel
- RICCARDO CAPELLI, Department of Applied Science and Technology, Politecnico di Torino, Italy

Publications

- ZUO K, MARJAULT HB, BREN KL, ROSSETTI G, NECHUSHTAI R, CARLONI P.
The two redox states of the human NEET proteins' [2Fe–2S] clusters.
JBIC J. Biol. Inorg. Chem. 2021, 26, 763–774.

Natural Sciences

Natural Sciences - Statistical Physics, Soft Matter, Biological Physics, Nonlinear Dynamics | DFG 310

Metadynamics-based design of ligands targeting COVID-19 3CLPRO main protease with high potency and increased residence time

Project ID: rwth0637

PAOLO CARLONI,
Department of Physics, RWTH Aachen University, Computational Biomedicine, Institute of Advanced Simulation (IAS-5) and Institute of Neuroscience and Medicine (INM-9), Forschungszentrum Jülich, Germany; JARA Institute: Molecular Neuroscience and Imaging, Institute of Neuroscience and Medicine (INM-11), Forschungszentrum Jülich, Germany

GIULIA ROSSETTI,
Institute of Advanced Simulation (IAS-5) and Institute of Neuroscience and Medicine (INM-9), Forschungszentrum Jülich, Germany; Jülich Supercomputing Center (JSC), Forschungszentrum Jülich, Germany; Department of Neurology, University Hospital Aachen (UKA), RWTH Aachen University

SIMONE ALBANI,
Faculty of Mathematics, Computer Science and Natural Sciences, RWTH Aachen University, Institute of Advanced Simulation (IAS-5) and Institute of Neuroscience and Medicine (INM-9), Forschungszentrum Jülich, Germany

LINH GIA HOANG,
Institute of Neuroscience and Medicine (INM-11), Forschungszentrum Jülich, Germany

EMILIANO IPPOLITI,
Institute of Advanced Simulation (IAS-5) and Institute of Neuroscience and Medicine (INM-9), Forschungszentrum Jülich, Germany

Project Report

We investigated the binding of the ligand X77 to SARS-CoV-2 main protease, based on the available structural information of the complex (Figure 1) (PDB: 6W63, 7Q5M, 7PHZ).

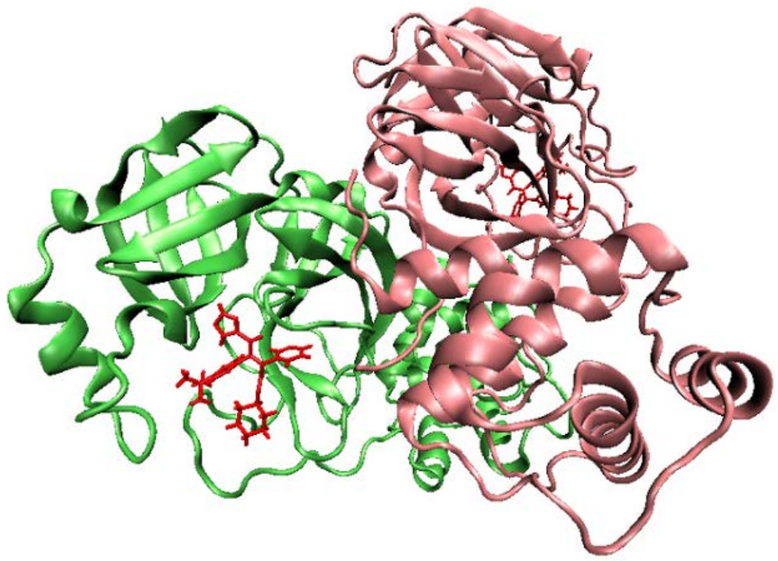

Figure 1. One crystal structure of ligand X77 binding SARS-CoV-2 main protease from Protein Data Bank (PDB ID: 6W63)

We performed a variety of metadynamics enhanced sampling simulations using different variants of the approach: well-tempered metadynamics [1], localized volumed-based metadynamics (LV-METAD) [2] and OPES [3]. The calculations were preceded by submicrosecond standard molecular dynamics simulations to equilibrate the systems (Figure 2).

The calculations were based on the Amberff14SB force field [4].

The calculations have led to a detailed prediction of the free energy landscape associated with ligand binding. In particular, we find the presence of several meta-stable poses, which are currently being analyzed. Our predicted affinity will be compared with the experimental data measured by our collaborator Prof. A. Zaliani (Fraunhofer). A paper reporting this research will be submitted soon.

Figure 2. Snapshot of the simulation box in a molecular dynamics simulation performed in this project

References

[1] BARDUCCI A, BUSSI G, PARRINELLO M. (2008). Well-tempered metadynamics: a smoothly converging and tunable free-energy method. Physical review letters, 100(2), 020603. https://doi.org/10.1103/PhysRevLett.100.020603

[2] ZHAO Q, CAPELLI R, CARLONI P, LÜSCHER B, LI J, ROSSETTI G. (2021). Enhaced Sampling Approach to the Induced-Fit Docking Problem in Protein-Ligand Binding: The Case of Mono-ADP-Ribosylation Hydrolase Inhibitors. Journal of chemical theory and computation, 17(12), 7899–7911. https://doi.org/10.1021/acs.jctc.1c00649

[3] INVERNIZZI M, PARRINELLO M. Rethinking metadynamics: From bias potentials to probability distributions. The Journal of Physical Chemistry Letters, 11(7):2731–2736, 2020.

[4] MAIER JA, MARTINEZ C, KASAVAJHALA K, WICKSTROM L, HAUSER KE, SIMMERLING C. 2015). ff14SB: Improving the Accuracy of Protein Side Chain and Backbone Parameters from ff99SB. Journal of chemical theory and computation, 11(8), 3696–3713. https://doi.org/10.1021/acs.jctc.5b00255

Selected national and international cooperations

- PROF. ZALIANI, Fraunhofer Institute for Translational Medicine and Pharmacology (ITMP), Hamburg, Germany

Statistical Physics, Soft Matter, Biological Physics, Nonlinear Dynamics | DFG 310

Ab-initio study of the inherent structures and the configurational entropy of liquid phase-change materials

Project ID: jara0214

RICCARDO MAZZARELLO,
Institute for Theoretical Solid State Physics, RWTH Aachen University

Current affiliation:
Sapienza University of Rome, Department of Physics, Rome, Italy

YAZHI XU,
VALENTIN EVANG,
Institute for Theoretical Solid State Physics, RWTH Aachen University

MATTHIAS WUTTIG,
I. Institute of Physics (IA), RWTH Aachen University

Project Report

We have carried out two main projects using the computational resources from JARA0214. Both projects deal with the kinetic properties of the liquid and amorphous state of phase-change materials (PCMs) [i]. The first project has focused on the crystallization of GeSb2Te4, an important PCM used in non-volatile, electronic memory devices (phase-change memories) and rewritable Blu-Ray discs [1-3]. We have performed ab initio molecular dynamics (AIMD) crystallization simulations using nanometer-scale (>1,000 atoms) models over one nanosecond, representing the largest-scale AIMD simulation of PCMs to date. We have developed a novel protocol based on the smooth overlap atomic population (SOAP) kernel method [iv] to examine the trajectories and elucidate atomic details during rapid crystallization. We have recently submitted a manuscript about this project to Advanced Materials, in which our AIMD simulations of crystallization have been combined with a theoretical analysis of the electronic properties of the resulting crystalline models [4]. Project 2 is devoted to the computational investigation of the potential energy landscape (PES) of supercooled liquid PCMs, starting from $Ge_2Sb_2Te_5$. Such investigation is crucial to understand the properties of the supercooled liquid phase and of the glass transition. Finally, some computing time of this JARA project was used to finalize simulations for a project on point defects in PbSbTe alloys, which has recently been published in Advanced Materials [5].

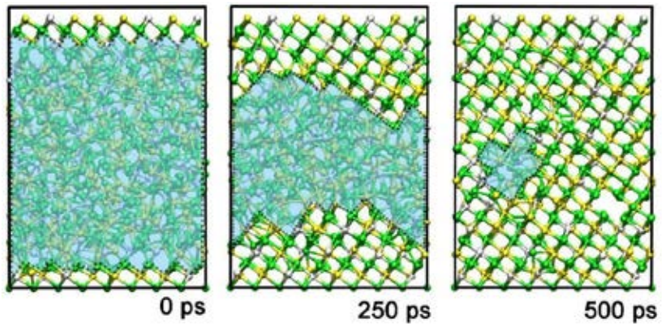

Figure 1. Snapshots of the ab initio crystallization of a 1,008-atom model of the $GeSb_2Te_4$ phase-change material. The system was first melted and then quenched to 300 K keeping two (111) crystalline layers fixed to create a planar amorphous–crystalline interface. Afterwards, the models was re-heated at ~630 K, at which it crystallized into a cubic rocksalt phase in less than 600 ps.

References:

[1] RAOUX S, WEŁNIC W, IELMINI D. Chem. Rev. 110, 240 (2010).

[2] ZHANG W, MAZZARELLO R, WUTTIG M, MA E. Nat. Rev. Mater. 4, 150 (2019).

[3] CHOE J. Intel 3D XPoint Memory Die Removed from Intel Optane PCM (Phase Change Memory), https://www.techinsights.com/blog/intel-3d-xpoint-memory-die-removed-intel-optanetm-pcmphase-change-memory/ (accessed: October 2020).

[4] XU Y, ZHOU Y, WANG X, ZHANG W, MA E, DERINGER VL, MAZZARELLO R. "Unraveling Crystallization Mechanisms and Electronic Structure of Phase-Change Materials by Large-Scale Ab Initio Simulations", Adv. Mater. 34, 2109139 (2022).

[5] EVANG V, REINDL J, SCHÄFER L, ROCHOTZKI A, PLETZER-ZELGERT P, WUTTIG M, MAZZARELLO R. "Thermally Controlled Charge-Carrier Transitions in Disordered PbSbTe Chalcogenides", Adv. Mater. 34, 2106868 (2022).

Selected national and international cooperations

- WEI ZHANG, Xi'an Jiaotong University, Xi'an, China
- MARCO BERNASCONI, University of Milano-Bicocca, Milan, Italy

Natural Sciences

Statistical Physics, Soft Matter, Biological Physics, Nonlinear Dynamics | DFG 310

Tissue Growth and Evolution

Project ID: rwth0475

JENS ELGETI, JOHANNES KRÄMER,
Institute of Biological Information Processing, Theoretical Physics of Living matter (IBI-5/las-2), Forschungszentrum Jülich, Germany

Project Report

During 2021 a long period of time the project was on hold, due to a shortage of staff caused by "Basisbetrieb" at FZ Juelich, and a delay in hiring and onboarding new doctoral researchers. Thus, most of the granted resources where not used, and results are accordingly limited. This was already reported to the IT desk, and a short term extension until end of February 2022 has been granted.

During the accounting period in 2021, we studied the dynamics of tissue generated from a single stem cell. The standard picture of tissue renewal from by stem cells is, that the stem cell divides asymetrically, generating a transient amplifying cell (TA cell). These TA cells divide rapidly, but a limited number of times, finally differentiating into non-dividing cells. We found that, due to the inhomogeneous cell generation within the tissue results in a surprisingly dynamic motion of the stem cell. The rapidly growing TA cell population resides asymetrically to the stem cell pushing the cell around, resulting in large directed displacements.

Furthermore, we performed preliminary simulations on the interaction of two stem cells. The inhomogeneous cell division within the tissue was found to cause a repulsive interaction between stem cells, and their respective cell population.

A second project on Tissue motility based on the highlight result of 2020, the "liquid-vacuum-coexistence" for self propelled cells, resulted in a publication.

We found that our model of selfpropelled Brownian particles with extended interactons results in a fluid like cell colony, where however no cell escapes. Our siumalations show many characteristica of observations made in in vitro experiments on MDCK colonies such as exactly this "liquid-vaccum coexistence" and an overall tension in the colony center. Furthermore, such colonies also display long-range correlations in the local velocity field, which we did not observe in our model initially. We thus proposed an additional velocity alignment interaction, which acts to align the current velocity with the propulsion direction. This results in enhanced coordinated motion of cells, with swirls forming in the center of the colony. The velocity alignment interaction furthermore results in the formation of fingers at the periphery of the colony with strong outward alignment of the cell velocities, reminiscent of growth of real MDCK-Cell colonies.

Publications

- SARKAR D, GOMPPER G, ELGETI J. "A minimal model for structure, dynamics, and tension of monolayered cell colonies"; Communications Physics 4, Article number: 36(2021); http://dx.doi.org/10.1038/s42005-020-00515-x

Natural Sciences

Astronomy and Astrophysics | DFG 311

Cosmic-ray Physics with the AMS Experiment on the International Space Station

Project ID: jara0052

HENNING GAST,
STEFAN SCHAEL,
ROBIN SONNABEND,
LEILA ALI CAVASONZA,
SOFIA CHOURIDOU,
CHAN HOON CHUNG,
THOMAS KIRN,
MANBING LI,
SICHEN LI,
KLAUS LÜBELSMEYER,
FABIAN MACHATE,
NIKOLAY NIKONOV,
GEORG SCHWERING,
THORSTEN SIEDENBURG,
VALERY ZHUKOV
Department of Physics,
Institute I B,
RWTH Aachen University

Project Report

© NASA

The Alpha Magnetic Spectrometer (AMS) a detector designed for precision spectroscopy of cosmic rays that was installed on the International Space Station (ISS) in May 2011. With dimensions of 5x4x3 m³ and a weight of 7.5 tons, AMS is the largest cosmic-ray spectrometer ever built. Its construction began in 1995, and a successful prototype flight aboard the Space Shuttle Discovery proved the feasibility of the detector concept in 1998. Led by Nobel laureate Professor Samuel Ting from MIT, AMS has been constructed and is now operated by an international collaboration of more than 200 scientists and engineers, from Europe, America and Asia. The overall construction costs, including the flight of AMS to the Space Station aboard Space Shuttle Endeavour, have amounted to 1.5 billion US dollars. AMS is the only magnet spectrometer in space and the largest instrument for basic research on the ISS. In Germany, RWTH Aachen has been strongly involved in the AMS project since its inception. One of the main components of AMS, the transition radiation detector (TRD), has been designed and constructed by the I. Physikalisches Institut B under the direction of Professor Stefan Schael. Today, the Aachen group, comprising 20 scientists and students, plays a major role in the analysis of the data gathered by AMS and in the operation and calibration of the instrument.

Since their discovery in 1912, cosmic rays have held many surprises in stock for us, from the discovery of new elementary particles to the most violent processes taking place in the Universe and accelerating cosmic rays to enormous energies. As a multi-purpose instrument for the precision spectroscopy of cosmic rays, AMS was conceived to answer fundamental questions about our Universe: What is the nature of Dark Matter? What happened to the antimatter that must have been produced in the Big Bang? Where are cosmic rays accelerated and how do they propagate through the Milky Way? Answers to these questions will have a profound impact on our understanding about the inner workings of our Universe and help advance fundamental science. In particular, the search for dark matter complements the search for new elementary particles at the Large Hadron Collider (LHC) at CERN, Geneva.

AMS has recorded 200 billion individual particle crossings (called “events”), more than all previous cosmic-ray experiments combined. The raw data volume collected is on the order of 40 TB per year. AMS employs redundant subdetectors for particle identification and for energy or momentum measurements: the TRD, an electromagnetic calorimeter (ECAL), a ring-imaging Cherenkov counter (RICH), a silicon tracker and a time-of-flight system (TOF). Before any physics analysis of the data can be performed, the information from all these subdetectors has to be pieced together and complicated reconstruction algorithms have to be run for each of them. The resulting high-level data serves as the input for physics analyses and occupies a volume of 160 TB per year of AMS flight on disk. HPC resources are vital for the processing, calibration, and analysis of this enormous dataset.

Over twenty publications from the AMS collaboration have appeared in the renowned Physical Review Letters, twelve of which have been selected as an Editor’s suggestion. The findings have received considerable attention among astrophysicists and triggered an enormous amount of theoretical work.

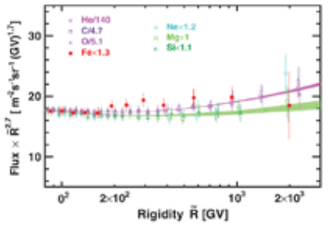

Figure 2: The rigidity dependence of the Fe flux compared with the rigidity dependence of the He, C, and O fluxes and the Ne,Mg, and Si fluxes above 80.5 GV. For display purposes only, the He, C, O, Ne, Si, and Fe fluxes were rescaled as indicated. (From Ref. [4])

The physics highlight of AMS in 2021 was the detailed study of several species of heavy ions in cosmic rays. Surprisingly, it was found that iron belongs to the He-C-O group of primary cosmic rays, but behaves differently than the Ne-Mg-Si group of primaries, even though it is closer in mass to the latter (Fig. 2). In addition, the study of the heavy secondary flourine revealed that there are two classes of secondary cosmic rays. Sodium and aluminum were found to fall into the same group of elements as nitrogen: they are well described as the sum of a primary and a secondary component.

The PhD thesis of Fabian Machate was defended in October 2021. It describes a study for a large acceptance analysis that allows the determination of electron fluxes with daily time resolution. It shows that significant short-term variations are visible in the daily electron fluxes up to ~20 GV.

Selected conference participations

- HENNING GAST, Properties of Light Primary and Secondary Cosmic Rays He-C-O and Li-Be-B Measured with the AMS on the ISS, 37th International Cosmic Ray Conference, Berlin, Germany, July 12-23, 2021
- STEFAN SCHAEL, New results from AMS-02 on the International Space Station and perspectives for AMS-100 at Lagrange Point 2, Queen’s University, Canada, November 26, 2021

Selected national and international cooperations

- PROFESSOR SAMUEL C. C. TING, Massachusetts Institute of Technology, USA
- PROFESSOR JAVIER BERDUGO, Centro de Investigaciones Energéticas, Medioambientales y Tecnológicas (CIEMAT), Spain
- PROFESSOR BRUNA BERTUCCI, INFN and University of Perugia, Italy
- PROFESSOR BERND HEBER, Christian-Albrechts-Universität zu Kiel, Germany
- PROFESSOR WEIWEI XU, Shandong Institute of Advanced Technology, China

Publications

- AGUILAR M ET AL. Periodicities in the Daily Proton Fluxes from 2011 to 2019 Measured by the Alpha Magnetic Spectrometer on the International Space Station from 1 to 100 GV, Phys. Rev. Lett. 127 (2021) 271102, DOI:https://doi.org/10.1103/PhysRevLett.127.271102
- AGUILAR M ET AL. Properties of a New Group of Cosmic Nuclei: Results from the Alpha Magnetic Spectrometer on Sodium, Aluminum, and Nitrogen, Phys. Rev. Lett. 127 (2021) 021101, DOI:https://doi.org/10.1103/PhysRevLett.127.021101; Erratum Phys. Rev. Lett. 127 (2021) 159901
- AGUILAR M ET AL. Properties of Heavy Secondary Fluorine Cosmic Rays: Results from the Alpha Magnetic Spectrometer, Phys. Rev. Lett. 126 (2021) 081102, DOI:https://doi.org/10.1103/PhysRevLett.126.081102
- AGUILAR M ET AL. Properties of Iron Primary Cosmic Rays: Results from the Alpha Magnetic Spectrometer, Phys. Rev. Lett. 126 (2021) 041104, DOI:https://doi.org/10.1103/PhysRevLett.126.041104
- MACHATE F. Study for large acceptance electron analysis with the Alpha Magnetic Spectrometer on the International Space Station, Dissertation, RWTH Aachen University (2021)

Engineering Sciences

Picture: Pexels

Engineering Sciences

Mechanics | DFG 402

Investigation of the 3D instationary flow in linear turbine cascade using scale resolving simulations

Project ID: jara0217
STEFAN HENNINGER,
NIMA FARD AFSHAR,
Institute of Jet Propulsion and Turbomachinery,
RWTH Aachen University

Project Report

Sub-project 1

The goal of this sub-project is to find the right trade-off regarding the mesh quality and computing cost. The mesh requirement for Hybrid RANS-LES (HRLES) methodologies, in which the RANS layer alleviates the harsh grid requirements, is studied. For the 3D simulation of cascade flow, the boundary layer on the blade and the boundary layer on the side walls are of special interest. Here the mesh density/quality shouldn't be as high as for wall-resolving LES calculations, but higher than the best practice RANS recommendations.

The first operating point (Re=90k) is used to quantify the mesh resolution. For this purpose, two meshes have been investigated with accordingly 32 and 55 million cells, based on the estimations in the literature for the appropriate non-dimensional wall plus values and where 90% of turbulent kinetic energy is resolved.

The IDDES simulations show a stronger dependency on the mesh resolution than SAS, which is inherently related to the formulations of the corresponding method.

Another aspect, closely related to the sub-project 2 is the ratio between the prescribed turbulent length scale and the grid width (l_t/max (Δx,Δy,Δz). Since the synthetic turbulence generator (STG) used for the simulations is prescribed as a combination of l_t and Reynolds stress tensor at the inlet, the mesh requirements for a correct turbulent decay are closely coupled to the prescribed l_t. The studies showed the necessity of a minimum ratio of 15 for l_t/max (Δx,Δy,Δz). Increasing the mentioned ratio (l_t/max (Δx,Δy,Δz) = 40) decreases the influence of the subgrid-stresses in the freestream and assures more LES content on the incoming turbulence. Although for the remaining studies the mesh with the ratio 15 was found to be satisfactory and was therefore used.

The studies showed that the coarse grid was not able to satisfy the criterion mentioned above fully and therefore will not be used further.

Sub-project 2

In sub-project 2 the STG based on the superposition of Fourier modes, implemented in TRACE, was tested on two different types of boundary conditions namely Riemann and unsteady 1d characteristic boundary conditions. The tests on the Riemann boundary condition in combination with the STG, showed the correct behavior regarding the turbulence generation, unlike the results of the unsteady 1d characteristic boundary conditions. Therefore, the Riemann boundary condition has been used for the remaining calculations.

Additionally, the turbulent boundary condition was quantified in terms of the correct turbulent decay. The combination of l_t and Reynolds stress tensor were chosen to reproduce the correct turbulent intensity decay according to the experimental values.As in sub-project 1., also here the calculations are limited to the first operating point Re= 90 k.

Sub-project 3

In subproject-3 both operating points Re=90k and Re=200k have been investigated via IDDES and SAS methods. The lower Reynolds number consist of a separation bubble which reattaches near the trailing edge. This Reynolds number includes a separation induced transition and is only fully captured when a transition model is activated. IDDES with transition model activated in RANS-mode is able to reproduce the pressure distribution correctly. When the transition model is deactivated, the pressure distribution doesn't agree with the measurements and therefore the transition onset point and separation is not predicted correctly. The IDDES results show a slightly better trend than RANS regarding the total pressure wake loss but not as good as LES results performed in the sub-project 4. SAS is not able to predict the separation accurately. Also, the predicted total pressure wake loss is less accurate than IDDES and closer to RANS values.

The higher Reynolds number Re=200k, which is the design point of this profile, also features a separation bubble. At this operating point, as a consequence of the higher turbulent content, the separation bubble is smaller and reattaches earlier on the suction side.

IDDES result (with and without transition model) at Re=200k don't perform as good as at the lower Reynolds number, when comparing the blade pressure distribution to measurements. This emphasizes the necessity to further improve and calibrate the transition modelling within the framework of IDDES. The SAS method shows, on the other hand, better results than IDDES Re=200k. This drawback should be investigated further in future projects.

Sub-project 4

In sub-project 4 two goals are pursued. The first goal, is to investigate the flow field of the low-pressure turbine with a more detailed approach, namely a wall resolving LES method. For this purpose, the WALE Subgrid Scale (SGS) model is used. The second goal is to provide reference data for the validation of the hybrid RANS/LES results achieved in the previous sub-projects. Additionally, the results are compared against measurements carried out in a high-speed linear cascade wind tunnel at the Bundeswehr University Munich.

In the first place, the turbulent boundary condition was quantified in terms of the correct turbulent decay, as in sub-project 2, which was done for HRLES. The combination of l_t and Reynolds stress tensor were chosen to reproduce the correct turbulent intensity decay according to the experimental values. Besides the turbulent decay another key factor here is to prescribe the correct endwall boundary layer compared to measurements. For this purpose, the boundary layer thickness and skin-friction Reynolds number are compared to experimental values. A correct prescription of the endwall boundary wall has been shown to be important to predict the wake loss and passage flow further downstream. The results of the LES-WALE simulation show a very promising match regarding the aerodynamic criteria such blade loading, pressure distribution and total pressure wake loss in the mid-section.

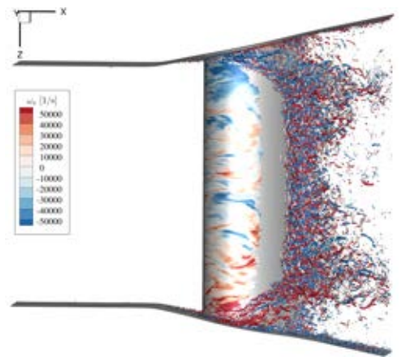

Selected conference participations

- NIMA FARD AFSHAR, High-Order Implicit Large Eddy Simulation of Flow over a Low-Reynolds Turbine Cascade, PyFR Seminar series online, July 15, 2021
- NIMA FARD AFSHAR, High-Order Implicit Large Eddy Simulation of Flow over a Low-Reynolds Turbine Cascade, HiFiLeD (2nd High-Fidelity Industrial LES/DNS Symposium) online, September 22-24, 2021

Selected national and international cooperations

- Peter Vincent, Imperial College, London, England
- Patrick Bechlars, MTU Aero Engines AG, Munich, Germany
- Christian Morsbach, German Aerospace Center (DLR), Cologne, Germany

Engineering Sciences

Mechanics | DFG 402

Investigation of the flow in a linear high pressure compressor cascade using scale resolving Simulations

Project ID: rwth0555
STEFAN HENNINGER,
NIMA FARD AFSHAR
Institute of Jet Propulsion and Turbomachinery,
RWTH Aachen University

Project Report

Hybrid RANS/LES (HRLES) is one SRS category, which bridges the gap between RANS and LES in regard to prediction accuracy of the results and required computing resources. The HRLES methods (i.e. various Detached Eddy Simulation (DES) formulations), with RANS modelling of the flow near the wall, and eddy-resolving simulation away from the wall, are believed to represent the mixing in turbulent flows and other secondary flow features formed in the end wall regions better than the state-of-the-art RANS.

The major goals targeted within this project can be concluded as follows:

1. Quantify the suitability of HRLES methods (one method in specific) to accurately predict the 3D flow field of high-pressure compressor cascade operating at high Reynolds number.
2. Analyzing the 3D flow of the high-pressure compressor cascade in terms of secondary flow structures, boundary layer development and loss mechanism, especially in the wake field.

The first goal is important because such HRLES methods are a promising methodology for simulating flows with higher Reynolds numbers in the near future. The reason is that wall resolved LES for such Reynolds numbers is still challenging in terms of computing resources. The second goal is important because a thorough understanding of secondary (near-wall) flow, which has been mostly neglected in the past, will help designers develop more sophisticated designs. The focus of the current study is the high-pressure compressor cascade (HPC cascade) operated at the Institute of Jet Propulsion and Turbomachinery (IST) of the RWTH Aachen University.

There are three simulations (3 operating points) planned to be performed within this computing period.

The mesh study for the HRLES was based on three different meshes, which were used to quantify the required mesh elements to resolve the turbulent structures. Additionally, the Pope criteria, in which 80% of the turbulent kinetic energy should be resolved, was sought for in the free stream regions. The second mesh, which consist of 47 mio. mesh elements, was found to be a good compromise between accuracy and computing resources.

At the lowest Reynolds number 490,000, the HRLES results show marginal improvement regarding the total pressure loss in the wake at midspan. Both RANS and HRLES show an offset regarding the peak of the total pressure wake loss but the shape (width) of the wake loss fits very well with the measurements. The total pressure wake loss of HRLES show almost no improvement in the near wall area, compared to RANS results.

The blade pressure distribution of both simulations matches very well with measurements. The reason for the only marginal improvement of the HRLES in the wake area has been shown to be the mesh density and/or quality, especially in the near wall and trailing edge areas. A further mesh refinement in the near wall area will result in higher computing resources and is not justified for HRLES. The HRLES methodology used in this project, switches between RANS and LES based on the turbulent length scale ratio of the corresponding method (l_{RANS}/l_{IDDES}) and is therefore highly coupled with the near wall mesh density.

At the highest Reynolds number 790,000, the results show nearly the same trend as for the lower Reynolds number. Also, at this operating point, there is a good match between both RANS and HRLES and the measurements regarding the blade pressure distribution. Here, the experience from the previous simulations regarding the mesh quality was adapted to come up with a more sophisticated mesh quality. The HRLES results show a better agreement with the measurement results, when comparing the total pressure wake loss (both peak values and shape) at midspan. Unfortunately, also at this operating point, the losses in the near wall area show almost no improvement, compared to RANS results. Also, here the near wall mesh density is believed to be responsible for the failure of the method.

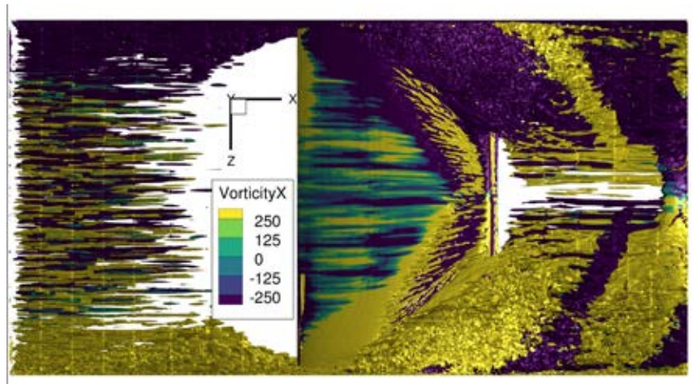

Selected national and international cooperations

- PATRICK BECHLARS, MTU Aero Engines AG, Munich, Germany
- CHRISTIAN MORSBACH, German Aerospace Center (DLR), Cologne, Germany

Mechanics | DFG 402

Phase field topology optimization to increase fracture toughness of thin shell structures

Project ID: rwth0625
KARSTEN PAUL,
ROGER SAUER,
MAREK BEHR
Chair for Computational Analysis of Technical Systems, RWTH Aachen University

Project Report

This work builds upon the research results stemming from two former compute projects, rwth0401 and rwth0433. Using the simulations performed in these compute projects, a phase field model for dynamic fracture of brittle shell structures has been developed. This framework has been further extended to model fracture on multi-patch shell structures.

The compute project rwth0625 has been mainly used in the year 2020, see also the progress report from 2020. During 2020, the models above have been studied more intensively to check for numerical robustness and efficiency. Further, this project's main aim was the development of a phase field approach for the topology optimization of shell structures. First, several phase separation processes with elastic misfit (solving for the phase field for a given elastic energy) have been carried out in 2021 using the compute resources from this project. The theory has then been extended to the coupled problem, in which it is simultaneously solved for the displacement and phase field, where the latter represents the geometry (e.g. phase 0 indicates void, and phase 1 indicates material). Already in this early stage of development, it became clear that the phase field approach is computationally too expensive for an efficient use in the context of topology optimization. This was proven theoretically, and supported by the computing time of the simulations. Thus, this idea was not pursued any longer, such that nearly no compute time was used in 2021 under this project. Also due to the Corona crisis, the research focus was then shifted from topology optimization of shell structures to the modeling of surface viscoelasticity, which is now pursued under compute project rwth0917.

Selected conference participations

- KARSTEN PAUL, CHRISTOPHER ZIMMERMANN, THANG X. DUONG, THOMAS J.R. HUGHES, CHAD M. LANDIS, KRANTHI K. MANDADAPU, ROGER A. SAUER, A phase field approach for dynamic brittle fracture of thin shell structures, 14th WCCM & ECCOMAS, Paris (virtual), January 11-15, 2021

- KARSTEN PAUL, THOMAS J.R. HUGHES, CHAD M. LANDIS, ROGER A. SAUER, Dynamic brittle fracture of thin shell structures based on a phase field approach, 16th USNCCM, Chicago (virtual), July 25-29, 2021

Selected national and international cooperations

- THOMAS J.R. HUGHES, Oden Institute of Computational Engineering and Sciences, UT Austin, Texas, USA
- CHAD M. LANDIS, Department of Aerospace Engineering and Engineering Mechanics, UT Austin, Texas, USA

Publications

- PAUL K, HUGHES TJR, LANDIS CM, SAUER RA, Dynamic Fracture of Brittle Shells in a Space-Time Adaptive Isogeometric Phase Field Framework, Current Trends and Open Problems in Computational Mechanics, Chapter 39, edited by Aldakheel F, Hudobivnik B, Soleimani M, Wessels H, Weißenfels C, Marino M, Springer International Publishing, in press

Heat Energy Technology, Thermal Machines, Fluid Mechanics | DFG 404

Investigation of the tip clearance flow in a linear compressor cascade using sale resolving simulations

Project ID: rwth0642
JOHANNES DEUTSCH
Institute of Jet Propulsion and Turbomachinery, RWTH Aachen University

Project Report

Tip clearance flows are responsible for around a third of the total losses in turbomachinery applications and are thus thoroughly investigated using experimental as well as computational methods. Within this computing project, we performed a simulation of the tip clearance flow in a compressor cascade using the Improved Delayed Detached Eddy Simulation (IDDES) method. For these simulations, we used the flow solver TRACE (Turbomachinery Research Aerodynamic Computational Environment) provided by the DLR's Institute of Propulsion Technology.

Within attached boundary layers, the IDDES method solves the unsteady Reynolds averaged Navier Stokes (RANS) equations and therefore models all turbulent fluctuations. In detached boundary layers, the turbulence is resolved following the approach of the Large Eddy Simulation (LES). The local switch between modelled and resolved turbulence is facilitated by a function that depends on the local resolution of the computational grid as well as the flow solution. Thus, the IDDES method can be categorized as seamless hybrid RANS/LES method.

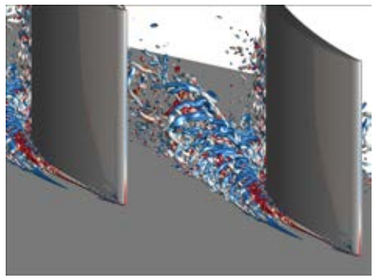

In the first period of the project, we derived the required mesh and time step resolution for the simulation of the full 3D domain. Therefore, we performed IDDES simulations with a domain reduced to the undisturbed flow in the blade passage. These simulations revealed a boundary layer separation that has not been reported in the experimental investigations. In consequence, we investigated the issue thoughtfully. It turned out that a bug in the flow solver that influenced the boundary layer protection caused the premature separation. With the fix applied, we did not observe a boundary layer separation.

In the second period, we performed the IDDES simulation of the tip clearance flow of the compressor cascade. The simulation took around 56 days on 912 cores on the compute cluster. We started the averaging of the flow quantities after four convective throughflows of the blade passage to exclude the observed initial transient. The averaging has been performed over 5 throughflows. In comparison to the available experimental data, the simulation predicts the core of the tip clearance vortex closer to the suction side. We analyzed the discrepancy in the results and identified a sudden drop in the turbulent kinetic energy in proximity to the separation of the vortex form the side wall in the beginning of its trajectory. This indicates a so-called "Gray-Area" problem that needs to be addressed in future applications of the IDDES method to tip clearance flows.

Five selected national and international cooperations

- FELIX MÖLLER, Institute of Test and Simulation for Gas Turbines, DLR, Cologne, Germany
- TOBAIS MAYENBERGER, MTU Aero Engines AG, Munich, Germany
- PATRICK BECHLARS, MTU Aero Engines AG, Munich, Germany

Engineering Sciences

Heat Energy Technology, Thermal Machines, Fluid Mechanics | DFG 404

Development of efficient numerical methods to quantitatively predict erosion rates - QUAVER

Project ID: bund0012

ANDREAS PETERS,
YOUJUN YANG,
BETTAR OULD EL MOCTAR,

Institut für Schiffstechnik,
Meerestechnik und Transportsysteme,
University Duisburg-Essen

Project Report

The pressure driven processes of vaporization and condensation of a fluid under constant temperature are called cavitation. Cavitation occurs as low static pressures and high flow velocities lead to low absolute pressures below the saturation pressure of the fluid. So called cavitation nuclei, non-condensable gas bubbles and solid particles, are the starting point for the growth of vapour filled cavitation bubbles which can accumulate in forms of cloud, sheet or vortex cavitation. As soon as the cavitation bubbles are exposed to higher surrounding pressures, they rapidly collapse and radiate pressure waves of high amplitudes. Bubble collapses that take place in the vicinity of a solid surface can cause surface damage which is known as erosion.

Maneuvering processes of ships at different speeds and in different sea states lead to differences of the propeller's inflow. Furthermore, the inflow of a conventional ship propeller is always inhomogeneous because of the influence of the ship's aft. Aside from efficiency losses and vibrations of the ship's structure, collapsing cavitation volumes may lead to erosion damage on the ship's propeller and rudder. Erosion is characterized by an initial plastic deformation of the material surface within an incubation period. If high loads from cavitation collapses occur repeatedly within the same area of a surface the material may break and lead to severe material loss. Proceeding erosion damages can cause failure of the propeller or rudder, making it impossible for the ship to manoeuver.

While experimental measurements are commonly used to predict cavitation erosion for ship propellers, they involve significant scale effects related to the cavitating flow and can only qualitatively assess erosion damage. Numerical approaches to predict cavitation erosion offer the potential to complement these measurements and to derive models quantitatively predict erosion.

The aim of this compute project was the development of numerical methods to quantitatively predict cavitation-induced erosion for ship appendages in terms of incubation time and erosion-rates. The developed approach, the Fast Solution Tool (FaST) enabled to efficiently predict cavitation erosion based on numerical flow simulations using a pressure-based solution algorithm. The algorithm was extended to consider compressibility effects of the liquid phase.

The newly developed erosion model uses information from the flow simulation to predict incubation times, mass loss rates, and erosion depths for given time intervals. Results of the flow simulation were validated against measurements from literature as well as own measurements in a cavitation tunnel. The erosion prediction was validated based on literature results and full-scale observations of erosion on a container ship propeller.

Simulations of the full ship geometry with propeller and rudder were, therefore, performed for different operating conditions of the ship to assess the potential risk of erosion for the propeller. The erosion prediction for the propeller agreed well with observations of the damage on the full-scale propeller for a similar operating condition.

Selected national and international cooperations

- FELIX SCHREINER, MAGNUS HAESE, ROMUALD SKODA, Lehrstuhl für Hydraulisches Strömungsmaschinen, Ruhr Universität Bochum (RUB), Deutschland
- TUNG NGUYEN, MICHAEL PALM, Voith GmbH & Co. KGaA, Heidenheim a. d. Brenz, Deutschland
- LUTZ KLEINSORGE, HAUKE BAUMFALK, JÖRN KLÜSS, Mecklenburger Metallguss GmbH (MMG), Waren (Müritz), Deutschland

Publications

- PETERS A, SKODA R, SCHREINER F, NGUYEN T, KLEINSORGE L, EL MOCTAR BO, YANG Y, BAUMFALK H, KLÜSS J, PALM M. (2021): „Kav4D – Numerische Vorhersage des zeitlichen Verlaufs kavitationsbedingter Erosionsschäden an Schiffspropulsions- und –manövrierorganen“, Statustagung Maritime Technologien, Tagungsband der Statustagung 2021, Schriftenreihe Projektträger Jülich, ISBN 978-3-95806-594-9.

Engineering Sciences

Heat Energy Technology, Thermal Machines, Fluid Mechanics | DFG 404

Parallel Stabilized Finite Element Methods for Non-Newtonian Flows and Fluid Structure Interaction Problems

Project ID: jara0185

MAREK BEHR,
STEFANIE ELGETI,
NORBERT HOSTERS,
MICHEL MAKE,
LINDA GESENHUES,
MAXIMILIAN SCHUSTER,
ANNA RANNO,
DANIEL HILGER,
THOMAS SPENKE,
STEFAN WITTSCHIEBER,
EUGEN SALZMANN,
KONSTANTIN KEY,
PATRICK ANTONY,
DANIEL WOLF,
LEONARDO BOLEDI,
TOBIAS BONGARTZ,
BLANCA FERRER,
VERONIKA TRAVNIKOVA,
FELIPE GONZALEZ,
Chair for Computational Analysis of Technical Systems,
RWTH Aachen University

Project Report

The objective of this project is the continued development of effective simulation methods for unsteady fluid flow problems. Typical application of the methods involve simulation of fuel and oil transport in piston ring packs, skin-pass rolling of aluminum, and various blood flow problems. The developed methods are implemented as part of our core multi-physics solver XNS, a Finite-Element Method (FEM) solver that is highly parallelized. Parallel execution of the solver is achieved through the use of message-passing communication libraries and is portable across a wide range of computer architectures. The modular design of XNS provides a flexible framework capable of solving complex coupled problems, and creates a strong basis for future method and solver extensions.

The main areas where novel computational methods are developed within this project can be aggregated by topic and application under the subgroups Fluid-Structure-Interaction, Hemodynamics, Two-Phase Flows, Production Engineering and Non-Newtonian Fluids and will be described in detail in the subsequent sections.Furthermore, simulations of skin-pass rolling procedures of aluminum sheets have been performed.

Our common objective is the development and usage of our in-house parallel finite element solver (XNS) for multi-physics problems, e.g. compressible and incompressible Navier- Stokes flow, linear elastic materials, non-Newtonian fluids, temperature, and scalar transport problems. In this section, we first outline the general methods and algorithms, that the solver makes use of.

The key method used in our flow solver XNS is based on the Deforming-Spatial-Domain/ Stabilized-Space-Time (DSD/SST) finite element formulation. The method is introduced in [25]. In the DSD/SST finite element formulation, a space-time discretization is used together with least-squares type stabilization. Space-time discretization means that time as well as space are discretized simultaneous with finite elements. Together with the stabilization, this method is well suited for the solution of problems governed by the Navier-Stokes equations in deforming domains. An extension of the finite element method used at our institute is the NURBS-Enhanced Finite Element Method (NEFEM). NEFEM increases the solution accuracy by using an exact representation of the domain boundary. Most of the computational domains are nowadays built using CAD models, which use Non-Uniform Rational B-Splines (NURBS) to model curves and surfaces. Standard FEM approximates these boundaries by polynomial interpolation. In contrast to that, NEFEM incorporates the NURBS description of the domain boundary into FEM. Thereby we obtain curved elements on the boundary. A further step towards the true geometry is taken by Isogeometric Analysis (IGA). In classical FEM, the polynomial basis chosen to approximate the unknown solution field is also used to represent the known geometry. In case the polynomial basis of the solution field is not equivalent to the one of the geometry, geometrical errors are automatically introduced. In order to avoid these errors, the isogeometric concepts reverse the construction of the polynomial interpolation. The known basis of the geometry (within our models we use NURBS) is used to approximate the unknown solution. We use a distributed memory parallelization with MPI, that is employed with an in-house library.

Selected honors, prizes and awards

- LINDA GESENHUES, GAMM Junior, elected by the Association of Applied Mathematics and Mechanics for an excellent PhD thesis in the fields of Applied Mathematics or Mechanics
- FABIAN KEY, GAMM Junior, elected by the Association of Applied Mathematics and Mechanics for an excellent PhD thesis in the fields of Applied Mathematics or Mechanics

Selected conference participations

- MAREK BEHR, IX International Conference on Coupled Problems in Science and Engineering: Plenary Lecture on Model Selection and Coupling in the Context of Biomedical Device Design
- HPC Asia 2021, Jeju, South Korea
- GAMM 91st Annual Meeting, Kassel, Germany
- International Congress on Theoretical and Applied Mathematics, Milan, Italy
- Mechanistic Machine Learning and Digital Twins for CSET, San Diego, USA
- Structural Membranes, Munich, Germany

Selected national and international cooperations

- “Model Reduction in Arteries with Drug-Eluting Stent“s, Politecnico di Milano, Milan, Italy
- SFB 1120 “Präzision aus Schmelze” Institut Für Kunststoffverarbeitung, RWTH Aachen University, and Institut für Leichtbau und Struktur-Biomechanik (ILSB), TU Vienna, Austria
- “CFD Simulation of Gas Flow via Piston Ring Pack and Impact on Fuel and Oil Transport” Ford Research Alliance, Aachen, Germany
- “Multiscale behavior of dense suspensions on highly parallel computing devices: from theory to applications“ Cyprus Institute, Cyprus, Universita Degli Studi di Roma Tor Vergata, Rome, Italy, and RWTH Aachen University
- “Neural Networks as reduced models for high-fidelity flow simulations in bioreactors and energy-efficient manufacturing processes” Forschungszentrum Jülich, Germany

Publications

- GESENHUES L, BEHR M. Simulating dense granular flow using the μ(I)-rheology within a space-time frame- work, International Journal for Numerical Methods in Fluids, 93, no. 9, 2889–2904, 2021.
- VON DANWITZ M, ANTONY P, KEY F, HOSTERS N, BEHR M. Four-dimensional elastically deformed simplex space-time meshes for domains with time-variant topology, International Journal for Numerical Methods in Flu- ids, 93, no. 12, 3490–3506.
- GUGLIETTA F, BEHR M, BIFERALE L, FALCUCCI G, SBRAGAGLIA M. Lattice Boltzmann simulations on the tumbling to tank-treading transition: effects of membrane viscosity, Philosophical Transactions of the Royal Society A: Mathematical, Physical and Engineering Sciences, 379, no. 2208, 20200395, Aug 2021.
- HUBE SA, BEHR M, ELGETI SN, SCHÖN M, SASSE J, HOPMANN C. Numerical Design of Distributive Mixing Elements, 2021.
- MAKE M, SPENKE T, HOSTERS N. Spline-Based Space-Time Finite Element Approach for Fluid- Structure Interaction Problems With a Focus on Fully Enclosed Domains, Preprint submitted to Computers and Mathematics with Applications, 2021.
- GUGLIETTA F, BEHR M, FALCUCCI G, SBRAGAGLIA M. Loading and relaxation dynamics of a red blood cell, Soft Matter, 17, 5978–5990, 2021.
- KEY F, BALLARIN F, EUSTERHOLZ S, ELGETI S, ROZZA G. Reduced Flow Model for Plastics Melt Inside an Extrusion Die, PAMM, 21, no. 1, e202100071, 2021.
- BOLEDI L, TERSCHANSKI B, ELGETI S, KOWALSKI J. “A level-set based space-time finite element approach to the modelling of solidification and melting processes”, 2021.
- SAELZER J, ALAMMARI Y, ZABEL A, BIERMANN D, LEE J, ELGETI S. Characterisation and modelling of friction depending on the tool topography and the intermediate medium, Procedia CIRP, 102, 435–440, 2021, 18th CIRP Conference on Modeling of Machining Operations (CMMO), Ljubljana, Slovenia, June 15-17, 2021.
- ZWICKE F, HOHLWECK T, HOPMANN C, ELGETI S. Inverse Design Based on Nonlinear Ther- moelastic Material Models, PAMM, 20, no. 1, e202000130, 2021.
- HELMIG J, KEY F, BEHR M, ELGETI S. Combining boundary-conforming finite element meshes on moving domains using a sliding mesh approach, International Journal for Numerical Methods in Fluids, 93, no.4, 1053-1073, 2021.

Engineering Sciences

Heat Energy Technology, Thermal Machines, Fluid Mechanics | DFG 404

Numerical analysis of wind-induced pressure fluctuations on open volumetric receivers in solar power tower plants (SPTP)

Project ID: jara0225

ROBERT PITZ-PAAL
PETER SCHWARZBÖZL
MAXIMILIAN DREXELIUS
DLR - Institute of Solar Research, Germany

Project Report

In the field of solar tower power plants, the technology of the open volumetric receiver (OVR) has proven to be very robust and efficient at experimental scales as well as at the pilot power plant in Jülich (1.5 MWel). The ceramic honeycomb structures of the OVR are irradiated by concentrated solar power and convectively increase the temperature of inflowing ambient air which is used as the heat transfer fluid (see [1]). Consequently, the next step in research and development of the technology is the scale-up towards market-relevant sizes. This project investigates a reference power plant with a tower height of around 200m and a thermal receiver placed in three separate cavities facing south, north-east and north-west with a combined thermal power of around 350 MWth (as presented in [2]). With upscaling and increasing tower height, ambient wind flow gains importance and the knowledge of wind-induced pressure fluctuations becomes a key factor in order to ensure safe and efficient operation of such power plant, as local pressure fluctuations directly influence the mass flow through the receiver.

The aim of this study is to simulate the wind flow around the reference plant with transient cfd simulations utilizing DES turbulence modelling. For this task the software openFOAM v6 and the Spalart-Allmaras DDES turbulence model were used. Two different flow velocities for a chosen wind direction have been analyzed. The results were further validated with wind tunnel experiments. Until this point the wind influence on open volumetric receivers has not yet been investigated. Work prior to this study was done in order to evaluate a similar receiver design (see [3]) in terms of the receiver efficiency and return air ratios for different loading and target temperatures with stationary RANS simulations. To evaluate the wind influence on the local pressure distribution, a CFD model of the tower was designed that contains the upper 50 m of the tower, which has a diameter of about 30 m (see Fig. 2) resulting in a mesh which contains about 192 Mio. hexahedral cells. For simplicity the receiver air flow has been ignored for this study, and the receiver has been simplified as a wall.

	SW-4	SW-14
Inlet Velocity [m/s]	4	14
Reynolds number [-]	10.46E+06	36.61E+06
Simulated Time [s]	130	40
CFL-number [-]	1	1
Mean Timestep [ms]	1.8	0.5

Table 1 sums up the key parameters of the simulated cases of flow around the solar tower.

FIG 1: Time series of local static pressure for the simulated cases of wind flow at the center of each cavity of the solar tower power plant.

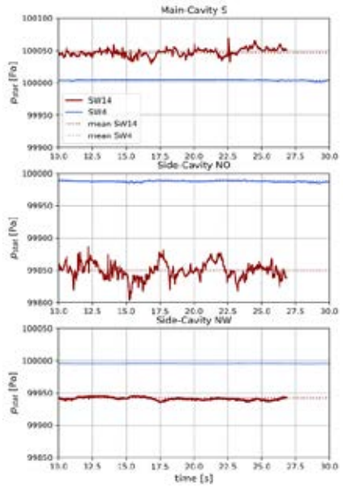

Fig. 1 shows the time series of static pressure probes in the center of each cavity under south-west-ward wind with a speed of 4 and 14 m/s. As Fig. 1 already indicates, the local r.m.s. values of the static pressure increase drastically with wind velocity. For these cases of 4 and 14 m/s wind r.m.s. values increase in about one order of magnitude. The local evaluation of r.m.s. values gives an indication of pressure fluctuations induced by flow separation at the edges of the geometry, which is highly depending on the flow direction. Fig. 1 also gives an impression about how severely the mean pressure level at each cavity changes depending on wind speed. Especially in the wake of the tower the drop in the mean pressure is very large with about -150 Pa. Due to the shift in mean pressure, dynamically changing flow directions can lead to pressure fluctuations in the order of 200 Pa for a wind speed of 14 m/s.

These results show that in terms of the severity of pressure fluctuations, changing flow direction is the more relevant mechanism in comparison to flow separation induced pressure fluctuation at constant wind directions.

For further validation of the simulation model, wind tunnel experiments in a high-pressure wind tunnel have been conducted. The measurement shows great alignment with the simulation results when comparing mean and r.m.s. values of local pressure probes distributed along the cavities and around the tower. Fig. 3 shows a cut through the field of lambda 2-values smaller than 2 for the simulation with an inlet velocity of 4 m/s. It gives an impression of the highly turbulent flow separation that occurs at the tower geometry, even though it is hard to distinguish between individual vortices.

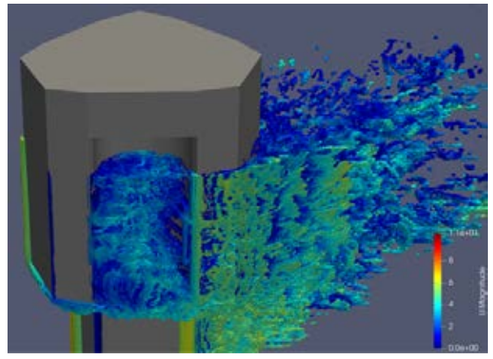

FIG 3: Flow visualization with the Lambda2-eigenvalue criterium, colored in the velocity magnitude - for the case of 4 m/s inlet velocity

Further work needs to be done in adding the receiver air flow to the model. In the concept power plant, the receiver consists of ceramic HitRec absorber cups [1] through which the heated air is sucked in. After heat transfer to the water-steam circuit the receiver air at a temperature of around 100 - 270°C is redirected to the front of the receiver again to increase the mean receiver inlet temperature and improve the thermal efficiency of the receiver. Modelling this flow and heat exchange is rather challenging because of the different scopes at which the wind around the tower (~ 30m diameter) and flow through the single channels of the receiver (~0.5mm) takes place. A modelling approach has been presented by Stadler et al. [3] whose application to wind simulation under LES turbulence modeling is yet to be proven. The improved model should be able not only to evaluate the wind influence on pressure fluctuations but also on thermal receiver efficiency caused by the interaction of ambient wind and the receiver return air flow.

References

[1] HOFFSCHMIDT ET AL. 2003 - Performance Evaluation of the 200-kWth HiTRec-II Open Volumetric Air Receiver

[2] SCHWARZBOEZL ET AL. 2020 - Annual Performance Assessment of a 50 MWe Commercial Solar Tower Plant with Improved Open Volumetric Receiver

[3] STADLER ET AL. 2019 - Performance assessment of an improved Open Volumetric Receiver Design with 240 MWth

Engineering Sciences

Heat Energy Technology, Thermal Machines, Fluid Mechanics | DFG 404

3D-CFD Simulation for Design Optimization of Fuel Cell Radial Compressor Stages

Project ID: rwth0553

JOHANNES KLÜTSCH,
Chair of Thermodynamics of Mobile Energy Conversion Systems (TME),
RWTH Aachen University

Project Report

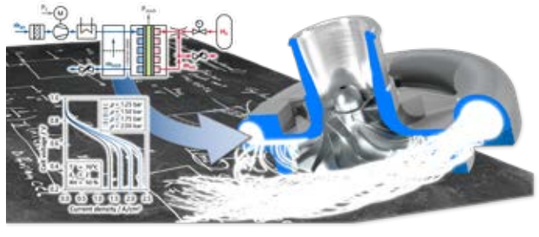

Introduction: Compared to battery-electric drive trains, polymer electrolyte membrane fuel cell (PEM-FC) drive trains offer the advantage of higher energy density and short refueling times making them particularly attractive for long-distance passenger- and freight-transport. PEM-FC drivetrains are supercharged on the cathode (air) side to increase efficiency and power density. Electrically driven radial compressors are preferably used for supercharging, as they are superior to other compressor types with regard to costs, service-life and noise emissions. However, the use in FC systems imposes high demands on the radial compressor design. A major challenge is the speed limitation imposed by the electric drive. In addition, oil-free operation must be ensured by a suitable design of the bearing system. Due to these boundary conditions, compressor designs known e. g. from exhaust gas turbocharger applications are only conditionally suitable for FC systems. Nevertheless, existing designs must be used in many cases, since an application-specific compressor development would be uneconomical for small expected production numbers. The resulting efficiency disadvantages must be accepted.

The project objective is the development of a guideline for the system efficiency-optimal design of FC supercharging systems and the respective aerodynamic radial compressor design.

Project Summary: The following figure gives an overview of the radial compressor design process.

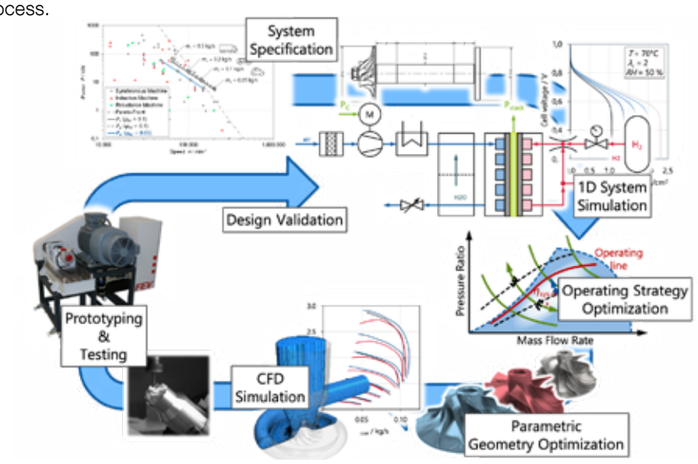

After identifying the influence of the FC powertrain architecture on the required compressor operating range by means of 1D system simulation, compressor candidate designs are generated and evaluated. For this, a preliminary design software has been developed at TME. The software consists of mean-line and steam surface flow models employing empirical correlations for impeller work input and dissipation. Low computational effort allows for compressor map estimation on desktop computers within seconds. To verify the flow models used during preliminary design as well as for geometry optimization within the detailed design step, extensive 3D-CFD simulations of multiple compressor geometries were carried out within the scope of the computation project. In the next step, simulations will be validated experimentally. A prototype of the optimized compressor geometry will be manufactured and tested evaluating aerodynamic performance as well as near surge line behavior in conjunction with the FC air path.

Simulation Setup: 3D-CFD simulations are carried out using the commercial software Siemens PLM StarCCM+ (version 2020.2). Flow is modeled as an ideal gas employing the k-ε Lag elliptic blending Reynolds-averaged Navier Stokes turbulence model. Exploiting rotational symmetry of impeller and diffuser, a blade passage model is derived. Here, a single blade element (or main & splitter blade passage, if applicable) is resolved, as shown in the following figure. An unstructured polyhedral mesh is used resulting in a cell count of $1.2 \cdot 10^6$ for the passage model and $7 \cdot 10^6$ for the full stage geometry, respectively. Model validation and mesh independency studies are carried out for a known automotive turbocharger compressor geometry.

Selected Results: FC radial compressor stages feature a significant efficiency deficit in comparison to “standard” designs used in turbocharger applications. This deficit is the result of excessive blade channel curvature as well as viscous losses in the blade passage and in the diffuser (low blade height and diffuser gap width). To evaluate the effect of the FC-specific design boundary conditions on aerodynamic performance, a geometry variation study was carried out in addition to the aforementioned geometry optimization process.

FC compressors employ air foil bearing systems which bearings offer lower specific stiffness compared to roller element or hydrodynamic bearings. Accordingly, a higher blade tip clearance must be provided to avoid blade-to-shroud contact. This can lead to excessive tip leakage losses. The following figure shows the effect of blade tip clearance on passage (impeller + diffuser) isentropic efficiency. For increased blade tip clearance s = 0.4 mm, the passage isentropic efficiency is reduced by 3.5 % on average. Reducing s to 0.15 mm yields an average efficiency increase of 3 %.

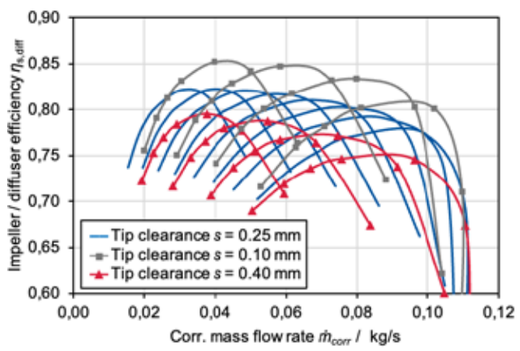

Figure 4: Passage isentropic efficiency for blade tip clearance variation

Summary and Conclusion: The application-specific requirements of the FC system necessitate a tailored compressor design. Efficiency deficits resulting from low stage flow coefficient operation (speed limit), can be partially compensated by impeller geometry optimization. Additionally, low blade tip clearance is vital for satisfactory compressor performance. Here, advances in air foil bearing technology can facilitate efficiency gains.

Coupling 1D system simulation with the integrated compressor design toolchain developed at TME makes the application-specific design of the air supply system economically feasible even for small production numbers.

Publications

- KLÜTSCH, PISCHINGER, SCHLOSSHAUER, LÜCKMANN, Simulation-driven Fuel Cell Air Compressor Design, MTZ worldwide, Issue 7-8/2021
- KLÜTSCH, WICK, SCHLOSSHAUER, LÜCKMANN, WALTERS, Simulation-Driven PEM Fuel Cell Compressor Design, 30th Aachen Colloquium Sustainable Mobility 2021

Engineering Sciences

Heat Energy Technology, Thermal Machines, Fluid Mechanics | DFG 404

Aerodynamic integration of an electro-hybrid powertrain for the silent air taxi

Project ID: rwth0612

JAN-PHILIPP HOFMANN,
Institute of Jet Propulsion and Turbomachinery,
RWTH Aachen University

OLAF WAGNER,
Institute of Aerospace Systems,
RWTH Aachen University

Project Report

The majority of the German population lives less than 25 km away from the nearest airfield. These small airports offer a considerable potential for directly connecting regional centers and rural regions in conjunction with significantly reducing travel times. A small aircraft as a means of transport ideally complements urban electric mobility and fits into other intermodal mobility concepts, such as the Urban Air Mobility Initiative. The necessary infrastructure at the ground already exists, but the establishment of a market for regional air mobility requires a new type of small aircraft. In order to meet the passenger requests as well as the acceptance of the residents, these aircrafts have to be more comfortable, safer and significantly quieter. These requirements are met by small twin-engine aircraft with an internal electro-hybrid powerplant and a propulsion via ducted propellers.

Major challenges in such an aircraft concept are the drag optimized integration of combustion engines in the rear part of the fuselage and electric machines in the pylons as well as the cooling of all powerplant components. Furthermore, the propulsors have to be positioned in such a way that the inlet distortions remain low even under high angles of attack (α) and in sliding conditions (β). The procedure and initial results for the optimization of the propulsor positions are described below.

The interaction between the propulsion system and aircraft was investigated by comparing two configurations, namely the aircraft without the pylon and fan and the aircraft with integrated pylon and fan. A numerical model was developed, and the interaction was investigated under cruise flight conditions, i.e., at an altitude of 3000m and an equivalent airspeed of 300km/h. It has been found that the aerodynamic performance of the aircraft is significantly influenced by the channel flow developing between the aircraft components wing, fuselage, pylon, and the nacelle. Based on this finding, the positioning of the fan was optimized. The design space for the optimization was defined, taking into account the installation position of the Rotax combustion engine, as well as flight mechanical aspects. With respect to the baseline position, the spanwise positioning of the fan varied between 15 cm in the outboard direction and 20 cm in the inboard direction. The location in the circumferential direction varied between 0 and 20°.

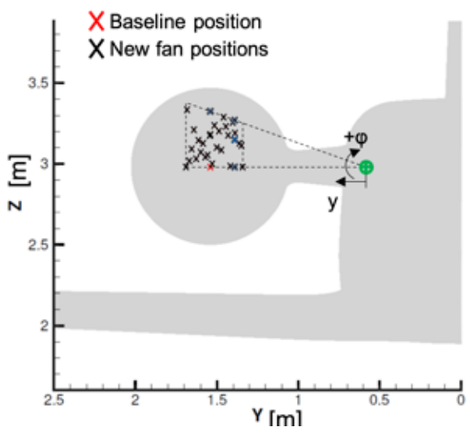

Figure 1: Illustration of the fan positions to be investigated within the design space

Consequently, 33 discrete fan positions were defined within the design space using a Latin hypercube sampling and are depicted in figure 1. For the new fan positions defined, stationary RANS computations have been carried out on a medium-sized computational grid with 95 million cells using the DLR TAU code. The inviscid fluxed were discretized using a central scheme with scalar dissipation, and the turbulence was modeled employing the k-ω Menter SST model.

The objective function of the optimization was defined as minimizing the drag while maximizing the lift to drag ratio L/D. Figure 2 depicts the drag reduction ΔC-Drag in % relative to the aircraft drag with the baseline fan position.

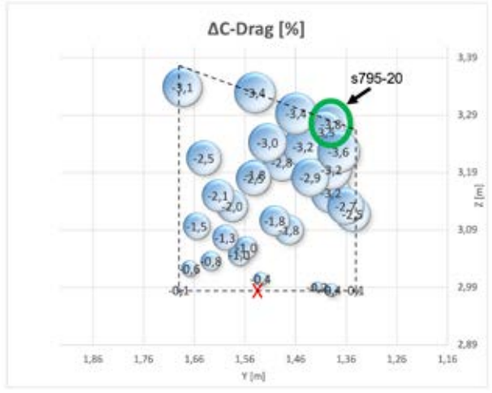

Figure 2: Drag reduction in % for the fan positions investigated relative to the aircraft drag with the baseline fan positions

It becomes evident that for a constant height Z and a variation of the fan position in spanwise direction Y, the drag changes only slightly. The largest drag reductions are achieved in the positions close to the fuselage and higher vertical distances from the wing, i.e., larger circumferential angles Φ. Thus, the vertical distance between the engine and the wing is the driving factor for reducing the aircraft drag. The lowest drag is found in position s795-20, with a drag reduction of 3.8%. With respect to the baseline, position s795-20 is 15 cm closer to the fuselage, and the engine is tilted upwards by 20° around the Rotax engine. Figure 3 depicts the axial velocity in a cut plane through the fan, pylon, fuselage, and wing for the baseline position and the optimized position s795-20. It can be noted that the fan shift from the baseline position to the optimized position leads to a significant reduction of the axial flow velocities within the channel flow between the fan, pylon, fuselage, and wing. As a result, the pressure drag of the wing is reduced by 19%, while the drag of the nacelle increases by 14.8%, yielding a total drag reduction of 3.8%. The opposing trend of the wing and nacelle drag indicates a complex aerodynamic coupling that is yet not fully understood and requires further investigations.

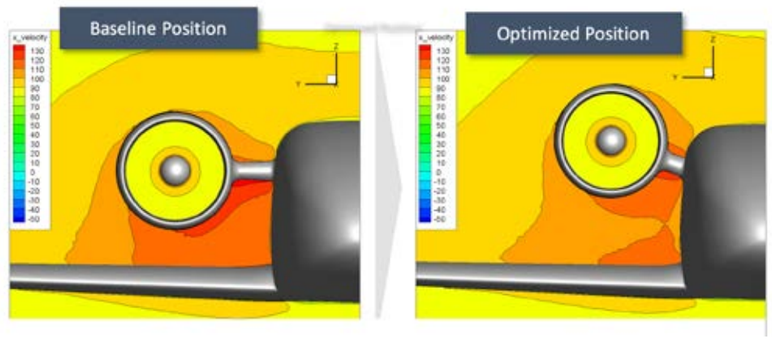

Figure 3: Counts of the axial velocity in a cut plane for the baseline and the optimized fan position

Engineering Sciences

Heat Energy Technology, Thermal Machines, Fluid Mechanics | DFG 404

Aerodynamic, Aeroelastic and Aeroacoustic Optimization of the Silent Air Taxi Ducted Fan

Project ID: jara0222
PETER JESCHKE,
STEFAN HENNINGER,
LUKAS STUHLDREIER,
PATRICK OKFEN,
JAN KOPPELBERG,
Institute of Jet Propulsion and Turbomachinery, RWTH Aachen University

Project Report

In addition to cutting down pollutant emissions, noiseless propulsion systems are key to enable air taxi operation in close proximity to residential areas. The WHO outlines that frequent noise exposure has a serious impact on human health and states an increase in heart rate or sleep stage changes as possible consequences [1]. Typically, general aviation aircraft are powered by propellers causing noise emissions in the order of magnitude of about 80 dB(A) – a value far above what is acceptable for high frequent operations next to residential areas. However, scientific knowledge can be used to reduce the emitted noise significantly. Investigations in the 1970s already demonstrated that a high number of blades and a propeller casing can cut noise emissions by up to 20 dB [2,3].

The Institute of Jet Propulsion and Turbomachinery (IST) participates in several research projects which address the development of a propulsion system for regional and urban air mobility. Among others, the design and optimization of a silent ducted fan is one of the tasks the IST is supposed to perform. As current fan and propeller designs differ quite a lot from the intended design, completely new aerodynamic, aeroelastic and aeroacoustic challenges have to be faced which have not been of any scientific interest before. In order to do so, numerical investigations for aerodynamics, aeroelastics and aeroacoustics are carried out by the IST. Consequently, the design of the ducted fan is a multidisciplinary process with contradicting demands. As a high degree of numerical simulation capability is needed to cope with these demands, this new area of research is addressed in the present computational project and a ducted fan is optimized for residential-friendly flight operation.

A propulsion system is supposed to provide sufficient thrust over the entire operating range of an aircraft. This includes demanding operating points such as for example rotation at severe crosswind condition or maximum climb. In these operating points the inflow direction deviates from the propulsor axis causing a circumferential variation of the flow conditions in the fan entry plane. As result incidence angles are locally increased, which enhances noise emissions, increases mechanical blade loading and degrades the stable operating range. Consequently, detailed inlet distortion investigation on a ducted fan are performed at the IST. Therefore, the CFD tooling is expanded to not only account for propulsor core flow but also consider the flow around the nacelle. A far field grid setup was developed by variations of global grid size, core engine grid size, far field grid size and y+ resolution for a zero angle of attack operation until grid independence was shown. It was found that a c-shaped grid topology enclosing the nacelle was needed to prevent numerical instabilities at the inlet lip. In addition, the required radial flow domain size for non-axisymmetric inflow was identified. The established setup then was used to investigate the aerodynamic inlet distortion performance at several operation points for various flow angles. Total pressure, static pressure and velocity magnitude were investigated at different axial locations to create an understanding of the interaction between distortion, rotor and nozzle.

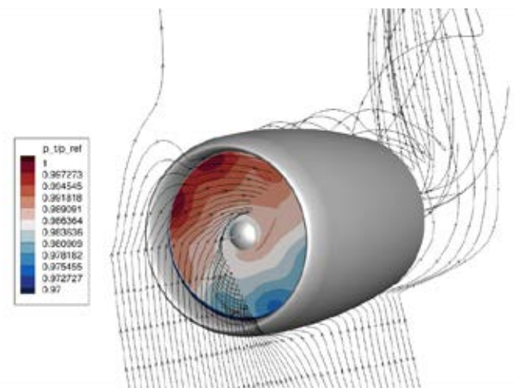

Figure 1: Ducted fan under crosswind conditions

For the analysis of the aeroacoustics of the ducted fan, the generation and propagation of the dominant tonal sound were investigated numerically in this computational project. Based on the known frequencies and the mode pattern in the duct, the required mesh resolution for sound excitation and propagation was determined in advance based on the acoustic wavelengths. The complete resolution of the flow condition in the channel and the relevant acoustic source and propagation mechanisms was checked using a mesh convergence study. In addition to the investigation of the mesh influence, the impact of the turbulence model was analyzed. For the final evaluation of the calculations, the influence of the analysis method was investigated for the necessary separation of the aerodynamic and acoustic fluctuations. Based on this, improvements to the numerical setup were derived and applied. With the results of the calculations, a deeper understanding of the sound excitation and propagation in a ducted fan was developed. The source mechanisms and the influence of the ducted fan geometry on the excitation and propagation of sound could be determined. Improvements of the geometry and the operating behavior to reduce the emitted sound were successfully implemented.

To evaluate the possibility of High-Cycle-Fatigue, the risk of blade flutter occurring in the operating range of the ducted fan was assessed. For a flutter assessment all inter-blade phase angles (IBPA) have to be considered, since the minimal damping can occur at any of these. The complete compressor map needs to be checked for possible flutter occurrences of the ducted fan. Because of the great amount of individual simulations needed to be conducted with the classical travelling wave mode approach, the aerodynamic influence coefficient (AIC) method is chosen instead. It uses a full annulus mesh, but only one simulation per operating point for a complete S-curve of the aerodynamic damping is needed. The downside of this method though, is that no nodal diameter effects can be captured and clean blade only mode shapes are assumed. But this assumption is valid in the presented case, as the mounting of the fan blades result in low disk coupling and therefore just a neglectable nodal diameter dependency. The results of the AIC-simulations are a full aerodynamic damping curve per mode and per operating point. However, for a flutter assessment only the minimal damping is relevant, since it is the least stable case. At flutter, the blades will automatically oscillate with the IBPA of the minimal damping, which needs to be negative. For the fundamental first flexural mode shape it was observed, that the minimal damping changes its sign to negative only close to the stall line at high shaft speeds. This is due to the flow separation close to the speed line and is therefore called stall flutter. The other investigated modes do not show a negative damping across the whole compressor map. Therefore, the flutter assessment indicated, that the fan blades are not prone to classical flutter in the relevant operating range.

References

[1] World Health Organization, Night noise guidelines for Europe, World Health Organization Regional Office for Europe, Copenhagen, 2009, 162 S.

[2] THE TECHNICAL EDITOR, "Dowty ducted propulsor flied," Flight International, 1977, pp. 209–211, URL: https://www.flightglobal.com/FlightPDFArchive/1977/1977%20-%202211.PDF [retrieved 25 November 2019].

[3] Davis DGM., "Ducted Propulsors for General Aviation," Aircraft Engineering and Aerospace Technology, Vol. 49, No. 9, 1977, pp. 5–7. doi: 10.1108/eb035403!

Publications

- JILKE L, Numerical Investigation of the Operating Behavior of a Ducted Fan for a Hybrid Electric Small Aircraft, Master's thesis, RWTH Aachen University
- DIRKES N, Numerical Investigation of Tonal Noise Emissions of a Ducted Fan for a Hybrid Electric Small Aircraft, Bachelor's thesis, RWTH Aachen University

Heat Energy Technology, Thermal Machines, Fluid Mechanics | DFG 404

Project **LONGRUN**: Development of efficient and environmentally friendly **LONG** distance powe**R**train for heavy d**U**ty trucks a**N**d coaches

Project ID: rwth0602

VIKRAM BETGERI,
Chair of Thermodynamics of Mobile Energy Conversion Systems, RWTH Aachen University

DEPPENKEMPER KAI,
FEV Europe Gmbh, Aachen, Germany

BRAM HAKSTEGE,
DAF Trucks N.V, Eindhoven, Netherlands

Project Report

Overview: Reduction of the real driving emissions, fuel consumption and its related CO_2 emission for heavy duty long haulage transport sector has been the primary motivation for the project LONGRUN. The objective of this research project is multifaceted and is primarily associated with development of different engines, drivelines /demonstrator vehicles with over 10% energy savings (Tank to Wheel) and related CO_2 reduction, 30% lower emission exhaust (NO_x, CO and others) and 50% peak thermal efficiency.

This project consortium consists of leading heavy duty OEMS of long haulage trucks and coaches, their suppliers and research partners, with an aim to develop innovative mobility solutions and to publish major technology and fuels roadmaps in time for revision of the CO_2 emission standards for heavy duty vehicles (third mobility package of the Commission) in 2022 and 2023. The objective (relevant work package) of this research work is the detailed investigation of brake thermal efficiency improvement measures of a heavy duty engine. Technology pathways which improves closed cycle efficiency, open cycle efficiency and waste heat recovery have been investigated with a holistic toolchain comprising of 1D engine process simulation, detailed 3D CFD simulation and experimental validation of heavy duty SCE engine.

Methodology: Engine technologies influencing combustion and gas exchange like high compression ratio piston, high injector flow rate, high peak firing capability, Miller valve timing and novel piston design concepts will be investigated for their efficiency potentials. Heat transfer improvement and exhaust energy recovery measures like piston thermal barrier coatings, insulated exhaust ports and electrically assisted turbocharger would additional be investigated for their energy saving/ efficiency potentials.

The overall methodology is illustrated in Figure 1. A Genetic Algorithm based optimization problem was set up in the 1D engine process simulation software GT- Suite for the given TC-DI engine with Miller cycle to explore the efficiency potentials. To investigate and optimize the in-cylinder mixture formation at high compression ratio and aggravated injector flow rates 3D CFD simulations coupled with combustion chemistry have been performed using CONVERGE. SCE engine experiments have been performed at the Fuel Science Centre test facility to validate the simulations.

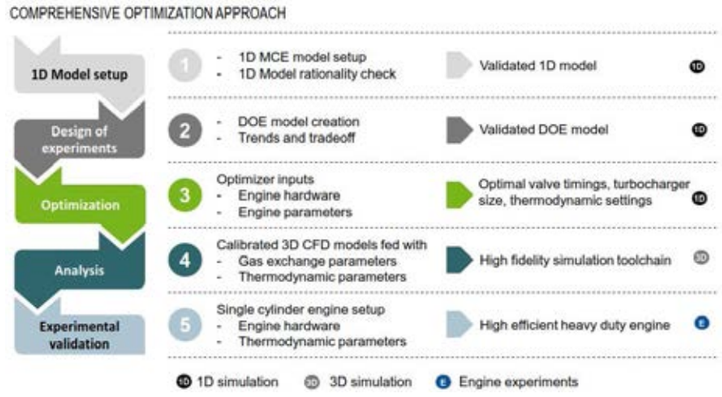

Figure 1. Comprehensive optimization approach

Results Preliminary model development: CFD models for a combination of new generation fast opening fuel injector with high compression ratio piston bowl. Such models form a prerequisite for optimization of high efficient, eco-friendly powertrain. Figure 2 shows the comparison between available measurement data with that of simulation prediction

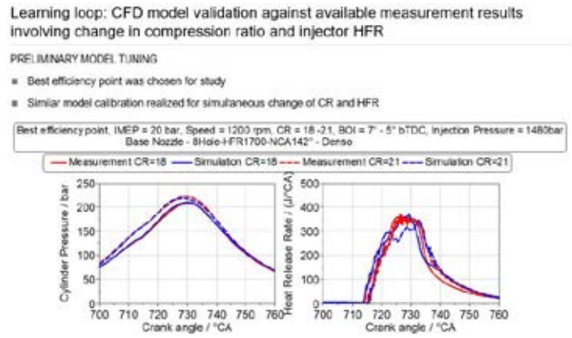

Fig. 2. Preliminary model development

During the optimization, the relevant hardware parameters like compression ratio, valve timings and their opening durations, turbine and compressor size, VTG rack position and engine control parameters where allowed to vary. The efficiency maps of turbocharger were scaled using the Mach similarity law during optimization. It is important that the 1D engine models are plausible and reliable to predict the trends associated with change in compression ratio, injector flow rate and peak firing pressure. Hence, they were iteratively validated with the available SCE measurement. The result of validation is shown in Figure 3, as noticed the change predicted by 1D simulation is in line with equivalent SCE measurements.

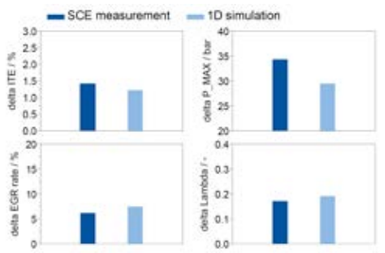

Fig. 3. Validation of 1D engine process model predictions

Compression ratio change = 18 to 21	IMEP = 20.98 bar, n = 1200 rpm, pinj = 1550bar
Injector flow rate change = 1700 cc/min to 2338 cc/min	pboost = 2650mbar, pback = 2720mbar

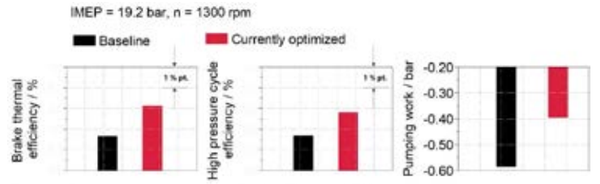

Fig. 4. 1D optimization result – Brake Thermal Efficiency improvement

Further, the results from the 1D optimizer is illustrated in Figure 4. This optimization reveals that the brake thermal efficiency can be increased by 1.5% points with reference to baseline configuration by a combination of an increased peak firing pressure, increased compression ratio (intake valve opening duration by 20% (LIVC) and increased compressor sizing. The increased BTE is due to improved high pressure cycle efficiency and a reduced pumping losses.

The overall BTE improvement currently obtained from various technologies jointly investigated with project partners is illustrated in Figure 5. Both 1D simulation and SCE measurements indicate towards a BTE benefit of up to 0.5% points from piston thermal barrier coating. With current investigation, an overall BTE of 49.3% point is obtained. Further potential existing in combustion system, energy preservation methods are still being investigated.

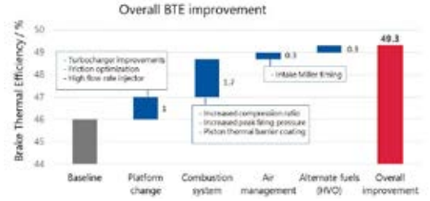

Fig. 5 Overall Brake Thermal Efficiency improvement - current status

Engineering Sciences

Heat Energy Technology, Thermal Machines, Fluid Mechanics | DFG 404

Joint project of VKA and ITV within the scope of the “Fuel Science Center”: “Investigation of low temperature combustion chemistry within a novel integrated kinetic model development framework” (ITV) and “Flame- and spray-wall interactions influence on unburned hydrocarbons and carbon monoxide emissions” (VKA)

Project ID: rwth0626

MARCUS FISCHER,
Chair of Thermodynamics of Mobile Energy Conversion Systems,
RWTH Aachen University

FLORIAN VOM LEHN,
Institute for Combustion Technology,
RWTH Aachen University

Project Report

In the scope of the computing project, the work at ITV included the extension of an optimization and uncertainty quantification framework for kinetic mechanisms. The framework builds on the method of uncertainty minimization using polynomial chaos expansions, which had been developed in previous work. Here, this approach, which was previously applied only to ignition delay time data, and has now been extended to allow for a joint consideration of different types of relevant low-temperature combustion targets, including jet-stirred reactor data. As an application case, the combustion kinetics of the novel bio-hybrid fuel dibutoxymethane (DBM) were investigated by developing a new detailed kinetic mechanism for this fuel component. The developed prior mechanism was further optimized by application of the extended framework and will soon be published.

Besides the mechanism development, the project also focused on the development of machine-learning-based models for prediction of fuel combustion properties. Specifically, a quantitative structure-property relationship model was developed for the first time to predict the laminar burning velocities of a wide range of fuels in dependence of both the molecular fuel structure and the physical conditions, i.e., pressure, temperature, and fuel-air equivalence ratio. For this purpose, an artificial neural network was trained based on a training set consisting of both the experimental LBV values and additional data obtained from numerical simulations with a detailed kinetic model. Cross-validation revealed a mean absolute error of 3.3 cm/s when applying the model to fuels, whose LBV datapoints were not used for training. In order to gain insights into the underlying fuel structure dependence of LBV, the model was then applied to analyze the functional group effects at unified conditions by means of sensitivity analysis and detailed fuel comparisons. The results demonstrate that a group contribution approach in combination with a machine learning methodology is capable of predicting the LBVs of a wide range of fuel structures with acceptable accuracy, which can be useful for future fuel design.

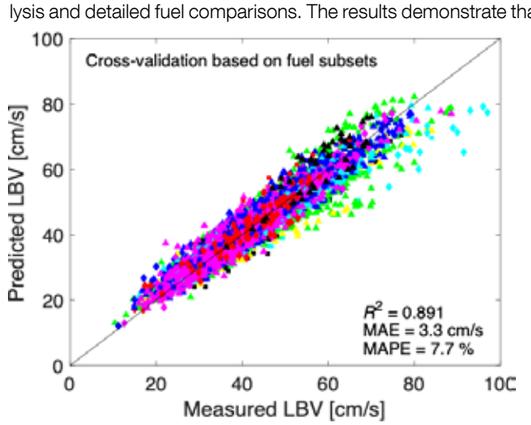

1-fold cross-validation based on fuel subsets of the artificial neural network trained for prediction of laminar burning velocity in dependence of the molecular fuel structure.

In the scope of the computing project the TME conducted several simulations to investigate the sampling process of a fast gas sampling valve inside an internal combustion single cylinder engine. This work should help to evaluate the results gained by the measurement methodology and derive the sample dilution. The wall quenching distance of the flame is about 20 µm thick for gasoline operation. Therefore only a small volume near the wall is of interest for the investigations. Upon valve opening the significant pressure difference between combustion chamber and the valve domain of Δp = 25 bar leads to high flow velocities at the valve. This leads to a sampling of not only the gas volume from the quenching zones but also to a sampling of combusted gas volume. The sampled gas volume sampled is calculated with the 3D-CFD simulation to $V_{GSV,1ms}$ = 2000 mm³, which is 0.4 % of the swept volume and 3.9 % of the compression volume of the engine. This correlates to a half sphere with a radius of 9.8 mm. Figure 2 shows the CFD results for the flow field during the sampling process at full valve stroke of the sampling valve and at the same time without sampling. It can be observed that the flow field into the valve is not symmetrical to one of the cylinder axis. The flow separation that occurs during sampling between in-cylinder flow and the flow inside the valve is located approximately 10 mm below the valve in the z-axis. The flow field in the vertical plane of the cylinder shows in negative z direction nearly the form of a quarter sphere. In positive z direction the flow is significantly influenced by the in-cylinder flow because it has the same vector as the flow into the GSV. Accordingly, the area of higher flow velocities reaches further into the negative y direction than below the GSV.

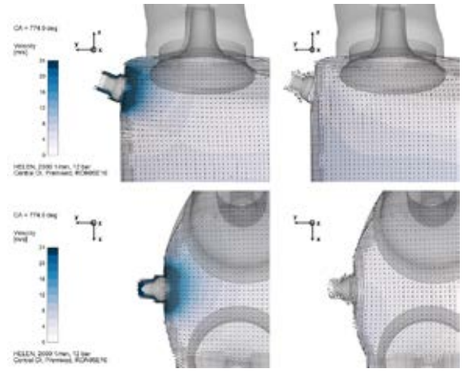

2-Flow field of the in-cylinder flow during sampling at full valve stroke (left) and without sampling (right)

Thus, a higher share of the gas sampled originates from the cylinder head walls. The interaction between in-cylinder flow and flow initiated by the GSV sampling can observed if one evaluates the flow field in the xy-plane. Here, the higher flow velocities can be observed towards the inlet valve and for this reason a higher share of the sampled gas originates from this region of the cylinder. To summarize, the sampled volume reaches up to 9.8 mm into the negative z direction and shows a non-symmetric shape in the xz and xy-plane. Therefore, we will not only sample the wall near gases from unburnt zones but also from zones which participate at the combustion. Accordingly, the wall-near gases will be already diluted at the sampling by products from complete combustion.

Selected conference participations

F. vom Lehn, B. Copa Cáceres, L. Cai, H. Pitsch, Laminar burning velocity prediction based on group contributions and artificial neural network, 10th European Combustion Meeting, Naples, Italy / Online, April 14-15, 2021

Selected national and international cooperations

- K. Alexander Heufer, Chair of High Pressure Gas Dynamics, RWTH Aachen University
- S. Mani Sarathy, King Abdullah University of Science and Technology, Thuwal, Saudi Arabia
- U. Simon, Institute of Inorganic Chemistry, RWTH Aachen University

Publications

- VOM LEHN F, CAI L, COPA CÁCERES B, PITSCH H. Exploring the fuel structure dependence of laminar burning velocity: A machine learning based group contribution approach, Combustion and Flame 232 (2021) 111525.
- WU X,* FISCHER M, NOLTE A, LENSSEN P, WANG B, OHLERTH T, WÖLL D, HEUFER KA, PISCHINGER S, SIMON U. Perovskite Catalyst for In-Cylinder Coating to Reduce Raw Pollutant Emissions of Internal Combustion Engines, ACS Omega, 7, 6, 5340–5349

Engineering Sciences

Heat Energy Technology, Thermal Machines, Fluid Mechanics | DFG 404

Soot Formation in Oxymethylene Ether Fuel Blends

Project ID: rwth0621

DOMINIK GOEB,
HEINZ PITSCH,
Institute for Combustion Technology,
RWTH Aachen University

Project Report

Coupling the power sector with its growing share of renewables to the transportation sector is an essential pathway to decreasing road traffic well-to-wheel CO_2 emissions. The link can be realized through tailor-made liquid e-fuels, which have the advantages of liquid fuels in terms of energy density, storage, existing infrastructure, and mature engine technology can be retained. Additional emission reduction potentials can be realized by tailoring the synthetic fuel's properties. Oxymethylene ethers (OME_x) with the molecular structure $CH_3O(CH_2O)_xC_{H3}$ have been proposed as a renewable replacement fuel or blend component for compression ignition engines. The formation of soot during the combustion of OME_x is suppressed. Hence, the soot-NOx tradeoff of classical diesel engines is eliminated, and a sizeable reduction in NOx emissions can be achieved by raising exhaust gas recirculation significantly. However, in particular OME_1 has significantly different fuel properties compared to diesel fuel, including a significantly lower boiling temperature and a significantly higher Cetane number, indicating longer ignition delay times.

Originally, the intention of this computing time project was the investigation of soot formation in the combustion of OME_x containing fuels, using a state-of-the-art hybrid method of moments (HMOM) physics-based soot model. However, validation simulations that were performed outside of this project within our group revealed significant flaws in the current formulation of that model, resulting in a violation of mass conservation for soot particles (Davidovic et al., submitted to Proceedings of the Combustion Institute (2022)). Thus, it was decided to instead focus on the spray ignition process of blends of OME_x with *n*-dodecane as diesel substitute, until a reformulated model is available. Here, previous work had shown that the ignition behavior of a fuel blend containing 35 vol% OME_1 was very similar to neat n-dodecane despite the much lower cetane number of OME_1. However, in the corresponding large-eddy simulations (LES) a fixed blend composition in liquid and gas phase was utilized, neglecting preferential diffusion effects (Goeb et al., Proceedings of the Combustion Institute (2021)). The computing time of this computing project was utilized to perform additional inert large-eddy simulations of different blends of OME_1 with *n*-dodecane, this time incorporating an appropriate multi-component evaporation model, as well as two-dimensional flamelet simulations of the ignition process of binary fuel blends.

Figure 1 shows the resulting unmixedness due to preferential evaporation, defined as the normalized deviation from the original liquid fuel composition, exemplary for a fuel blend containing 35 vol% OME_1. It can be concluded that the unmixedness is quickly approaching zero in the downstream region of the flame, indicating the negligible impact of preferential evaporation on the flame and thus also on pollutant formation.

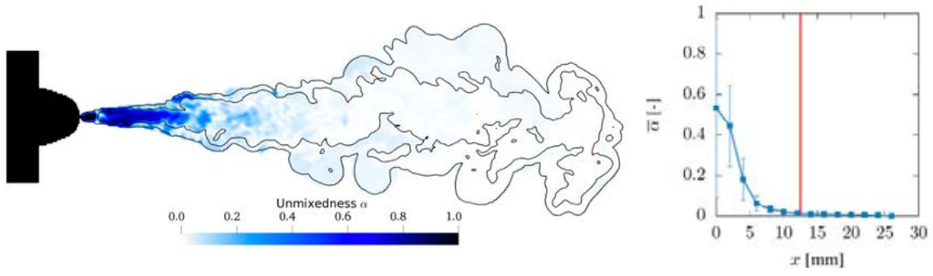

Figure 1: Left: Instantaneous unmixedness at 0:3 ms. The inner black contour represents an isoline of stoichiometric mixture Zst = 0.077, indicating the rich spray core, the outer black contour an isoline of Z = 10E-4, corresponding to the outer extent of the spray cone. Right: Radially averaged unmixedness along the spray axis with spatial standard deviation. The vertical red line indicates the experimentally determined flame lift-off length.

However, in the upstream mixing region close to the nozzle, which is potentially relevant for the ignition process, unmixedness is still high. Thus, to investigate how locally different mixtures impact the ignition behavior of a binary fuel blend, simulations of 2-dimensional flamelets were performed. For this, first the existing flamelet code was extensively validated and improved. In particular, the extremely stiff system of equations resulting from the derivation of the 2D flamelet equations proved to be challenging to solve numerically, and a significant amount of computing time was utilized in test runs to develop a stable numerical solution framework.

Figure 2 shows an exemplary resulting plot of temperature in 2D flamelet space, which covers all possible mixtures of the two fuels with each other and air, after ignition. One can clearly see which mixtures are already burning, and which are yet to ignite or currently showing cool flame temperature levels.

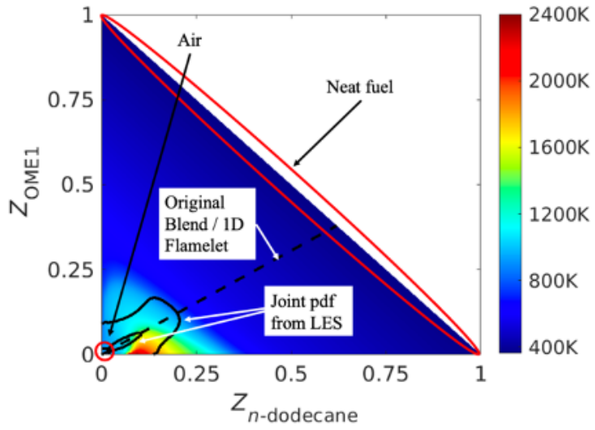

Figure 2: Explanation of temperature plot in 2D mixture fraction space.

The interaction, i.e., mixing, between different mixtures in flamelet space is modeled by the so-called scalar dissipation rates. For low, constant, and equal scalar dissipation rates, ignition of the different mixtures was found to be dominated by auto-ignition, not mixing, so that the influence of preferential evaporation combined with the significant difference in the ignition delay between the two fuels plays a negligible role in the overall ignition process.

In the next step, scalar dissipation and thus mixing rates were evaluated from the LES and then used in the 2D flamelet simulations. A significant impact of the much higher early scalar dissipation rates on the resulting ignition behavior in flamelet space is expected, but post-processing and analysis of the generated data are still ongoing.

Selected conference participations

- D. GOEB, M. DAVIDOVIC, M. BODE, L. CAI AND H. PITSCH. Impact of Preferential Evaporation on Ignition in Oxymethylene Ether - n-Dodecane-Blends. In Proceedings of the 10th European Combustion Meeting, Naples, Italy / Online, April 14-15, 2021

Engineering Sciences

Heat Energy Technology, Thermal Machines, Fluid Mechanics | DFG 404

Large Eddy Simulation of Knocking Combustion in Spark Ignition Engines

Project ID: rwth0644
MICHAEL BLOMBERG
Chair of Thermodynamics of Mobile Energy Conversion Systems, RWTH Aachen University

Project Report

Within this HPC project, scientists and students at the Chair of Thermodynamic of Mobile Energy Conversion Systems (tme) have worked on numerically more efficient 3D-CFD simulation models for internal combustion engines (ICE). The work was carried out within the FVV (Forschungsvereinigung Verbrennungskraftmaschinen) funded research project “Fast Knocking Prediction”. Engine knock describes the potentially harmful auto-ignition of unburnt gases in the combustion chamber leading to high pressure amplitudes, see Fig. 1, as well as high peak temperatures. Knocking is a stochastic phenomenon and is an efficiency limiting factor for spark ignited engines, independent of the fuel (conventional, fossil gasoline or potentially carbon-neutral fuels as methanol or hydrogen) and has been subject to research for the past decades. The overall project of “FVV Fast Knocking Prediction” was to find a novel knock controller to allow for engine operation closer to the thermodynamic optimum.

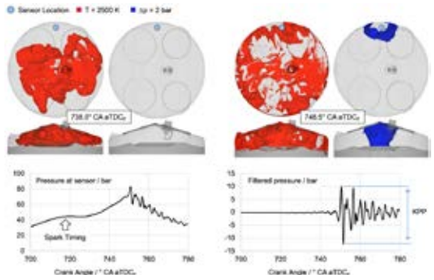

Fig. 1: Visualization of flame and pressure wave propagation before and after knock onset. Pressure trace recorded at depicted monitor point as well as the filtered signal to explain KPP (knock peak to peak).

To gain more fundamental knowledge about the stochastic phenomenon, 3D-CFD combustion simulations have been carried out. To cover cyclic variations, it was necessary to perform Large Eddy Simulations (LES). With LES coupled with detailed chemistry however, the combustion speed (laminar flame velocity) is strongly depending on the spatial resolution (grid size) and no convergence could be proven for feasible wallclock times of full-cycle engine simulations. Therefore, 2D laminar, premixed combustion cases have been set up in order to introduce and validate models which will accelerate the laminar flame speeds to the level of the converged solution. The chosen approach is based on the Thickened Flame theory and utilizes large tables of pre-calculated laminar flamespeeds.

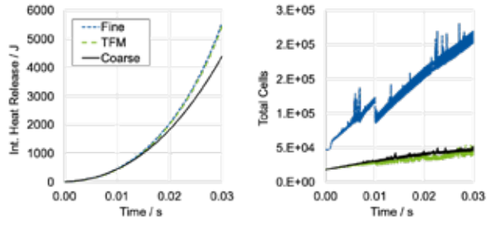

Fig. 2: Results of a 2D laminar, premixed combustion case for the converged solution “Fine”, a typically utilized grid resolution “Coarse” as well as the result with the Thickened Flame Model “TFM”.

This model approach was then carried over to the 3D cases at the knock boundary. As these cases are strictly turbulent (which will accelerate the premixed flame), the interaction between the Thickened Flame Model and the turbulence needed to be investigated. Therefore, test bench results of 500 recorded single cycles were used as a validation database for the evaluation of the heat release, the pressure trace and ultimately also the knock behavior. After successful calibration for one operating point, an engine speed variation was carried out, showing minor re-calibration effort is needed for the varying turbulence level induced by different piston velocities.

To gain further fundamental and statistically relevant results, 100 non-consecutive LES have been carried out. For that, the spark timing was chosen to achieve around 50 % of the operating points to be above the knock threshold, allowing for a statistical evaluation of potentially knock-relevant influence factors, both before spark timing as well as locally at the point of the auto-ignition. The results are depicted on Fig. 3 on the right. The cyclic variations (all simulations have been carried out with identical boundary conditions) are clearly visible, also the pressure fluctuations for the faster burning cycles with the higher pressure amplitude. On the right, the severity of the knock event is depicted over the center of combustion (50 % of fuel mass burned), showing a good extrapolation of the test data.

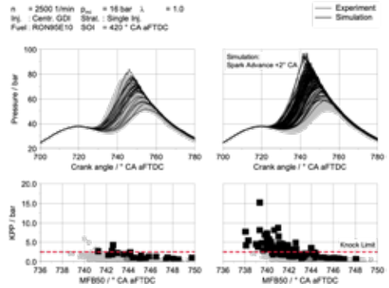

Fig. 3: Simulation result with Thickened Flame Model against experimental data. Left graphs show final model calibration of the Thickened Flame Model. To achieve a higher percentage of knocking cycles, a spark advance has been carried out and the number of cycles was increased to 100 (right graphs). MFB50: 50 % of fuel mass burned, KPP: Knock Peak to Peak, CA aFTDC: Crank Angle after Firing Top Dead Center, SOI: Start of Injection

To support the development of novel knock controllers within the project, probability density functions (PDF) for temperature, mixture and residual gas fraction distribution have been generated. At the same time, the size of hot spots leading to auto-ignition have been evaluated from the high frequency 3D output data. This hotspot distribution can be utilized by one-dimensional models and is relevant for an estimation of the energy hotspots are potentially carrying and whether an auto-ignition can lead to critical engine knock or if the ignition will lead to a deflagrative combustion.

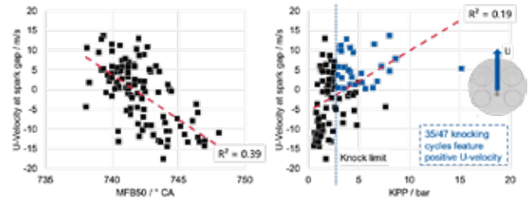

Fig. 4: Correlations for MFB50 (point at which 50 % of the fuel mass is burned) and KPP (Knock Peak to Peak) with the U-Velocity at spark gap at spark timing.

Finally, influence factors before spark timing have been investigated. The detection of phenomena before spark timing might enable future knock controllers to influence the combustion phasing and prevent engine knock. Unfortunately, no early indicators of engine knock have been identified. The most significant, however still weak, correlation found was with respect to high flow velocities at the spark plug, leading to a strong deflection of the early flame kernel and faster combustion (linear correlation, R^2 = 39 %, see Fig. 4). Fast combustion then leads to higher pressures and temperatures in the unburnt, increasing the chance of auto-ignition and knock events (R^2 = 19 %).

While no fundamentally new hypothesis or pre-indicators with respect to engine knock have been identified, a large step toward numerically more efficient combustion simulation with LES has been achieved. The results of the 100 single working cycles above the knock limit allow for modelling with even further reduced numerical effort (RANS 3D-CFD, 1D engine process simulation). Finally, the complete methodology is easily applicable for novel, carbon-neutral fuels such as Hydrogen, Ammonia or Methanol.

Selected conference participations

- MICHAEL BLOMBERG, Experimental and numerical studies at knock limited spark advance, WKM Symposium, Stuttgart, June 15, 2021
- MICHAEL BLOMBERG, Using CONVERGE CFD to describe knocking combustion with RANS and LES (TFM), Converge User Conference, September 30, 2021

Heat Energy Technology, Thermal Machines, Fluid Mechanics | DFG 404

Development of a super-resolution generative adversarial network with physics-based loss function in the context of turbulent reacting flows

Project ID: rwth0658
LUDOVICO NISTA,
TEMISTOCLE GRENGA,
CHRISTOPH SCHUMANN
Institute for Combustion Technology,
RWTH Aachen University

Project Report

Super-Resolution Generative Adversarial Networks (SRGANs) have been applied in photo-realistic single image enhancement. Here, the input to the generator is a low-resolution image and the model learns to recover the missing finer textures. In the context of turbulence, SRGANs can be used to increase details of low-resolution simulations. To resolve the multi-scale behavior of turbulence, highly refined grids that capture all turbulent scaless must be used. This approach, called Direct Numerical Simulation (DNS), is computationally expensive, prohibiting applications at industrial conditions. To reduce computational cost, the smallest scales of turbulence are not resolved in Large Eddy Simulations (LES), which dramatically reduces the computational expense. In a LES, the unresolved, filtered influences need to be modeled with a subfilter-scale (closure) model. In turbulent combustion, the turbulent flow field is further impacted by the heat release associated with combustion chemistry as density and viscosity variations occur. The presence of reactions can be at length scales that are not resolved (filtered) by LES. Using an SRGAN, we investigated if it is possible to reconstruct the high-resolution velocity fields of different premixed hydrogen/air turbulent combustion regimes from the lower-resolution data of a LES.

Given the promising results achieved in the context of inert turbulence (Bode et al., Proc. Comb. Inst. 38(2):2617-2625, 2021), a similar network configuration was applied to two asymptotic regimes of turbulent combustion. In one of these regimes, the flame is thick relative to the smallest turbulent length scales and turbulence behaves mostly like non-reacting turbulence. In the other regime, the flame is comparatively thin, and the budgets of Turbulent Kinetic Energy (TKE) are strongly impacted by the combustion heat release. The computational time allotted in the context of this project was utilized to first develop the Machine Learning (ML) framework and then to train the GAN in different configurations: using data from only one regime and applying the network to the same regime and using data from both regimes combined (mixed). High-Resolution (HR) data was generated by means of DNS (MacArt et al., Combust Flame 191: 468-485, 2018) and Low-Resolution (LR) data was obtained by filtering the data to obtain input fields similar to LES. The training procedure is explained further in (Nista et al., Proceedings of the 10th European Combustion Meeting, 2021).

To assess the network's ability to close the filtered momentum equation, one of the equations solved by LES, a component of the unresolved subfilter-scale stress tensor $\boldsymbol{\tau}_{ij}^{r}$, predicted by the trained GAN is compared to the most employed closure model in the literature, the static Smagorinsky model. Figure 1 depicts this comparison in case of consistent training and application in the thin flame regime, although the same conclusions can be drawn for the thick flame regime. The alignment of the GAN's prediction with the diagonal is superior, the error is significantly lower and the correlation of all tensor components with the DNS exceeds 90%, confirming that the network can learn the individual combustion regimes and indicating that it might outperform commonly employed models.

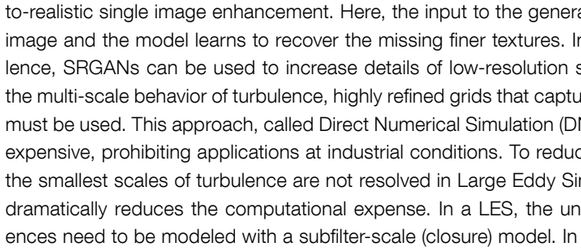

Figure 1: Joint Probability Density Functions (jPDFs) of the first diagonal component of the subfilter-scale stress tensor in case of consistent training and application in the thin flame regime. Left: comparison of the network's prediction (GAN) with the ground truth (DNS), right: comparison of the static Smagorinsky model (Cs=0.17) with the DNS. RMSE = Root Mean Squared Error.

To judge whether the GAN may be applied universally, and thus to verify its generalization ability, it was trained on random data from both datasets. The closure of the momentum equation is evaluated with jPDFs in figure 2. Qualitatively, the subfilter stresses are close to the individual training. The RMSE increases and the correlations with the DNS decrease slightly but there are no artifacts or strong outliers in the jPDF.

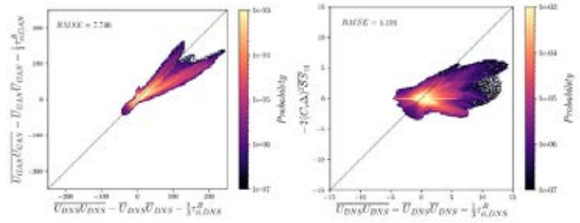

Figure 2: jPDFs of the first diagonal component of the subfilter-scale stress tensor in case of mixed training and application in the thin flame regime (left) and the thick flame regime (right).

The budgets of the TKE are profoundly different in a thick and a thin flame, and the network needs to be able to distinguish well between the regimes. This is evaluated in figure 3, where the TKE budgets are plotted over the progress variable, a measure of combustion advancement, for the mixed training. The network can reconstruct the budgets remarkably well and correctly identifies that the main source of TKE in the thin flame regime is the velocity-pressure gradient (P), whereas the mean shear (P) is a sink of TKE over the entire flame brush. To the contrary, the latter term is the major source of TKE in the thick flame regime. The largest differences exist for the smallest dissipative scales of turbulence (ε), as is expected.

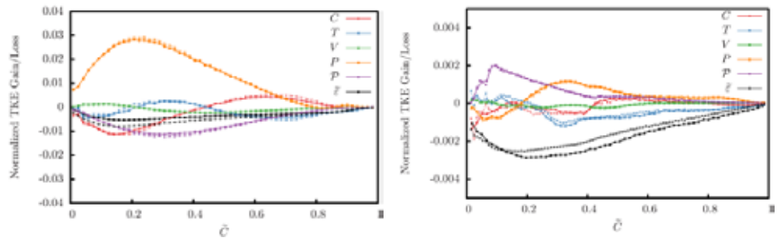

Figure 3: Budgets of the TKE plotted over the progress variable in case of mixed training and application in the thin flame regime (left) and the thick flame regime (right). C=convective transport, T=turbulent transport, V=viscous transport, P=velocity-pressure gradient, P=mean shear, ε=viscous dissipation. The thick solid lines are for the network's prediction, the thin, dashed lines are the DNS ground truth.

The work performed so far is evaluated a-priori, meaning that modeled subfilter-scale terms are compared with the exact solution computed from DNS. It is still unknown if the trained GAN is applicable, accurate and stable as closure model in a LES numerical solver. Hence, we are currently investigating whether this a-posteriori application of the model is equally promising.

Selected conference participations

- T. GRENGA, L. NISTA, C. SCHUMANN, A. N. KARIMI, G. SCIALABBA, A. ATTILI AND H. PITSCH. Predictive data driven turbulence-combustion model through Super Resolution Generative Adversarial Network. In Proceedings of the 10th European Combustion Meeting, Naples, Italy, April 14-15, 2021

Selected National and international cooperations

- PROF. ANTONIO ATTILI, School of Engineering, University of Edinburgh, Edinburgh, UK
- PROF. MORRIS RIEDEL, University of Iceland & Jülich Supercomputing Center, Jülich

Engineering Sciences

Heat Energy Technology, Thermal Machines, Fluid Mechanics | DFG 404

Gas-liquid flow delivery with centrifugal pumps
Development of a validated and efficient simulation method to extend the operating range of centrifugal pumps for handling gas-laden liquids.

Project ID: bund0013
ROMUALD SKODA,
MARKUS HUNDSHAGEN
Chair of Hydraulic Fluid Machinery,
Ruhr University Bochum, Germany

Project Report

Centrifugal pumps are employed in various industrial and engineering applications to transport two-phase mixtures as liquid and non-condensable gas. Several examples of the two-phase pump operation can be found, e.g., in the chemical and process industry or geothermal power stations. In recent optical flow measurements of our project partners from the University of Magdeburg on a transparent volute-type radial centrifugal pump, an accumulation of air bubbles to adherent gas pockets within the impeller blade channels was observed [5]. A transition of unsteady bubbly flow towards an attached gas pocket at the blade suction side was found for increasing water's air loading. Due to the presence of these attached gas pockets, the water is guided inefficiently through the blade passages, which may result in a drop in pump performance and pump surging.

Predicting two-phase flows in centrifugal pumps with state-of-the-art computational fluid dynamic (CFD) methods is only possible by accepting significant uncertainties. We could show that the standard Euler-Euler two-fluid (EE2F) model for the simulation of dispersed bubbles can only approximately capture the pump performance drop, partially with a qualitative mismatch of the location of gas accumulation within the impeller [2]. On the other hand, an interphase-resolving model in terms of the volume-of-fluid (VOF) approach is appropriate to resolve the liquid-gas interface and the coherent gas aggregation if a sufficient spatial grid resolution is provided. However, with the VOF model, it was possible to resolve coherent void structures with the employed computational grids, but finely dispersed gas bubbles could not be resolved [3]. Therefore, a proper head drop could not be captured [3]. The resolution of the disperse phase within the VOF approach would lead to an extremely high computational effort, which cannot be guaranteed even by current HPC systems. Based on these findings, a hybrid two-phase (H2P) flow solver was adopted within this study, which features VOF properties when air accumulations form, while the EE2F approach is used in the dispersed part of the flow. For the time being, a monodisperse bubble size distribution is applied in the dispersed flow region. An extension to polydisperse population balance modeling will be undertaken in the next step. In the measurements, a high unsteadiness of the two-phase flow was observed [5]. For centrifugal pump flows, we could show that a scale-adaptive simulation model can directly resolve large turbulent structures down to the local grid cell size and is more beneficial than standard statistical URANS turbulence models for predicting highly unsteady flow regions [1]. Therefore, a scale-adaptive turbulence model is utilized in this study. The simulation results reveal that the prediction of coherent gas pockets in centrifugal pump impellers is significantly improved by dynamically introducing the interphase sharpening within the H2P approach [4]. The better prediction of gas pockets with the H2P model compared to the EE2F model is exemplarily shown in Figure 1. The temporal standard deviation of the air volume fraction $\alpha_{a,RMS}$ is presented for an inlet air volume fraction of $\varepsilon = 5\%$. While the temporal variation of the gas pockets within the EE2F model simulation reflects the behavior of the agglomerated bubbles flow regime, the H2P model simulation shows steady gas pockets with an unsteady wake. This behavior reflects the temporal characteristics of the gas pockets observed in the measurements, and this flow morphology is called pocket flow regime [5].

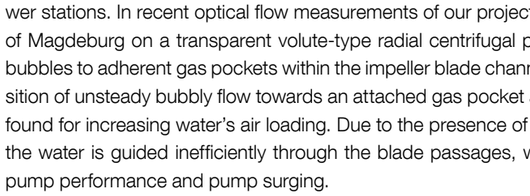

Figure 1: Contour plots of the temporal standard deviation of air volume fraction $\alpha a,RMS$ at impeller midspan and $\varepsilon = 5\%$ operation point; Results have been obtained by the EE2F model simulation with a bubble diameter of 1.5 mm (a) and the H2P model simulation with 1.0 mm (b).

The transition from bubbly via alternating pocket flow to steady pocket flow could also be captured within the H2P model simulations, which goes clearly beyond the capabilities of conventional EE2F and VOF methods [4]. A sample comparison of contour plots at impeller midspan of time-averaged air volume fraction $\overline{\alpha_a}$ in the H2P model simulations and the experimental observed ensemble-averaged accumulation zones for different ε is presented in Figure 2. A very good agreement between simulation results and measurement data is observable for the investigated operation range, and the transition of flow regimes was captured well by the H2P model simulations.

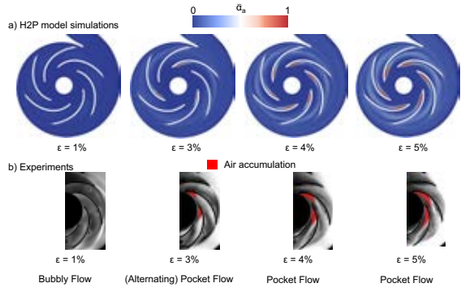

Figure 2: Contour plots for time-averaged air volume fraction at $\overline{\alpha_a}$ impeller midspan with a monodisperse bubble diameter of 1.0 mm for the H2P model simulations (a), and corresponding ensemble-averaged experimental results of a grey-scale analysis (b).

While the capabilities of an H2P approach for pump flows could be shown for the first time, remaining uncertainties are primarily traced back to the assumption of an invariant bubble diameter in the monodisperse air phase. Therefore, in the next step, we intend to use a population balance model together with breakup and coalescence kernels to reflect the polydisperse bubble spectrum. The question will be answered if the polydisperse modeling increases the predictability of the CFD method or if a recalibration of bubble interaction models for two-phase pump flows is necessary. The above-presented results were published in a journal publication [4] and a conference proceeding [3].

Selected conference participations

- MARKUS HUNDSHAGEN, Assessment of multi-phase CFD methods for gas-laden liquid flows in centrifugal pumps with particular emphasis on the change of flow morphology. 14th European Conference on Turbomachinery Fluid Dynamics & Thermodynamics (ETC14), Gdansk (online), Poland, April 12-16, 2021
- MARKUS HUNDSHAGEN, 3D-CFD simulations of the transition from bubbly to pocket flow regime in two-phase radial centrifugal pump flows. 18th Multiphase Flow Conference, Dresden (online), Germany, November 10-12, 2021

Selected national and international cooperations

- DOMINIQUE THÉVENIN, MICHAEL MANSOUR, Lab. of Fluid Dynamics & Technical Flows, University of Magdeburg "Otto Von Guericke", Germany
- CHRISTIAN HASSE, BICH-DIEP NGUYEN, Profil area Thermo-Fluids & Interfaces, TU Darmstadt, Germany
- GÉRARD BOIS, ENSAM. Laboratoire de Mecanique des Fluides de Lille, France

Publications

- HUNDSHAGEN M, RAVE K, MANSOUR M, THÉVENIN D, SKODA R. (2021). Assessment of multi-phase CFD methods for gas-laden liquid flows in centrifugal pumps with particular emphasis on the change of flow morphology. Proc. 14th European Conference on Turbomachinery Fluid Dynamics & Thermodynamics (ETC14), Paper-ID: ETC2021-529, Gdansk, Poland, April 12-16, 2021. DOI: 10.29008/ETC2021-529.

References:

[1] Hundshagen M, Casimir N, Pesch A, Falsafi S, Skoda R. "Assessment of scale-adaptive turbulence models for volute-type centrifugal pumps at part load operation," Int. J. Heat Fluid Flow, vol. 85, 2020 doi: 10.1016/j.ijheatfluidflow.2020.108621.

[2] Hundshagen M, Mansour M, Thévenin D, Skoda R. "3D Simulation of Gas-Laden Liquid Flows in Centrifugal Pumps and the Assessment of Two-Fluid CFD Methods," Exp. Comput. Multiph. Flow, vol. 3, pp. 186–207, 2021 doi: 10.1007/s42757-020-0080-4.

[3] Hundshagen M, Rave K, Mansour M, Thévenin D, Skoda R. "Assessment of multi-phase CFD methods for gas-laden liquid flows in centrifugal pumps with particular emphasis on the change of flow morphology," Proceeding of 14th European Turbomachinery Conference on Turbomachinery Fluid Dynamics and Thermodynamics, Gdansk, Poland, April 12-16, 2021.

[4] Hundshagen M, Rave K, Nguyen BD, Popp S, Hasse C, Mansour M, Thévenin D, Skoda R. "Two-Phase Flow Simulations of Liquid/Gas Transport in Radial Centrifugal Pumps With Special Emphasis on the Transition From Bubbles to Adherent Gas Accumulations," ASME J. Fluids Eng., vol. 144, no. 10, 2022 doi: 10.1115/1.4054264.

[5] Mansour M, Kopparthy S, Thévenin D. "Investigations on the effect of rotational speed on the transport of air-water two-phase flows by centrifugal pumps," Int. J. Heat Fluid Flow, vol. 94, 2022 doi: 10.1016/j.ijheatfluidflow.2022.108939.

Heat Energy Technology, Thermal Machines, Fluid Mechanics | DFG 404

SBES of an eccentrically mounted variable stator vane

Project ID: rwth0670
JOHANNES JANSSEN,
Institute of Jet Propulsion and Turbomachinery,
RWTH Aachen University

Project Report

The front stages of gas turbine compressors are equipped with adjustable stators. In shrouded compressor designs, as mainly used in aero engines, the stator blades are mounted in the hub by means of a round so-called penny. Due to the necessary separation between moving and stationary components, a cavity remains between the penny and the hub, the so-called penny cavity. This cavity is flowed through, resulting in additional total pressure losses, whereby those total pressure losses dominate which are present due to the re-entry of the leakage into the passage. In the past research, the additional losses were quantified using flow simulations and experiments for a standard geometry of the cavity.

In the present project, a modified geometry in which the blade is eccentrically mounted is to be investigated. For this purpose, scale-resolving simulations were carried out using the ANSYS CFX software. The stress-blended eddy simulation (SBES) method developed by ANSYS was carried out, which is a subtype of the detached eddy simulation (DES). Since it was shown during the project that a zonal approach to translating the RANS inlet boundary conditions into synthetic turbulence is a beneficial turbulence treatment, this extension was used.

The results of the mesh study of the predecessor project could be used for the meshing, so that no further mesh study had to be carried out. The scale-resolving simulations were successfully completed. The procedure was such that the calculation required approx. 5000 time steps for settling, so that a recording of the transient quantities was only made after the settling process had been completed. The flow field was averaged over an averaging period of approx. 25000 time steps until the mean value of physically relevant quantities (e.g. the static pressure or the velocity) no longer changed significantly at previously defined monitor points. The measurement uncertainty of the associated measurements was used as a measure of the required accuracy.

It could be shown that the results of the scale-resolving simulations agree very well with the experimental results. In particular, in comparison with similarly performed steady-state simulations, the effects that are present due to the cavity geometry are much better reproduced. The influence of the eccentricity and the resulting cavity geometry can be clearly seen in the results of the scale-resolved simulations and can also be explained physically.

Selected conference participations

- JOHANNES JANSSEN, DANIEL POHL, PETER JESCHKE, ALEXANDER HALCOUSSIS, RAINER HAIN, THOMAS FUCHS, Effect of an Axially Tilted Variable Stator Vane Platform on Penny Cavity and Main Flow, ASME Turbo Expo 2021: Turbomachinery Technical Conference and Exposition, online, June 07-11, 2021

Publications

- JANSSEN J, POHL D, JESCHKE P, HALCOUSSIS A, HAIN R, FUCHS T. Effect of an Axially Tilted Variable Stator Vane Platform on Penny Cavity and Main Flow, Journal of turbomachinery, 2021, Vol 144, no. 2: 021010

Materials in Sintering Processes and Generative Manufacturing Processes | DFG 405

Mechanical Properties of Nanocomposites of Silica and Graphene Aerogels: An All-atom Simulation Study

Project ID: jara0201
BERND MARKERT,
SANDEEP P. PATIL,
Institute of General Mechanics,
RWTH Aachen University

Project Report

Many potential applications of silica aerogel are limited due to its low-tensile strength and brittle nature. To mitigate the above limitations, recently, many researchers have been focusing on composites of silica aerogels by the addition of glass fibers and other reinforcements. The idea of this proposal is to study the mechanical properties of silica aerogel reinforced with graphene aerogel, graphene aerogel reinforced with glass fibers, graphene aerogel reinforced with carbon nanotubes.

These reinforcement agents would be randomly distributed and provide for opportunities to study their effects on the silica aerogel. On the one hand, experimentally fabricating these reinforced silica aerogels is still challenging with only a few successful examples. On the other hand, to the best of our knowledge, surprisingly, graphene aerogel reinforced silica aerogels have not been yet studied in a computational study.

Computer simulations act as a bridge between the theory and the experiment and provide a powerful insight into the systems. Therefore we propose a detailed and systematic study of the mechanical properties of reinforced silica aerogel and reinforced graphene aerogel material using molecular dynamics (MD) simulations.

Selected national and international cooperations

- HYUNG-HO PARK, Department of Materials Science and Engineering, Yonsei University, Seoul, South Korea

Publications

- PATIL SP, BACHHAV BS, MARKERT B. "Thermal conductivity of glass fiber-reinforced silica aerogels using molecular dynamics simulations." Ceramics International 48.2 (2022): 2250-2256.
- PATIL, SP. "Enhanced mechanical properties of double-walled carbon nanotubes reinforced silica aerogels: An all-atom simulation study." Scripta Materialia 196 (2021): 113757.
- KULKARNI A, ET AL. "An All-Atom Simulation Study of Gas Detonation Forming Technique." Metals 11.4 (2021): 611.
- PATIL SP., ET AL. "Mechanical modeling and simulation of aerogels: A review." Ceramics International 47.3 (2021): 2981-2998.
- PATIL SP, KULKARNI A, MARKERT B. "Shockwave response of graphene aerogels: an all-atom simulation study." Computational Materials Science 189 (2021): 110252.
- AL-MAHARMA AY, ET AL. "The Effect of Functionally-Graded Voids and GNPs on the Damage Tolerance of Polyurethane Foam Core." PAMM 20.1 (2021): e202000082.

Engineering Sciences

Materials Science | DFG 406

Quantum mechanically guided materials design

Project ID: jara0131

PAVEL ONDRAČKA,
Materials Chemistry,
RWTH Aachen University / Masaryk University, Brno, Czech Republic

SIMON EVERTZ,
Materials Chemistry,
RWTH Aachen University, Germany / Max-Planck-Institut für Eisenforschung, Düsseldorf, Germany

DENIS MUSIC, PHD,
Materials Chemistry, RWTH Aachen University / Department of Materials Science and Mathematics, Malmö University, Malmö, Sweden

DIMITRI BOGDANOVSKI,
LOAY ELALFY,
JOCHEN M. SCHNEIDER,
Materials Chemistry,
RWTH Aachen University

Project Report

Within the framework of the JARA0131 project, density-functional-theory based investigations of different material classes such as transition metal aluminum oxynitrides, metallic glasses and compositionally complex oxides were carried out. Key observables are the phase stability, electronic structure, elastic constants and mechanical properties and also kinetic factors such as diffusion activation energy barriers, enabling evaluation of essential macroscopic properties such as thermal stability or oxidation resistance. In tandem with physical vapor deposition synthesis and a wide array of analytical tools, this approach is a core concept of the MCh strategy to rationally guide the design of tailor-made functional materials through the interplay of simulations, combinatorial synthesis and analytics. Two notable results published in 2021 shall be presented here as examples.

Enhanced thermal stability of (Ti,Al)N coatings by oxygen incorporation

Thermal stability is a key property for several applications of protective coatings and is influenced by multiple factors, chemical composition among them. In this combined experimental and theoretical study, the thermal stability of metastable cubic (Ti,Al)N and (Ti,Al)(O_xN_{1-x}) coatings was investigated on the experimental side by means of X-ray diffraction analysis, atom probe tomography (APT) and energy-dispersive X-ray spectroscopy (EDX). It was shown that the transformation to a wurtzite solid solution occurs at 1300 °C for the oxynitride coating vs. 1000 °C for the oxygen-free system, yielding a clear thermal stability enhancement, with the main driver being a lower O solubility in the wurtzite phase compared to the oxynitride. For the growth of the wurtzite phase, only the metal atoms require sufficient mobility, as revealed by APT and EDX, while oxynitride growth requires mobility of non-metal atoms as well.

On the simulation side, these mobility differences were investigated by means of vacancy formation energy calculations and by calculations of single-atom diffusion activation energy barriers, employing density-functional-theory based approaches as implemented in the VASP package. The (Ti,Al)(O,N) structural models were constructed from literature with respect to the distribution of the metal species on their sublattice. Subsequently, 20 at% of N were substituted with O and metal vacancies were created to ensure charge neutrality. Computation of the energies of formation vs. the constituting elements of the cubic (Ti,Al)N system and of the oxynitride ($Ti_{0.44}Al_{0.44}$)($O_{0.38}N_{0.62}$) revealed a decrease in formation energy from –1.347 eV per atom to –1.799 eV per atom, indicating that addition of O to the nitride system is energetically favorable. Furthermore, it was shown that the energetic cost of vacancy formation on the non-metal sublattice in the oxynitride is nearly twice as high as that on the metal sublattice, requiring higher temperatures for the former to occur. This is well in line with the increase in thermal stability in the oxynitride.

For the calculation of diffusion activation energy barriers, a single atom of the probed species was moved along a [110] trajectory towards the nearest vacancy, with the barrier magnitude determined by the energy difference at the saddle point of the trajectory and the equilibrium configuration. The coordinates of the probed atom were fixed while those of all other atoms were optimized. This approach is computationally rather inexpensive, in contrast to costly molecular dynamics simulations, yet provides a good first approximation of the activation energy barriers. Generally, the highest barriers were found for N (3.73 eV in (Ti,Al)N), with the lowest found for Al (2.54 in (Ti,Al)N). Upon addition of O, the barriers for all species decreased, with the main trend of N being the strongest, followed by Ti, O and Al, being unchanged. In this manner, the different mobility of the individual species was elucidated and correlated with the vacancy formation energies, reinforcing the idea that mass transport on the metal sublattice occurs much more easily.

Metavalent bonding induced abnormal phonon transport in diamondlike structures

In this purely theoretical study, the thermal conductivity of $CuInSe_2$, $CuInTe_2$, $AgInSe_2$ and $AgInTe_2$ was examined. It has been known from prior studies that these compounds behave anomalously in terms of their thermal conductivity, which is generally lower for systems containing heavier atoms (Keyes' rule), yet the reverse is true for $CuInTe_2$ vs. $CuInSe_2$ and $AgInTe_2$ vs. $AgInSe_2$. To elucidate the hitherto ununderstood reason for this behavior, the electronic and phononic structures of the described materials were studied by means of density-functional theory calculations and lattice dynamics simulations (as implemented in the phonopy package). To that end, after structural optimization and calculation of the electronic energies, 64-atom supercells of the individual systems were created and both harmonic and anharmonic interatomic force constants were obtained via the finite displacement method. This allows for the calculation of the phonon frequencies, visualization of vibrational modes and finally, through solution of the Boltzmann transport equation, the lattice thermal conductivity.

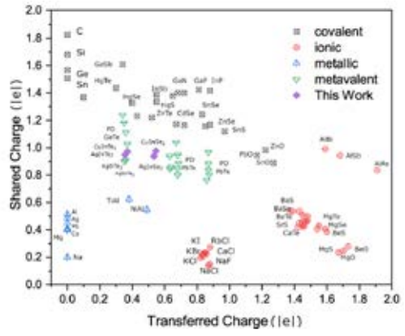

Figure 1: Bonding character map with the shared charge and the transferred charge between atoms as the main descriptors, showing that $CuInTe_2$, $CuInSe_2$, $AgInTe_2$ and $AgInSe_2$ can all be grouped in the metavalent region based on comparisons with literature data. Figure taken from L. Elalfy et al. "Metavalent bonding induced abnormal phonon transport in diamondlike structures: Beyond conventional theory", Phys. Rev. B, 2021, 103(7), 075203.

This approach reproduced the aforementioned anomalous behavior, and a detailed analysis of the phonon band structure revealed that the transverse acoustic phonon bands have a larger negative Grüneisen parameter in the case of the lighter selenides. This usually indicates a higher phonon anharmonicity, lower phonon lifetime and thus lower thermal conductivity, in line with the obtained values. Furthermore, a negative Grüneisen parameter hints towards a bonding mismatch, which was confirmed via examination of the electronic structure: the interatomic charge transfer in the studied compounds suggests a metavalent bonding scenario, inducing a lattice distortion caused by the difference in ionic radii and electronegativity. This distortion, in turn, gives rise to higher phononic anharmonicity, thus eventually causing the anomalous lower thermal conductivity of the lighter selenides.

Selected conference participations

- MARCUS HANS, 'Spinodal Decomposition of Reactively Sputtered (V,Al)N Thin Films', ICMCTF 2021 Virtual Conference, April 25-30, 2021

Selected national and international cooperations

- DAVID HOLEC, Department of Materials Science, Montanuniversität Leoben, Austria
- DENIS MUSIC, Materials Science, RWTH Aachen University, Aachen, Germany / Department of Materials Science and Mathematics, Malmö University, Sweden
- DANIEL PRIMETZHOFER, Department of Physics & Astronomy, Uppsala University, Sweden
- MING HU, Department of Mechanical Engineering, University of South Carolina, Columbia, USA
- CHRISTIAN LIEBSCHER, Max-Planck-Institut für Eisenforschung, Düsseldorf, Germany

Publications

- HOLZAPFEL DM, MUSIC D, HANS M, ET AL. "Enhanced thermal stability of (Ti,Al)N coatings by oxygen incorporation" Acta Materialia 2021, 218, 117204.
- ELALFY L, MUSIC D, HU M. "Metavalent bonding induced abnormal phonon transport in diamondlike structures: Beyond conventional theory" Phys. Rev. B. 2021, 103(7), 075203.
- MARSHAL A, SINGH P, MUSIC D, ET AL. "Effect of synthesis temperature on the phase formation of NiTiAlFeCr compositionally complex alloy thin films" J. Alloys Compd. 2021, 854, 155178.

Engineering Sciences

Materials Science | DFG 406

Quantum mechanically guided design of wear-protective coatings for polymer forming tools

Project ID: jara0151

JOCHEN M. SCHNEIDER, Materials Chemistry, RWTH Aachen University

PAVEL ONDRAČKA, Materials Chemistry, RWTH Aachen University / Masaryk University, Brno, Czech Republic

SIMON EVERTZ, Materials Chemistry, RWTH Aachen, Germany / Max-Planck-Institut für Eisenforschung, Düsseldorf, Germany

DIMITRI BOGDANOVSKI, LUKAS LÖFLER, SOHEIL KARIMI AGHDA, MSC., Materials Chemistry, RWTH Aachen University

Project Report

We employ quantum-mechanical density functional theory simulations to design specifically tailored structural and functional materials and rationally guide their synthesis. These simulations allow us to understand the composition-dependent phase stabilities, electrical and magnetic behaviours and mechanical properties. Together with the experimental analyses tools, including atom probe tomography, scanning tunnelling electron microscopy, X-ray diffraction, energy-dispersive X-ray spectroscopy and X-ray photo spectroscopy, simulations and their interpretation form our core strategy of quantum-mechanically guided materials design. This tandem approach was used to investigate a vast range of novel materials classes, including nitrides, high entropy alloys, nanolaminates and metallic glasses within this JARA project pertaining to several DFG-funded projects. The results have been communicated in peer-reviewed, international scientific journals. A selection of two of these projects is presented in the following.

Unravelling the ion-energy-dependent structure evolution and its implications for the elastic properties of (V,Al)N thin films

Ion-irradiation-induced changes in the structure and mechanical properties of metastable cubic (V,Al)N deposited by reactive high-power pulsed magnetron sputtering are systematically investigated by correlating experiments and ab initio simulations in the ion kinetic energy (E_{kin}) range from 4 to 233 eV. In order to study high-energy ions, ab initio molecular simulations (AIMD) ion bombardment and the thermal spike model were used together. The impact of low-energy Ar atoms (E_{kin} = 35 eV) was studied by placing Ar atoms atop V, Al and N atom sites on the surface of a VAlN slab. For 1000 fs, the impact and the following nucleation and annihilation of defects were simulated. Using the defect structure obtained with AIMD and the Kinchin-Pease relation, the defect density could be correlated to the kinetic energy. The knowledge of this relation allowed us to use the thermal spike model to model impacts at higher energies, thus circumventing computational issues of energy dissipation in the small cells. Here a subvolume of the cell was removed from the cell, heated up to high thermal loads from 10000 to 20000 K and then reinserted into the cell. The resulting structure was then relaxed at 0 K, and the remaining defect density was correlated to the kinetic energy of incoming ions. The simulations show an increase in vacancy and Frenkel pair concentration with increasing kinetic energy. At 165 eV the number of Frenkel pairs reaches a maximum as annihilation processes become more common and the number of defects decreases. The ion bombardment induces compressive stresses in the cells, which fit very well with the stresses measured in the experiments. It is evident that the evolution of film stress and mechanical properties can be explained on the basis of the ab initio calculations, capturing the complex interplay of ion-irradiation-induced defect generation and annihilation.

Ab initio-guided X-ray photoelectron spectroscopy quantification of Ti vacancies in $Ti_{1-\delta}O_xN_{1-x}$ thin films

Ab initio calculations were employed to investigate the effect of oxygen concentration-dependent Ti vacancy formation on the core electron binding energy (BE) shifts in cubic titanium oxynitride ($Ti_{1-\delta}O_xN_{1-x}$). The BE was determined by evaluating the energy difference between the ground state and the final state, in which an electron is removed from a specific level and placed in the valence band. The chosen method does not deliver accurate absolute BE values, but it is able to give precise energy differences. In the scope of this work, the binding energy of all N 1s states in three special quasirandom (SQS) cells was calculated using the Wien2k DFT code, after full structural relaxation with VASP. It was shown that the presence of a Ti vacancy reduces the 1s core electron binding energy of the first N neighbours by ~0.6 eV and that this effect is additive with respect to the number of vacancies. Hence it is predicted that the Ti vacancy concentration can be revealed from the intensity of the shifted components in the N1s core spectra region. This notion was critically appraised by fitting the N1s region obtained via X-ray photoelectron spectroscopy (XPS) measurements of $Ti_{1-\delta}O_xN_{1-x}$ thin films deposited by high power pulsed magnetron sputtering. A model to quantify the Ti vacancy concentration based on the intensity ratio between the N 1s signal components, corresponding to N atoms with locally different Ti vacancy concentrations, was developed. Herein a random vacancy distribution was assumed, and the influence of surface oxidation from atmospheric exposure after deposition was considered. The thus estimated vacancy concentrations are consistent with a model calculating the vacancy concentration based on the O concentration determined by elastic recoil detection analysis (ERDA) and textbook oxidation states, and hence, electroneutrality. Thus, we have unequivocally established that the formation and population of Ti vacancies in cubic $Ti_{1-\delta}O_xN_{1-x}$ thin films can be quantified by XPS measurements from N1s core electron binding energy shifts.

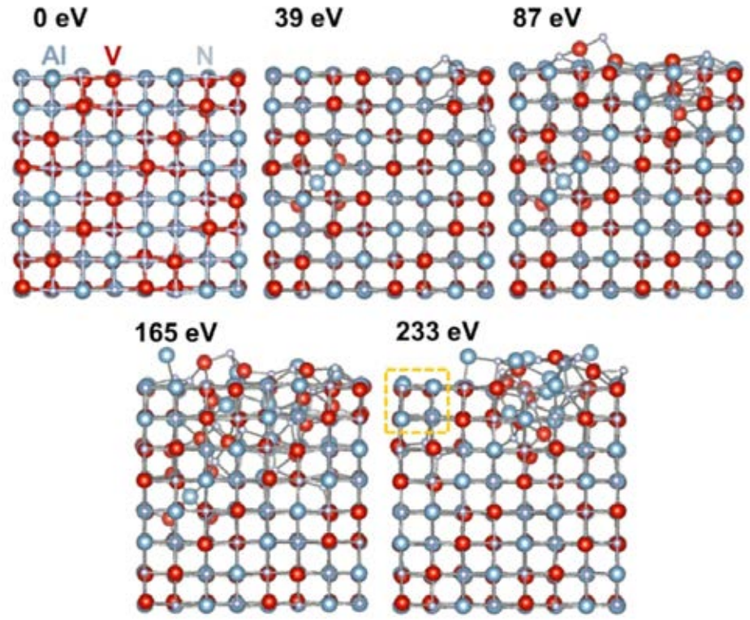

Figure 1 Thermal spike model for $V_{0.5}Al_{0.5}N$ (200) surface, corresponding to energetic ion irradiations. The initial kinetic energy of impinging ion E_{kin} is shown above each final defect structure. In the defect structure with E = 233 eV, a dashed square (in orange) represents the recovered surface region due to defect annihilation. Taken from S. K. Aghda, Acta Materialia, Volume 214, 2021

Selected conference participations

- SOHEIL KARIMI AGHDA, HIPIMS conference 2021 (virtual conference), June 16 - 18, 2021
- SOHEIL KARIMI AGHDA, AVS 67 virtual symposium, October 25 - 28, 2021
- LENA PATTERER, AVS 67 virtual symposium, October 25 - 28, 2021

Publications

- KARIMI AGHDA S, ET AL. „Unravelling the ion-energy-dependent structure evolution and its implications for the elastic properties of (V,Al)N thin films" Acta Materialia 2021, 214
- RUESS H, ET AL. "Effect of target peak power density on the phase formation, microstructure evolution, and mechanical properties of Cr_2AlC MAX-phase coatings" J. Eur. Ceram. Soc. 2021, 41(3)

Engineering Sciences

Materials Science | DFG 406

Quantum-mechanical investigations of phase stability and thermal conductivity in MAX phases and compositionally complex oxides

Project ID: jara0221
DIMITRI BOGDANOVSKI
Materials Chemistry

PETER PÖLLMANN,
JOCHEN M. SCHNEIDER,
Materials Chemistry,
RWTH Aachen University

Project Report

In the course of 2021 in the present project, the investigative focus was shifted from the originally envisioned MAX phases towards the structurally highly similar and currently intensively investigated MAB phases, consisting of interlinked polyhedra of transition metal (M = Cr, Mo etc.) and boron atoms, separated by A element mono- or bilayers. The phase stabilities, electronic structure and thermodynamic potentials of several MAB phases were thus explored in the framework of this project, with a particular focus on two compositions and their derivatives, MoAlB and CrAlB.

One study particularly focused on both ground-state energies of formation and temperature-dependent Gibbs' energies of formation within the quaternary Mo–Cr–Al–B system. The goal was to elucidate why the ternary, equistoichiometric CrAlB phase has not been found experimentally so far while its structural analogue, MoAlB, has been obtained in both bulk and thin film form. Starting from the experimentally determined MoAlB structure, structural models in which Mo atoms were successively replaced by Cr to yield a range of compositions were optimized using density functional theory (DFT) calculations via the VASP package. The energies of formation at 0 K for said optimized systems were then calculated, both vs. the elements and vs. the most stable competing phases known from literature, Mo_2AlB_2 or MoB on the Mo side and Cr_2AlB_2 on the Cr side. It was found that CrAlB is stable vs. the elements in the ground state, but indeed unstable vs. both Mo_2AlB_2/Cr_2AlB_2 and MoB/Cr_2AlB_2. However, the formation of the Cr-rich quaternary system is exothermic at Mo/Cr ratios of approx. 0.2 (vs. MoB) or 0.33 (vs. Mo_2AlB_2) and above, yielding first hints towards the viability of stabilizing Cr-rich (Mo,Cr)AlB via alloying with Mo.

These investigations were then extended further, using the phonopy suite for a lattice-dynamics-based approach in order to obtain electronic and phononic contributions to the Helmholtz energy via the phonon frequencies. Such calculations are performed for several volumes deviating from the equilibrium volume of the respective system in order to account for volume dependency. This results in a set of ***E(V)*** calculations with subsequent lattice dynamics simulations for each of these volumes. Temperature- and volume-dependent thermodynamic potentials are finally obtained via fitting the electronic and phononic energies at different ***V*** to the Birch-Murnaghan equations of state. While computationally highly expensive, this recipe allows the calculation of all essential thermodynamic potentials through the Guggenheim scheme for an arbitrary temperature range.

Analysis of the temperature dependence of the Gibbs energies of formation confirmed the ground-state findings: while MoAlB is stable vs. the elements and all main competing phases throughout the examined temperature range (0 to 1500 K), CrAlB is unstable vs. Cr_2AlB_2 and Al. Upon alloying with Mo, the quaternary system is stabilized, with higher Mo contents allowing stabilization at higher temperatures: e.g., $Mo_{0.375}Cr_{0.625}AlB$ is stable vs Mo_2AlB_2 and Cr_2AlB_2 up to ca. 620 K, while $Mo_{0.5}Cr_{0.5}AlB$ is predicted to be stable up to 1000 K. Such DFT-derived thermodynamic potentials may serve as predictive guidelines for future synthesis attempts of hitherto unobtained materials.

A second, combined experimental-computational study focused on the formation of the two-dimensional MoB phase from MoAlB via direct synthesis. While formation of such two-dimensional MBenes is known from literature, performed using chemical etching of bulk MoAlB to deintercalate the Al layers, in the experimental section of the present study direct formation of the MBene phase was observed for the first time in a physical vapor deposition scenario. The MoB region coexists with a pristine MoAlB phase as well as several derivative defect phases in a multiphase thin film and was identified using sophisticated high-resolution scanning tunneling electron microscopy techniques (STEM) at the Max-Planck-Institut für Eisenforschung. On the simulation side of this study, the MoB phase was modeled by taking the structural data of MoAlB, removal of the Al layer and subsequent full structural optimization. The resulting quasi-2D structure was analyzed in terms of atomic positions and bond lengths projected in the ab plane, thus mimicking the surface layer observed in the STEM images, in order to serve as a reference model for bond length determination and species identification in STEM. The projected in-plane bond distances from DFT and those identified in the STEM images were in excellent agreement with each other. In addition, the energies of formation of both the MoB phase as well as the other coexisting defect phases were calculated relative to the energy of formation of pristine MoAlB, with the energy requirement for MoB formation being approx. 0.115 eV per atom – an energy barrier easily overcome during magnetron sputtering and in line with prior findings of synthesis of metastable systems.

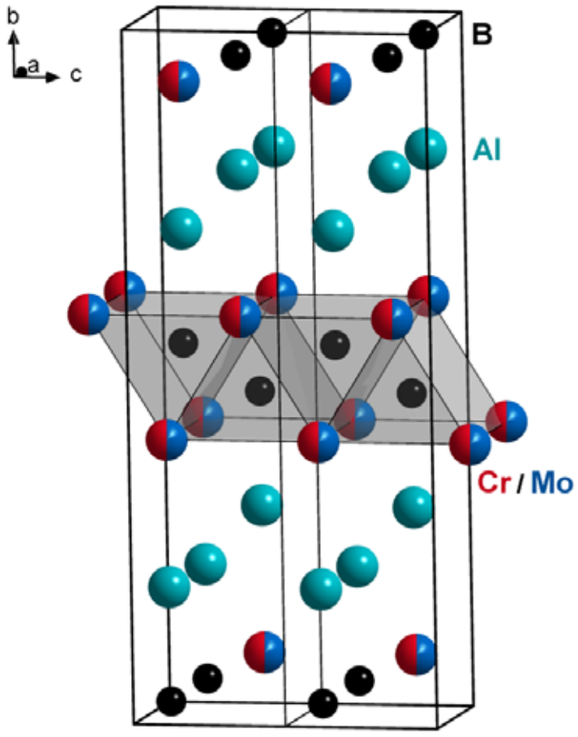

Figure 1: Structural model of an exemplary 1×1×2 supercell of $Mo_{0.5}Cr_{0.5}AlB$ supercell; successive replacement of Mo with Cr allows for various compositions to be simulated. The M_6B trigonal prisms, a key structural motif in MAB phases, are marked in grey. Figure from a manuscript currently in review at Nanoscale.

Selected national and international cooperations

- RAJIB SAHU AND CHRISTINA SCHEU, Max-Planck-Institut für Eisenforschung, Düsseldorf, Germany

Publications

- SAHU R, BOGDANOVSKI D, ACHENBACH JO, ET AL. „Direct MoB Mbene domain formation in magnetron sputtered MoAlB thin films" Nanoscale 2021, 13, 18077.
- BOGDANOVSKI D, PÖLLMANN PJ, SCHNEIDER JM. „An ab initio investigation of the temperature dependent energetic barriers towards CrAlB and (Mo,Cr)AlB formation in a metastable synthesis scenario" Nanoscale, currently in review

Engineering Sciences

Materials Science | DFG 406

Atomistic simulations of plasticity in complex crystals

Project ID: rwth0591

ZHUOCHENG XIE,
SANDRA KORTE-KERZEL,
MATTIS SEEHAUS,
Institute of Physical Metallurgy and Metal Physics,
RWTH Aachen University

Project Report

In this proposed project, the plasticity of complex intermetallic crystals was investigated using atomistic simulations. How these complex crystal structures plastically deform were explored using atomistic simulations and correlating with micro- and nanomechanical testing. How local plasticity of fundamental building blocks influence the deformation behavior of large and complex unit cells were studied in detail. The ultimate goal of this research project is to understand and predict plasticity in intermetallics and transfer the identified general descriptors to data mining purpose to boost materials design and development. The atomistic simulations play an indispensable role in understanding the deformation mechanisms of these complex intermetallic crystals in atomic length scale and femtosecond time resolution.

During the reporting period, we focused on the methodology development to characterize complex crystal structures and their defects as well as the deformation mechanisms of complex crystals and their composites. The identification of defects in crystal structures is crucial for the analysis of atomistic simulations. Many methods to characterize defects that are based on the classification of local atomic arrangement are available for simple crystalline structures. However, there is currently no method to identify both, the crystal structures and internal defects of topologically close-packed (TCP) phases such as Laves phases. We propose a new method, Laves phase Crystal Analysis (LaCA), to characterize the atomic arrangement in Laves crystals by interweaving existing structural analysis algorithms.

The new method can identify the polytypes C14 and C15 of Laves phases, typical crystallographic defects in these phases, and common deformation mechanisms such as synchroshear and non-basal dislocations. Defects in the C36 Laves phase are detectable through deviations from the periodic arrangement of the C14 and C15 structures that make up this phase. We performed large-scale atomistic simulations with millions of atoms to simulate the nanomechanical testing on Laves phases, and LaCA allows the automatic identification of mixtures of different typical crystallographic defects (see Figure 1). LaCA is a robust algorithm, which has been extended to other complex crystal structures, including $CaCu_5$ and $Mg_{17}Al_{12}$.

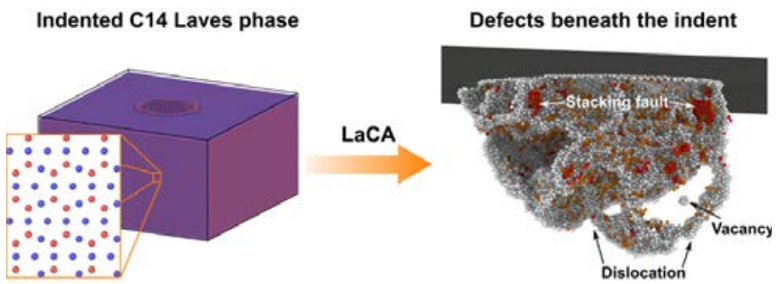

Figure 1: Defect characterization of indented C14 Laves phase using Laves phase crystal analysis (LaCA).

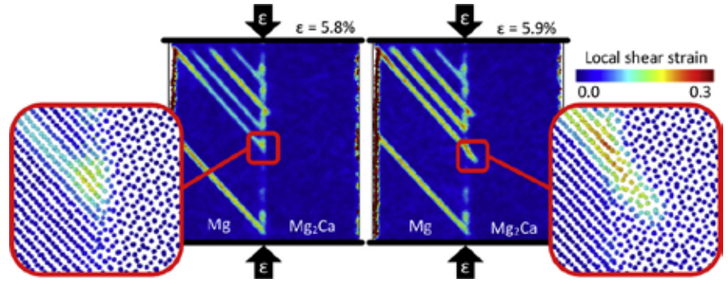

Figure 2: Slip transfer at interfaces in Mg-Ca alloy, as predicted by molecular dynamics simulation.

Large-scale atomistic simulations have been conducted on the interfaces between Mg and Mg-based intermetallic phases since the mechanical properties of Mg alloys are greatly influenced by the Mg-intermetallic interfaces. Nanomechanical experiments presented the evidence of slip transfer from the Mg matrix to the $(Mg,Al)_2Ca$ Laves phase at room temperature and the associated nano-scale mechanisms were explored by means of atomistic simulations (see Figure 2). We identify two possible mechanisms for transferring Mg basal slip into Laves phases depending on the crystallographic orientation: a direct and an indirect slip transfer triggered by full and partial dislocations, respectively. The importance of interfacial sliding on preventing the transfer of plasticity from one phase to the other was identified in both experiments and simulations.

To better understand the plastic deformation of Al_2Cu theta-phase and its composite materials, we performed molecular statics simulations on Al_2Cu theta-phase to evaluate all possible slip systems and correlated the simulation outcomes with the experiments of micropillar compression. The obtained slip systems were analyzed using a geometrical consideration of the interplanar distances in conjunction with the simulations to obtain the generalized stacking fault energies and effective Burgers vectors.

During the reporting period, one Master thesis and one mini-thesis were finished with the support of this HPC project. Except the above-mentioned research outcomes, we are still working on other relevant research topics using the granted computational resources from this project.

Selected national and international cooperations

- JULIEN GUÉNOLÉ, LEM3, Université de Lorraine, CNRS, France
- ERIK BITZEK, Max-Planck-Institut für Eisenforschung, Germany
- SANG HO OH, Korea Institute of Energy Technology, Korea
- DANIEL KIENER, Montanuniversität Leoben, Austria

Publications

- XIE Z, ET AL., Laves phase crystal analysis (LaCA): Atomistic identification of lattice defects in C14 and C15 topologically close-packed phases, Journal of Materials Research, 36 (2021) 2010–2024.
- ANDRE D, XIE Z, OTT F, PÜRSTL JT, LOHREY N, CLEGG WJ, SANDLÖBES-HAUT S, KORTE-KERZEL S. Dislocation-mediated plasticity in the Al2Cu θ-phase, Acta Materialia, 209 (2021) 116748.
- GUÉNOLÉ J, ZUBAIR M, ROY S, XIE Z, LIPIŃSKA-CHWAŁEK M, SANDLÖBES-HAUT S, KORTE-KERZEL S. Exploring the transfer of plasticity across Laves phase interfaces in a dual phase magnesium alloy, Materials & Design, 202 (2021) 109572.

Engineering Sciences

Computer Science | DFG 409

Privacy-Preserving Machine Learning for Intrusion Detection

Project ID: rwth0438
ULRIKE MEYER
ARTHUR DRICHEL
MALTE BREUER
VINCENT DRURY
SEBASTIAN SCHÄFER
BENEDIKT HOLMES
Research Group IT-Security,
RWTH Aachen University

Project Report

The security of complex systems and networks often depends on data aggregated from several sources such as enduser devices, or industry control systems. These devices can create a vast amount of alerts, that make it hard for analysts to discern attacks from benign behavior. There exist several approaches for Intrusion Detection Systems (IDS) and Intrusion Prevention Systems (IPS) to handle these alerts, including machine learning approaches, to filter relevant output. However, such approaches raise questions on privacy, as they often include interactions with enduser systems and can be used to create user profiles or monitor user activity. Furthermore, the question arises how threats can be addressed preemptively, e.g., by leveraging public information to identify and secure vulnerable systems. The goal of this project is to research privacypreserving machine learning approaches to several known problem domains.

Detection of Domain Generation Algorithms: Botnets can have severe effects on the availability and confidentiality of systems. Botnet creators often use Domain Generation Algorithms (DGAs) to communicate with infected systems to make it harder to block their commands. Machine learning (ML) classifiers can be used to monitor the Domain Name System (DNS) traffic of a network enabling network operators to find and clean infected systems.In this part of the project, we engineered two novel classifiers which are based on residual neural networks (ResNets), one for DGA binary and one for DGA multiclass classification. While the binary classifier is able to separate benign from malicious domain names, the multiclass classifier is able to attribute domain names to the DGAs which generated them, enabling the execution of malware specific countermeasures. Both classifiers achieve or even outperform state-of-the-art classification performance. Further, we developed and implemented several collaborative ML approaches to train DGA classifiers cooperatively in a privacypreserving fashion which increases a classifier's detection performance and can reduce its false positive rate by up to 51.7%. In terms of investigating the explainability properties of the ResNet classifier, we developed the feature-based multiclass classifier EXPLAIN. We visualize the classification performance of ResNet and EXPLAIN in form of a combined confusion matrix in Fig.1.

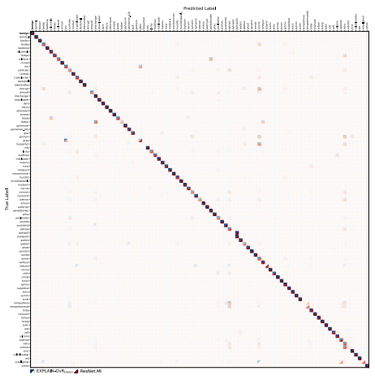

Figure 1: Combined confusion matrix.

Passive Detection of Outdated Software: To preemptively detect systems vulnerable to Malware, DNS queries can be analyzed and classified. This can help operators to create an overview of their network, including the usage of outdated and vulnerable software. If outdated, misconfigured, or unauthorized software can be detected in a network, it is possible to update, block, or at least notify the responsible administrators, in order to prevent possible attacks in the future. In this part of the project, we developed different approaches for this task based on rules or statistical models, machine learning, and process mining. We mostly rely on DNS traffic for the identification of applications.
However, we additionally worked on deep learning approaches that also utilize network flows. While the detection accuracy is comparable to the classification of only DNS, the advantage is that it can be applied if the DNS traffic is encrypted, e.g., when DNS over HTTPS (DoH) is used. For the DNS only case, we developed a rule-based pipeline including automatic traffic labeling and rule extraction. For the process mining approach, we currently develop a complete pipeline based on our prototypes. Additionally, we developed a tool for automatically labeling network packets with application names. This tool is the basis for data generation to develop our rule-based, process mining-based, and deep learning-based approaches.

Automated Detection of Phishing Websites: Phishing is a severe threat to endusers, and as a result to whole organizations. It can be used to deliver Malware, or steal confidential information from users by directing them to malicious websites. This sub-project aims to research different types of phishing detection, preemptive as well as reactive, to improve the security of end-users, and organizations. Defenses against phishing attacks are already integrated into different software solutions, e.g., in the form of blocklists in popular browsers. However, these reactive blocklists leave a short period of time, a "window of opportunity", in which an attack cannot yet be detected. This leaves potential victims of phishing attacks unprotected. Certificate Transparency (CT) logs offer a possibility to detect these attacks earlier, as the acquisition of a certificate is likely to happen before the attack is mounted. In this part of the project, we developed a pipeline that can be utilized to work with the massive scale of data that is included in these logs. The pipeline offers functionality to train classifiers on certificate data, test the classifiers on certificates obtained from real CT logs, and finally use the trained classifiers to detect the certificates of phishing websites as soon as they are added to the logs.

Simulation of Privacy-Preserving Applications: In this part of the project we develop a distributed system that enables the computation of an optimal exchange constellation between patient with incompatible living donors in the context of kidney donor exchange in an automated, privacy-preserving, and fair fashion. We have already developed Secure Multi- Party Computation (SMPC) protocols that support different exchange structures such as crossover exchanges where only two patient-donor pairs are involved. Furthermore, we have run simulations to compare the performance of a kidney exchange platform using our protocols to a non privacy-preserving approach and measured the number of transplants for both scenarios. Our simulations have shown that the performance difference between the two approaches is negligible for those constellations that are most likely to occur in practice.

Selected national and international cooperations

- SUSANNE WETZEL, Stevens Institute of Technology, New Jersey, USA
- EU PROJECT SAPPAN (Fraunhofer FIT, Sankt Augustin, Germany, University of Stuttgart, Stuttgart, Germany CESNET, Prague, Czech Republic, Dreamlab Technologies, Bern, Switzerland, Hewlett Packard Enterprise, Galway, Ireland, F-Secure, Helsinki, Finland)
- DOMINIK TEUBERT, Siemens CERT, Munich, Germany

Publications

- DRICHEL A, FAERBER N, MEYER U. 2021. First Step Towards EXPLAINable DGA Multiclass Classification. In International Conference on Availability, Reliability & Security. ACM.
- DRICHEL A, DRURY V, VON BRANDT J, MEYER U. 2021. Finding Phish in a Haystack: A Pipeline for Phishing Classification on Certificate Transparency Logs. In International Workshop on Cyber Crime. ACM.
- DRICHEL A, HOLMES B, VON BRANDT J, MEYER U. 2021. The More, the Better? A Study on Collaborative Machine Learning for DGA Detection. In Workshop on Cyber-Security Arms Race. ACM.
- HOLMES B, DRICHEL A, MEYER U. 2021. Sharing FANCI Features : A Privacy Analysis of Feature Extraction for DGA Detection. In International Conference on Cyber-Technologies and Cyber- Systems. IARIA XPS Press.
- DRICHEL A, GURABI MA, AMELUNG T, MEYER U. 2021. Towards Privacy-Preserving Classification-as-a-Service for DGA Detection. In International Conference on Privacy, Security and Trust. IEEE.

Engineering Sciences

Computer Science | DFG 409

CFD Simulations Ecurie Aix

Project ID: rwth0213

UWE NAUMANN
Informatik 12,
Software and Tools
for Computational Engineering,
RWTH Aachen University

ALEXANDER MÜLLER
PHILIPP KUNZE
PASCAL KRUSE
LUCAS TROSSEN
JOHANNES LOSACKER
FELIX IJEWSKI
JAVIER MANCHEÑO DEVIS
GERRIT WEBER

Project Report

Introduction: Every year we, as the Formula Student Team of RWTH Aachen University, develop a completely new electric race car and revise a previous car to be able to drive autonomously. For our Aerodynamics team, the electric vehicle is the main focus. We try to find the best geometries for our car within the regulatory constraints and while keeping performance compromises with other design areas in mind. To help us design and improve our aerodynamic package, we carry out extensive CFD simulations, using Siemens Star-CCM+.

Methods: Over the years, our simulations have been developed further and further to improve accuracy, resulting in several simulation approaches being used currently, depending on the desired information about the different aerodynamic phenomena and influences on the racetrack. These include a straight-line half car simulation using a symmetry plane which consists of around 50 million cells, a full car simulation with a yawed car and turned front tires as well as a cornering simulation, the latter two both using around 90 million cells. In our development process, we mainly use the straight-line and yaw-angle simulations as they provide much quicker turnaround times and yield enough information. The yawed car is used to include the influence of various driving states on our aerodynamic performance. This is especially important because the purpose of our high-downforce vehicle concept is to increase performance in grip-limited driving conditions, which means those are also the situations in which the car state differs most from the neutral state. This is also the reason for the development of the cornering simulation. Here, the car can be fully transformed to represent real driving situations in corners, including a curved wind tunnel which makes sure that the air flow relative to the vehicle matches the real air flow during cornering. For these simulations we are switching from the k-epsilon turbulence model

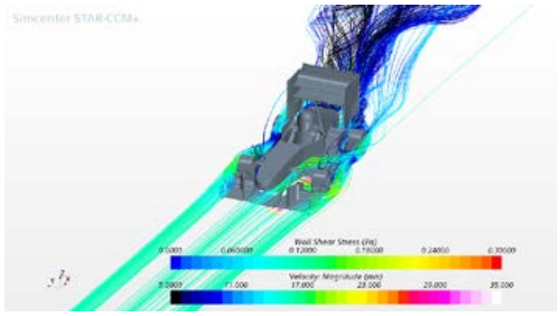

Figure 1: Simulation result of the car visualizing streamlines

Apart from the external aerodynamics, we also use CFD simulations for the design of our cooling systems. These include a water-cooling circuit for our four electric motors and the corresponding inverters as well as an air-cooled battery. Apart from system simulation in MATLAB Simulink and Siemens Amesim, we use thermal CFD simulations to analyze their behaviour.

Results: Over the course of 2021, we put a lot of effort in developing a completely new aerodynamic package including the development of a new front wing, undertray, rear wing, tire wake components of smaller size and a new cooling package. The next upcoming new car will be able to compete in both autonomous and electric disciplines. With the merge of our driverless (autonomous) car and our electric car and other major geometry changes like a new monocoque and a new wheel package we saw the need of developing a new aerodynamic package as well.

Our aerodynamic package is currently in a state where it is performing better than our predescessing concept despite still having key areas to improve on in this current state. We are aiming to increase our downforce in comparison to our previous car by 20% until the end of this season.

In terms of cooling we were able to increase the heat flux in our cooling sleeves for our four distinctive motors by over 100% while maintaining the same pressure drop. Also, we are currently developing our own microtube radiators. This type of radiator enables a much higher heat dissipation, taking advantage of the principle of the Carman's vortex street. Our estimations done in a MATLAB model show a potentially higher heat dissipation of over 25% with a 60% reduction in weight and size. This is also enhanced by the new design of our inverter cooling plate which also reduced it's weight by 10% and it's pressure drop by 60%.

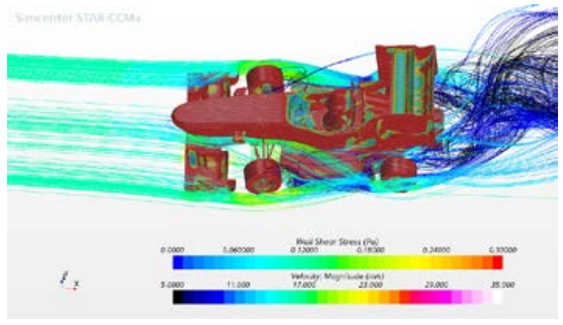

Figure 2: Simulation result of the car showing shear forces acting on the surface visualizing streamlines

Furthermore, after an elongated period of development in home office compromised by the pandemic we were able to finalize and manufacture the past concept of our racing car, the "eace09". This past summer of 2021 where the races/events take part, has brought us to the best results as a team so far. We were able to collect a lot of trophies, particularly an "Overall 1st" win on the RedBull Ring in Austria.

This past season, having been the most successful season in our club's history was substantially supported by the possibility of using the high-performance computing capabilities of the RWTH Compute Cluster for the development of our aerodynamics.

Summary: The team Ecurie Aix participates in the Formula Student, the biggest international development competition of its kind, for which a new race car is build every year. Formula Student does not only generate immense attraction for industrial partners, but also for scientific institutions, since the research often overlaps and yields scientific theses and future employees. The development of a race car does not simply contain of craftsmanship in the workshop. It requires an intense conceptualization, for example the development of the car's aerodynamic parts in thousands of CFD simulations. Since these complex simulations cannot be performed by the student's notebooks, Ecurie Aix was granted to use the high-performance computing possibilities of the RWTH Compute Cluster for the development of the aerodynamic package.

Selected honors, prizes and awards

- Ecurie Aix Formula Student Team, Formula Student Austria Overall 1st, RedBull Ring Spielberg, Austria

Engineering Sciences

Computer Science | DFG 409

Investigation of the SPEChpc 2021 Benchmark Suites

Project ID: rwth0663
SANDRA WIENKE
BO WANG
NINA LÖSEKE
SEVERIN SCHÜLLER,
IT Center
RWTH Aachen University

Project Report

The Standard Performance Evaluation Corporation (SPEC) is a non-profit corporation formed to establish, maintain and endorse standardized benchmarks and tools to evaluate performance and energy efficiency for the newest generation of computing systems. SPEC develops benchmark suites and reviews and publishes submitted results. RWTH Aachen University is a member of the SPEC High Performance Group (HPG) that focuses on benchmark suites for parallel processing. Staff from the IT Center actively engages in the SPEC HPG committee as technical representatives.

In October 2021, SPEC HPG released the new (application-based) SPEChpc 2021 benchmark suites [1]. The suites target at heterogeneous multi-node systems with several levels of parallelism, as found in today's and future CPU or GPU clusters. These levels of parallelism are addressed by "MPI+X" where "X" can be one of the following node-level programming paradigms: OpenMP on the host, OpenACC, OpenMP target offloading. To evaluate HPC systems of different sizes, SPEChpc 2021 offers four suites that provide datasets from "tiny" to "large". These benchmark suites support comparisons of systems and software stacks, the procurement and acceptance process of HPC systems worldwide, and research on heterogeneous clusters.

As part of the benchmark development and release of the SPEChpc 2021 benchmark suites, it is essential that the SPEC HPG committee members test the benchmark suites in different HPC system environments with different workloads. This project has supported these testing activities to eliminate compiler issues, improve benchmark performance and to enable future users with a smooth installation and run process of the benchmark suites. Simultaneously, the SPEChpc benchmark suites have been used for regression testing at RWTH Aachen University. To this end, comparisons of the achieved SPEC scores on CLAIX to other test systems showed significant negative performance differences for some of the benchmarks. With a detailed performance analysis, we found that the execution times differ mostly in the amount of MPI time, specifically, in MPI_Allreduce collective operations. This cross-node execution time imbalance is caused by: (1) dropping memory bandwidth and (2) (system and network) noise (also refer to [2]). As a result, additional job-based bandwidth checks were implemented for CLAIX, and suspicious DIMMs are regularly reported and replaced by the vendor. Furthermore, performance reduction induced by noise could be tackled by not fully loading the compute nodes with MPI ranks, but leave one core empty per NUMA domain. However, further investigations are necessary to find the actual cause of the noise and its extremely high performance impact. Nevertheless, these findings also help to improve performance of other (bulk synchronous) HPC applications running on CLAIX.

Finally, this project allowed to publish performance results for SPEChpc 2021 on the SPEC website for CLAIX-2018 [3]. These SPEC results follow strict run rules and are peer-reviewed. Such SPEC results foster the fair comparison of systems and software stacks.

References

[1] SPEC: "SPEChpc™ 2021 Benchmark Suites", https://www.spec.org/hpc2021/

[2] Brunst H, Chandrasekaran S, Ciorba FM, Hagerty N, Henschel R, Juckeland G, Li J, Melesse Vergara VG, Wienke S, Zavala M. "First Experiences in Performance Benchmarking with the New SPEChpc 2021 Suites", accepted at the IEEE/ACM International Symposium on Cluster, Cloud and Internet Computing (CCGrid) 2022, preprint available at https://doi.org/10.48550/arXiv.2203.06751

[3] SPEC: "SPEChpc 2021 Results", https://www.spec.org/hpc2021/results/

Selected national and international cooperations

Standard Performance Evaluation Corporation: High Performance Group, http://spec.org/hpg/

Thinking the Future
Zukunft denken